The University Of Sheffield.

Spinning Silk *ex vivo*

Andreas Köppel

Supervisor: Dr. Chris Holland

A thesis submitted in partial fulfilment of the requirements for the degree of Doctor of Philosophy

Natural Materials Group

Department of Materials Science and Engineering

The University of Sheffield

Submission Date: November 2019

Thesis abstract

This thesis presents new insights into how strong and tough silk fibres can be spun under benign conditions in Nature. This new knowledge provides inspiration for the development of novel bio-inspired processes and feedstocks that will hopefully be able to produce environmentally friendly high-performance materials.

Silk spinning has fascinated humans throughout history and lately, primarily due to its outstanding property-processing relationship. The mechanical properties of silk fibres easily compete with synthetic fibres but are spun at only ambient conditions without the need for harsh solvents. However, recreating this process has proven challenging to date. Although the main mechanisms such as shear flow as well as pH and the ionic environment are well explored, their interactions especially in the context of extensional flow have not been addressed to date.

Therefore, in this work I investigate the effect of extensional flow on native silk proteins. My findings show that although being the main flow field in fibre spinning, extensional flow alone is not sufficient to create silk fibres at natural spinning speeds. Extending this work by combining both a pH change and subsequent extensional stretching, I have shown that native silk proteins exhibit improved spinnability and ultimately can be spun into fibres that even outperform native silk.

Following, I investigated the effect of metal ions on the flow properties of silk and found that the sensitivity of the silk feedstock to alignment and aggregation can be altered by adding metal ions such as KCl, $CaCl_2$, LiBr and LiCl.

Acknowledgements

First and foremost, I would like to thank my supervisor Dr. Chris Holland for giving me the opportunity to conduct this very interesting research in the Natural Materials Group. I am very thankful for his continuous support and enthusiasm, the helpful discussions and his inspiration which helped me become a better researcher over the course of my PhD. I thank Dr. Pete Laity for help with experimental interpretations and sharing his seemingly never-ending knowledge about silk, fibre spinning and various characterisation techniques.

Additionally, I want to thank Dr. Jamie Sparkes, Dr. Anastasia Brif, Egdar Barajas-Ledesma, Nicola Stehling, Dr. Richard Hodgkinson, Dr. Hyo-Won Kwak, Dr. Petr Lepcio, Hana Postulkova and Yogendra Pratap Singh for moral support, help with various things in the lab and creating a nice office atmosphere where I really enjoyed working.

I would like to extend my deepest gratitude to my examiners Dr. Ann Terry and Dr. Jonny Blaker who kindly accepted to examine my work. I am very thankful for their contributions to the improvement of the quality of my thesis. For taking the role as provisional internal examiner I would like to thank Dr. Claire Corkhill.

I would like to thank Dr. Sarah Langridge and the Scientific Advisory Board members of the Dr. Jeff Wadsworth-Battelle Fellowship scheme for awarding me the fellowship that allowed me to spend four months in the USA at the end of my PhD.

For funding I would like to thank the Engineering and Physical Sciences Council (EPSRC) and the Horizon 2020 programme by the European Union.

On a personal note, I would like to thank Siu Ki Ng, my family and friends for their continuous support throughout my PhD.

Table of Contents

List of Figures

List of Tables

CHAPTER 1:

Introduction to Silk

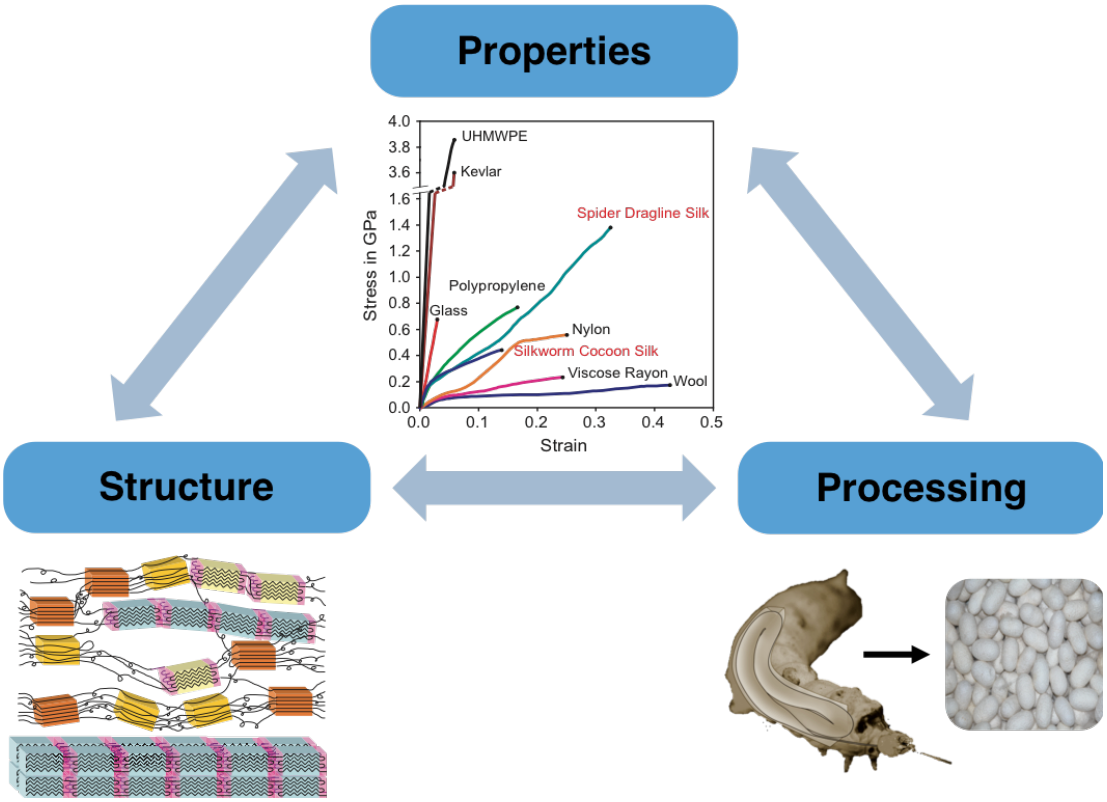

This chapter provides an introduction to silkworm and spider silk explaining why it is interesting to study these fascinating materials. Additionally, the natural silk spinning process is described as well as different approaches trying to spin artificial silk fibres. The section “Artificial silk spinning” of this chapter is based on my review paper “Progress and Trends in Artificial Silk Spinning: A Systematic Review” published in the journal ACS Biomaterials Science & Engineering.[1]

1.1 What is silk and why is it interesting?

Silks are generally defined as structural proteins that are spun, on demand, into fibres for use outside the body by thousands of arthropod species such as silkworms, honey bees, dragon flies, lacewings and spiders (Figure 1).[2-3] Some silks have evolved over hundreds of millions of years for a specific purpose such as web construction, prey capture, offspring and self-protection alongside many others. The biodiversity of silks results in a great variety of physical properties, composition and structures.[4-6]

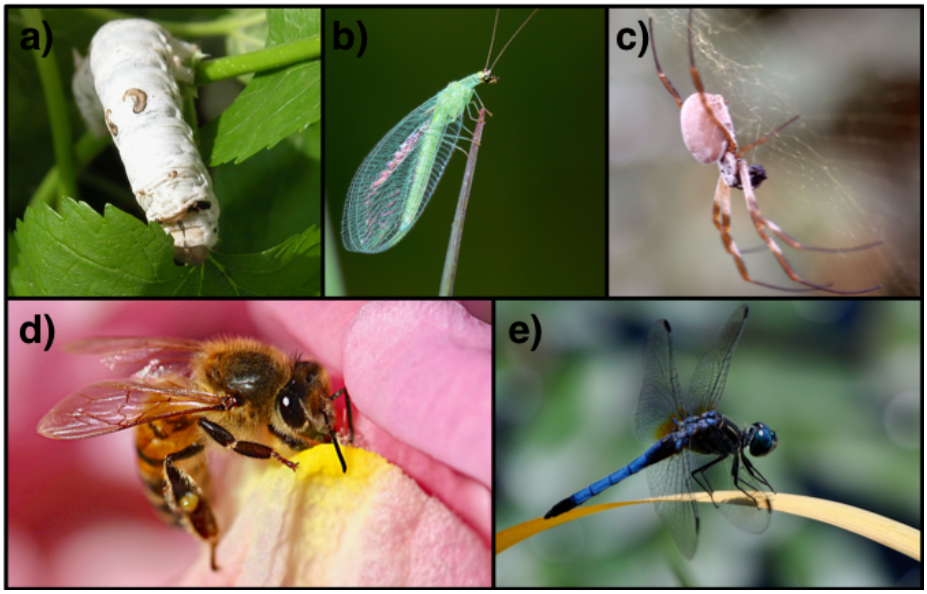

Figure 1: Examples of common silk spinners. **a** Silkworms **b** Lacewings. Credit: Green lacewing (https://flic.kr/p/2aVF9nQ) from Brad Smith licensed under CC BY-NC 2.0 **c** Spiders **d** Honey bees. Credit: Honey bee (https://flic.kr/p/2aVF9nQ) from Renee Grayson licensed under CC BY 2.0 **e** Dragonflies. Credit: Dragon fly (https://flic.kr/p/bCtx3v) from Tom Shockey licensed under CC BY 2.0.

However, the term ‘silk’ is most commonly associated with textiles, specifically the fibres unravelled from cocoons spun by the silkworm *Bombyx mori*.[7] This ‘queen of textiles’ has been used by humans for thousands of years in the production of luxury apparel due to its appearance, soft touch and durability, and is today produced on a commercial scale in quantities of hundreds of thousands of tonnes per annum.[8-9]

Another type of silk that found early uses by humans is spider silk, which combines outstanding mechanical properties with biodegradability and biocompatibility. Ancient Greeks used it to heal bleeding wounds, while Australian aborigines used the silk of a tropical spider to make fishing lines and New Guinea natives manufactured fishing nets and bags.[10]

Nowadays, silkworm and spider silk receive increased attention from a sustainable processing point of view as they possess a very interesting property-processing relationship. The silk fibres are spun at ambient temperatures under very mild conditions with only water as solvent and yet have remarkable mechanical and biodegradable properties.[11-13] This sophisticated spinning process, which has been shown to be 1000 times more efficient compared to the current processes for making synthetic polymer fibres,[14] creates a multi-scale hierarchical structure in the fibres which is responsible for its mechanical properties.

Silkworm silk for example, which has not specifically been evolved for single fibre load-bearing applications but rather for forming a non-woven composite protective cocoon around the silkworm moth, possesses a strength of 360 MPa and a toughness of 50.5 MJ/m^3 which is better than other natural fibres and in a similar range with nylon and polypropylene fibres (Figure 2).[15]

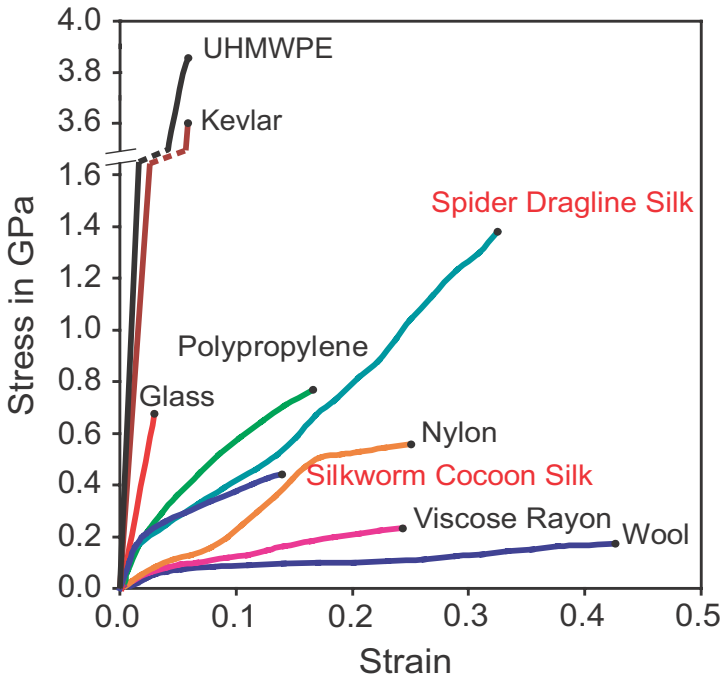

Figure 2: Stress-strain curves of *Bombyx mori* and spider dragline silk. The mechanical properties of other synthetic and natural fibres are shown as a comparison. This image was taken from the Natural Materials Group's image library.

On the other hand, spider dragline silk which serves as web frame and radii as well as a life line when spiders are in danger has a remarkable combination of high strength and toughness (1150 MPa and 214.5 MJ/m^3)[16] which cannot be found elsewhere in Nature and any other synthetic materials. The properties are not only superior to all natural fibres such as wool, cotton, etc., but even outperform synthetic fibres (Figure 2).[5, 17-19]

More specifically, spider dragline silk can absorb 3-4 times more energy before breaking compared to Kevlar, one of the strongest man-made fibres (Table 1).[20] Another example of such superb properties is the orb weaving spider *Caerostris darwini* which produces webs that span 15 m wide rivers. Its dragline silk has a strength of 1652 MPa and an extensibility of 52 % making it the strongest and toughest natural fibre known (354 MJ/m^3).[21]

Table 1: Tensile properties of silk compared to other materials. Data extracted from [15-17].

Material	Stiffness / GPa	Strength / GPa	Extensibility / %	Toughness / MJ/m^3
Nephila edulis dragline silk	7.9	1.2	39	215
Bombyx mori cocoon silk	8.5	0.4	19	51
Wool (100% RH[a])	0.5	0.2	50	60
Elastin	0.001	0.002	150	2
Synthetic rubber	0.001	0.05	850	100
Nylon fibre	5	1	18	80
Kevlar 49 fibre	130	3.6	2.7	50
Carbon fibre	300	4	1.3	25
High tensile steel	200	1.5	0.8	6

[a] RH, relative humidity.

1.2 Silkworm and spider silk

The silkworm *Bombyx mori* (Figure 3a) spins a single fibre which is around 700-1500 m long and wrapped around the animal in a figure of eight pattern to form a cocoon for self-protection during metamorphosis (Figure 3b).[22-23] The fibre is a composite made up of two different proteins – fibroin and sericin. Two fibroin monofilaments, also called brins, which are individually 7-12 μm in diameter and have a circular to elliptical shape, form the main structural part of the fibre (diameter ~20 μm).[24] Sericin serves as a sticky, glue-like coating around the brins which helps to bond the fibres together during cocoon formation (see Figure 3c).[25]

Silk fibroin is a macromolecular complex which consists of proteins called heavy chain (H-fibroin), light chain (L-fibroin) and fibrohexamerin (P25), a glycoprotein, which are present in a molar ratio of 6:6:1.[26] H-fibroin and L-fibroin are covalently bonded together by a disulphide bond and P25 is associated with them by non-covalent forces.[26-28]

Figure 3: *Bombyx mori* silkworm silk. **a** The Chinese silkworm *Bombyx mori*. **b** Cocoon spun by the silkworm *Bombyx mori*. **c** Structure of the *Bombyx mori* silk fibre. The two fibroin monofilaments are covered by a sericin layer. Scalebar: 10 μm. Reprinted by permission from Springer Nature: Nature, Surprising Strength of Silkworm Silk, Shao and Vollrath), Copyright 2002.

The 5,263-residue H-fibroin chain has a molecular weight of 391 kDa and consists of the following amino acids: glycine (45.9 %), alanine (30.3 %), serine (12.1 %), tyrosine (5.3 %), valine (1.8 %) and small amounts of other amino acids.[29] The primary structure can be roughly divided into 12 highly repetitive and 11 irregular regions alternating along the chain. Glycine-X repeat units, where X is alanine, serine, tyrosine, valine and threonine, form the repetitive domains, with GAGAGS being the main motif.[29] The non-repetitive domains with 42-43 residues mainly consist of charged, aromatic and bulky amino residues with larger side groups, for example phenylalanine (Phe), tyrosine (Tyr) and tryptophan (Trp).[29]

The L-fibroin chain has a much lower molecular weight (25 kDa) and consists of irregular amino acid sequences. The role of the light chain in the silk formation process is not entirely clear yet.[28]

The glycoprotein P25 has a molecular weight of around 30 kDa and is secreted together with H-fibroin.[30] It is considered important in maintaining the integrity of silk fibres by forming hydrophobic interactions with the H-fibroin chain(s).[26] P25 is unique as it is the only N-glycosylated protein within the fibroin complex.[26]

The solid silk fibre consists of disordered and ordered domains which are responsible for the remarkable mechanical properties (Figure 4). The ordered domains are highly oriented parallel to the fibre axis and are formed by crystalline β-sheets due to inter- and intramolecular forces such as hydrogen bonding, van der Waals forces and hydrophobic interactions in the repetitive domains of the H-fibroin chain.[31] The size, aspect ratio and orientation of the β-sheet crystallites define the strength and stiffness of the silk fibre.[5, 32] In contrast, the disordered domains which are mainly amorphous regions, that can be oriented to various degrees, determine the extensibility and therefore the toughness of the fibre.[31] Depending on the processing conditions the mechanical properties of the silk fibre can be significantly altered. It was shown that by force-reeling the fibre from the animal the strength and stiffness increase while the extensibility is reduced due to the higher orientation of the crystalline and amorphous parts.[33-34]

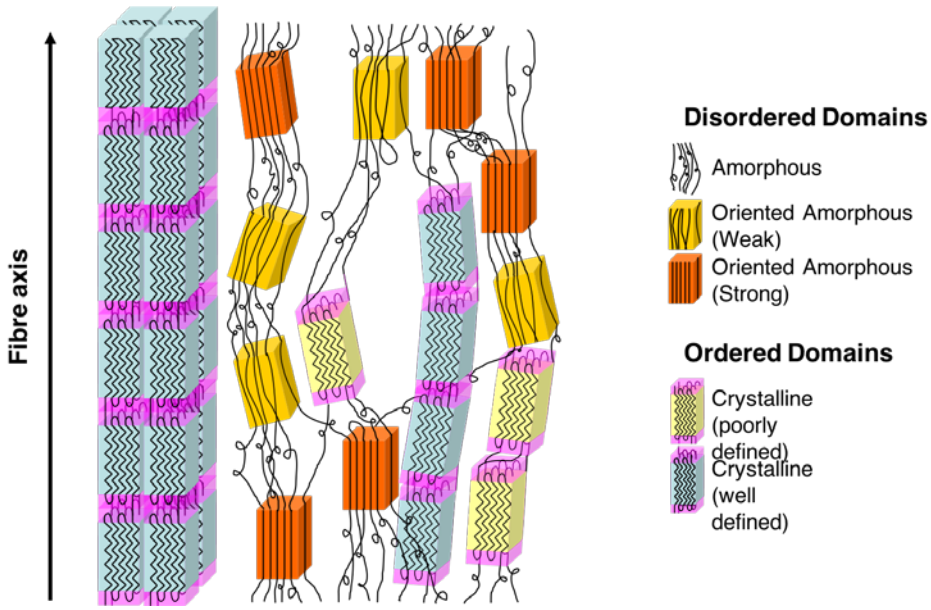

Figure 4: The structure of silk fibres. The ordered (crystalline) domains are responsible for the strength and stiffness of the fibres whereas the disordered (amorphous) regions govern the fibre's extensibility. This image was taken from the Natural Materials Group's image library.

In contrast, spiders can change the mechanical properties of their silks by spinning from up to seven different glands. The mechanical properties of each silk are optimally tuned for serving its own purpose such as web construction, prey capture and offspring protection (Figure 5).[5-6] Dragline silk which spiders use for the construction of the web frame and radii is spun from the major ampullate gland. Due to the exceptional mechanical properties of dragline silk, especially the one from *Nephila* spiders (*Nephila clavipes*[35-36] and *Nephila edulis*[37-38]), it is the most intensively studied silk along with *Bombyx mori* silk.[39-40] The dragline fibre with a diameter from 3-6 μm is significantly thinner compared to silkworm silk.[5]

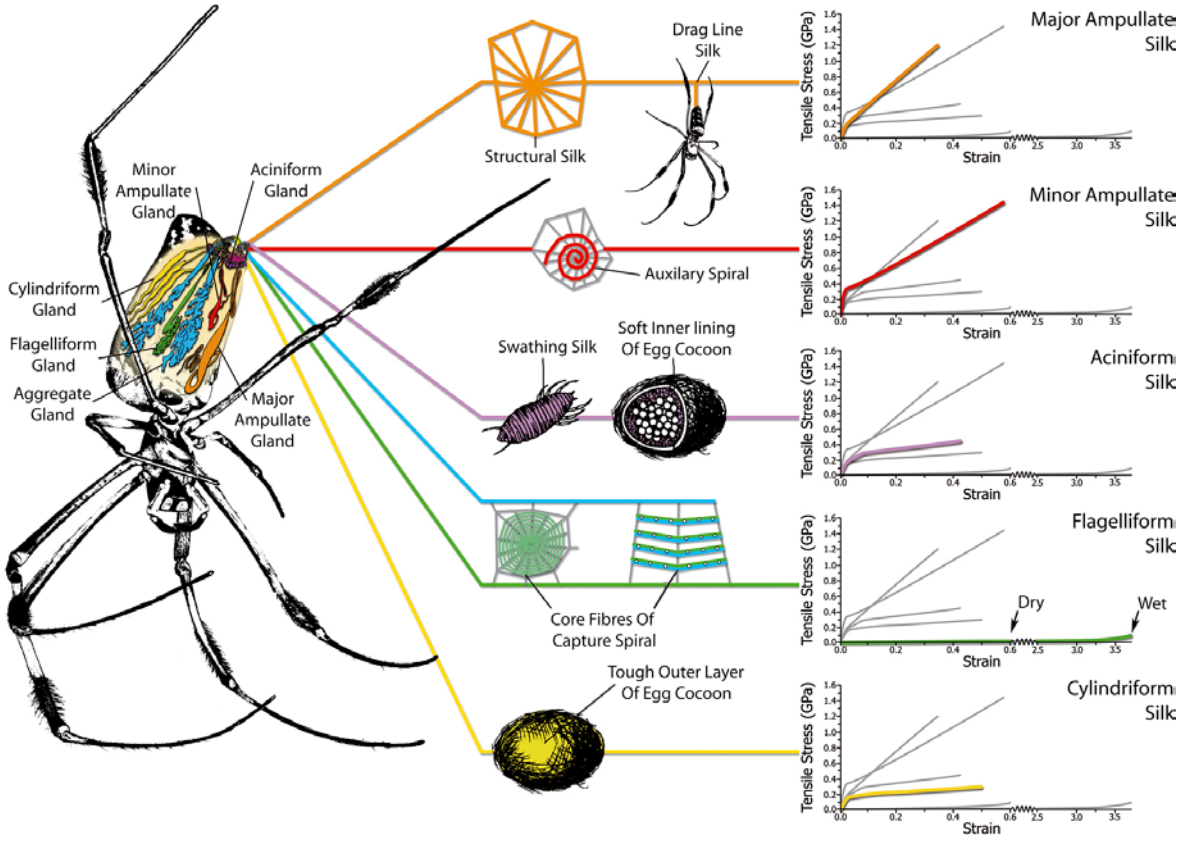

Figure 5: The different silk glands and uses for each spider silk. There is a huge variation in the mechanical properties of each spider silk as they are used for very different purposes. This image was taken from the Natural Materials Group's image library.

Dragline silks consist of two protein components which are named MaSp1 and MaSp2 (Major ampullate Spidroins) for *Nephila clavipes* spiders. The amino acid composition of dragline silk is basically similar to the heavy fibroin chain from *Bombyx mori* with highly repetitive regions of glycine and alanine that are encompassed by non-repetitive terminal regions.[20] The primary amino sequences however are very different.[20] The spidroins consist of alternating alanine- and glycine-rich repeat units that are assigned to various structural motifs.[41] In MaSp1 for example, polyalanine units $(A)_n$ are assigned to the crystalline β-sheet regions and GGX repeats mainly form α-helix structures. Whereas, the main glycine repeat in MaSp2 GPGXX is suggested to be involved in forming β-turns.[41-42]

1.3 Natural silk spinning

This section describes the key mechanisms behind how silk is transformed from an aqueous silk solution into a solid, insoluble fibre. As *Bombyx mori* is the main focus in this research, the natural spinning process of this silkworm will be described in detail. However, fibre formation in spiders is similar despite having different silk glands, protein structures and a final fibre that is optimised for serving different functions.[20, 42]

Silk is processed in highly specialised glands which in case of the silkworm can be divided into three divisions: posterior, middle and anterior division (Figure 6).[43] In the narrow, entwined posterior division the fibroin proteins are synthesised by epithelial cells and expressed into the lumen of the gland.[26, 30] In this part, the aqueous protein solution has a pH value of 6.9 and the fibroin concentration is around 12 wt%.[44] The protein solution is then transported into the middle division, a broader S-shaped part, where it is stored for spinning as a highly viscous liquid (~26 wt%).[43, 45] At this section in the gland the pH is around 5.2 and sericin is secreted around the fibroin proteins as a separate layer without mixing.[43-44]

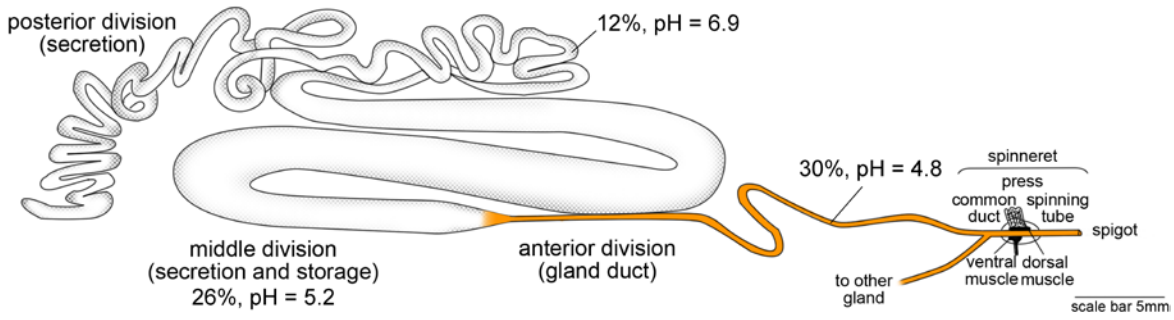

Figure 6: The silk gland of the silkworm *Bombyx mori*. In this schematic only one of the two glands is shown. This image was taken from the Natural Materials Group's image library.

At the end of the middle division the proteins flow down a tapered part into the anterior division also called the gland duct. There, the diameter narrows down to around 50 μm while the metal ion composition changes and the pH further decreases to 4.8 due to vesicular proton pumps and a special type of epithelial cells that produce carbonic anhydrase.[44, 46-47] Previous research has found that copper, magnesium, zinc, sodium and potassium ion levels increase from the posterior to the anterior division while calcium levels significantly decrease.[45, 48-50] It has been postulated that ionic bonding between the metal anions and negatively charged side groups is responsible for controlling the viscosity in the silk gland[51] and providing optimised storage conditions for the proteins prior to spinning.[49] Starting from the tapering part of the silk duct it is thought that the protein molecules align under shear and elongational forces due to their liquid crystalline behaviour.[5, 47, 52] The proteins then gel due to the decrease in pH by suppressing the negatively charged amino acid residues in the fibroin proteins.[47-48, 53-55]

During gelation the viscosity increases, and the silk feedstock can actively be pulled into a solid fibre by the silkworm. The fibre pulling creates an extensional flow field which causes the proteins to detach from the duct wall which is known as the internal draw down taper.[47, 56] The extensional flow field orients and aligns the molecules which leads to the formation of approximately half of the total β-sheets and the removal of the water shell around the fibroin.[47] Before the silk fibre emerges from the spigot, both silk glands join and the

filaments pass the silk press which is thought to act as a restriction die that results in further water removal and molecular alignment.[47]

As a conclusion, the common key factors involved in natural fibre formation in both spiders and silkworms are changes in metal ion concentration[45, 48-50] and pH[44, 46-47, 57] together with shear and elongational forces when the fibre is pulled from the gland.[5, 43, 56, 58-59]

1.4 Artificial silk spinning

Silk's benign natural production combined with the interesting structure-property relationship has inspired researchers for more than 100 years in their attempts to spin artificial silks. Such bespoke fibres produced under environmentally friendly conditions can then be used for a range of new applications ranging from sutures, wound dressings and scaffolds for tissue engineering[6, 60-62] to reinforcing polymer composites.[63]

The following section provides an overview of all approaches for spinning artificial silk fibres in literature to date. Artificial silk spinning is comprised of three main parts which are illustrated in Figure 7. The first step is the preparation of the spinning dope, followed by the choice of the spinning setup and lastly various post-processing steps to improve the fibre properties.

i) Spinning dope

As in nature, artificial fibre spinning begins with the creation of a spinning dope. In case of silk, the feedstock is either made from native, regenerated or recombinant proteins. Native dope is obtained by dissecting silkworms or spiders and extracting the silk proteins directly from the silk gland.[64-66] Whilst this feedstock is considered the gold standard, its preparation is both time consuming and expensive and thus not feasible for large-scale production.

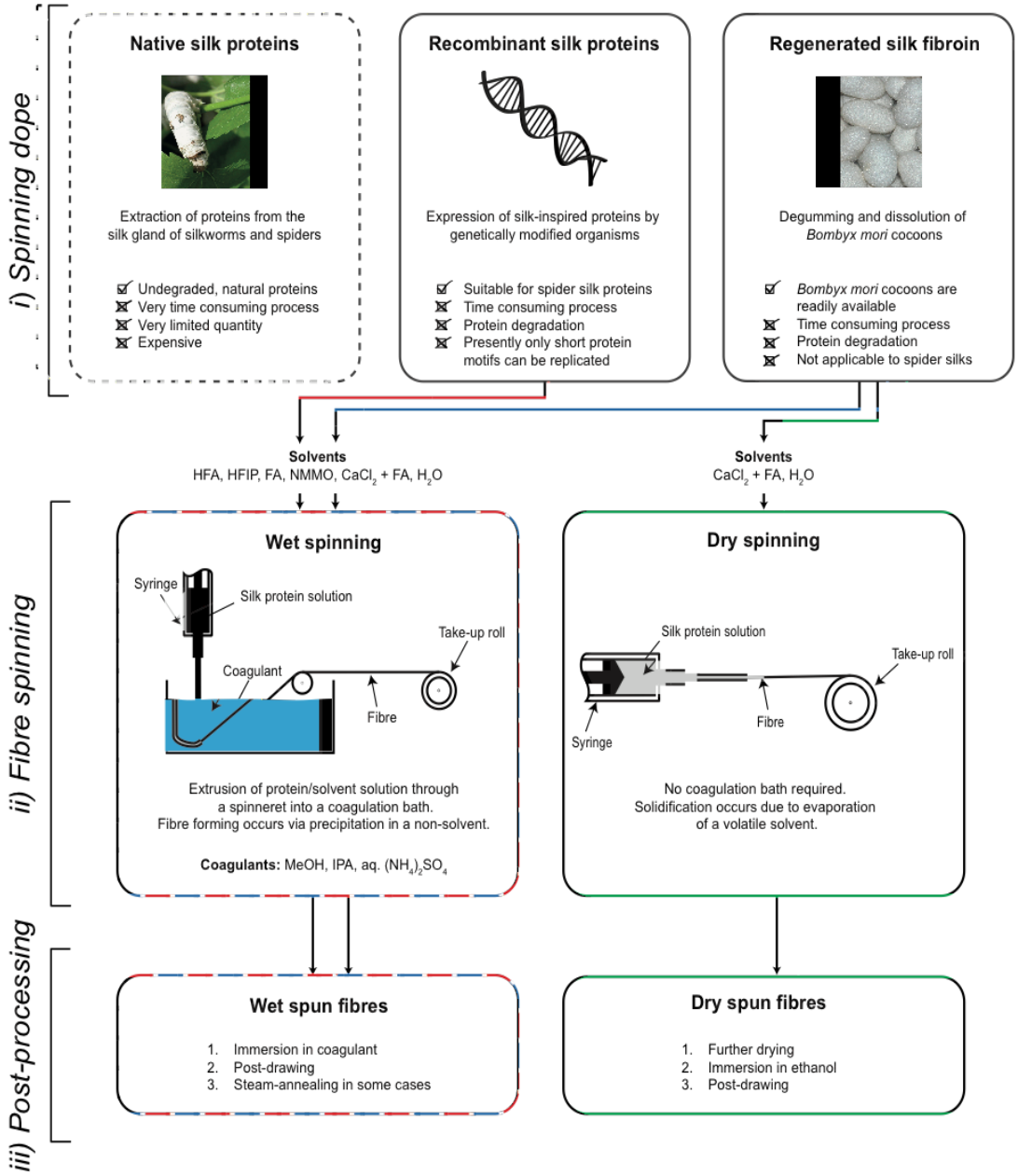

Figure 7: Scheme showing the different approaches for artificial silk fibre production. The different colours represent RSF wet spun fibres (blue), RSF dry spun fibres (green) and recombinant wet spun fibres (red). For consistency, this colouring is maintained throughout the entire chapter. Abbreviations: hexafluoroacetone hydrate (HFA), hexafluoroisopropanol (HFIP), formic acid (FA), n-methylmorpholine-n-oxide (NMMO), methanol (MeOH), isopropanol (IPA).

The second approach is the recombinant synthesis of silk-inspired proteins. Various silk protein motifs have been expressed by genetically modified organisms such as bacteria[67], yeasts[68] and insect cells[69], along with both mammalian[70] and plant cells[71]. Whilst industrially scalable, it is currently limited by the fact that it is very difficult to replicate the full length and sequence of a natural silk protein (i.e. 100's of kDa), and thus the resulting dopes contain silk-inspired proteins of a reduced molecular weight.[41, 72-74] Only recently it has been reported that synthetic spidroins with a molecular weight of 556 kDa could be recombinantly produced which hopefully can help opening new doors for artificial silk spinning.[75]

Finally, it is possible to resolubilise previously spun silk fibres via a process called regeneration (also known as reconstitution).[66, 76-78] Spider silk regeneration is challenged by the fact that these animals regularly produce small amounts of silk throughout their lives, thus acquiring sufficient raw material takes multiple spiders and several days of reeling as only around 0.8 mg of dragline spider silk can be reeled from one spider per day.[77] However a few studies have achieved this technical feat and spun fibres from the resulting solution.[76-77]

This is in stark contrast to silkworms, which produce a large quantity of silk once in their life cycle for cocoon construction.[79] These cocoons are in plentiful supply and can readily be regenerated into large quantities of feedstock using well established techniques.[80] In general, *B. mori* silk regeneration is a three-step process: First is the removal of the glue-like sericin coating of the fibres by a process known as degumming.[81] In most cases this is done by boiling the cocoons in water with either sodium carbonate[82], marseilles soap[83], or mixtures of both[84]. Second, fibres are dissolved in strong chaotropic agents (LiBr, $CaCl_2$, $Ca(NO_3)_2$) which disrupt their hydrogen bonded crystalline structure and enable rehydration of the proteins.[85-86] Finally these chaotropic agents are dialysed away, leaving a silk feedstock solution ready to use.

Whilst regeneration is undoubtedly the most popular approach for silk feedstock preparation, over the past decade it has emerged that the silk proteins undergo partial degradation during this process. [87-89] This is likely due to the degumming step and such degradation in turn affects the regenerated silk's processing potential and ultimate mechanical properties.[66, 90-91] As a result, there are currently concerted efforts to improve this process and enable higher quality regenerated silks with more native like properties to be exploited.[88, 92-93]

In summary, it is clear that there appear to be trade-offs for each approach in the production of an artificial silk dope with respect to achieving quality (native) or quantity (recombinant or regeneration).

ii) Fibre spinning

Due to their relative availability, regenerated and recombinant silk proteins have been used extensively by researchers to spin artificial fibres via both dry[94-102] and wet[67, 70, 72-74, 82-84, 103-145] extrusion based spinning, as well as electrospinning[90, 125, 146-152] processes and occasionally hand-drawn droplet spinning.[113, 153] Here, the discussion is limited to dry and wet spun fibres (Figure 7) as these are the only methods to spin individual fibres in a controlled manner as electrospinning is mainly used for the preparation of nonwoven mats. Dry spinning is the process by which solidification of the fibre occurs due to evaporation of a volatile solvent.[154] For wet spinning the protein/solvent solution is extruded through a spinneret directly into a non-solvent coagulation bath which initiates solidification into a fibre via precipitation.[154] A variation which bridges both wet and dry spinning processes also exists which involves a small air gap prior to the coagulation bath and is known as dry-jet wet spinning.[154]

iii) Post-processing

In general, as-spun silk fibres produced by both wet and dry spinning techniques are often brittle and have poor mechanical properties.[97, 99, 131, 143] Therefore different post-processing methods have been applied to improve the mechanical performance via modulating protein order[15, 95] and decreasing fibre diameter[131] (Figure 7). For wet spun fibres, the most common post-processing methods are immersion in the coagulant for extended periods, manually or automatically applied post-drawing with different ratios, and in some cases steam-annealing.[83, 107, 121] It appears that dry spun fibres have to be further dehydrated and later immersed in ethanol for continuing crystallisation.[94-95, 99] Additionally, wet and dry spun fibres are post-drawn to increase both the order and alignment of the molecules.[74, 100, 102, 129, 131, 143]

1.5 Progress and trends in artificial silk spinning to date

With so many variables in the process of artificial silk spinning, a direct comparison of mechanical properties is often difficult. Differences in the preparation of the spinning dope for example have a huge impact on the final performance of the spun fibres. The chemicals used for degumming and dissolution of the natural fibres alongside the processing time determine the degradation of the silk proteins and thus the molecular weight which directly impacts the mechanical properties[87, 93]. Other influencing factors are the protein concentration of the spinning dope, the choice of solvent and coagulant and the post-processing conditions, to name the most important ones. However, when analysing the literature, it is possible to observe some interesting trends over time that shed light onto both challenges that have been overcome, and those still to be met. A complete list of all spinning approaches reported in literature to date together with the fibre properties can be found in Table 2, with data summarised in Figure 8. As a reference, the properties of spider dragline silk from *Nephila edulis*[16] and natural *Bombyx mori* silk[15] are shown as well.

Table 2: Overview of mechanical properties and processing conditions of all artificial silk fibres reported in literature. Information about how data was converted between different units can be found in Appendix A1.

		Processing parameters					Fibre properties				
		M_W	Protein conc.	Solvent	Coagulant	Draw ratio	Strength	Extensibility	Stiffness	Toughness	Diameter
RSF wet spinning	Reference	kDa	wt% or (w/v)%	-	-	-	MPa	%	GPa	MJ/m^3	µm
	Yazawa *et al.* 1960	-	n.a.	concentrated magnesium nitrate	saturated ammonium solution	n.a.	2.5 g/den	20-25	n.a.	n.a.	n.a.
	Ishizaka *et al.* 1989	-	12	85 % phosphoric acid + 5.7 wt% dimethylformamide	25% aqueous sodium sulfate	9.3	2.1 g/den	10.1	n.a.	n.a.	n.a.
	Matsumoto *et al.* 1996	-	20	40 wt% $LiBr{\cdot}H_2O$ in ethanol; ethanol with different water contents	methanol, ethanol, isopropanol with 10% aq.LiBr	3.2	130 [a]	11	6.7 [a]	12.9 [b]	118.5
	Yao *et al.* 2002	-	10	hexafluoroacetone hydrate (HFA)	methanol	3	321.2 [a,b]	16.1 [b]	5.3 [a,b]	37.6 [a,b]	40-50 [a]
	Zhao *et al.* 2003	-	10	hexafluoro-iso-propanol (HFIP)	methanol	3	193 [b]	19 [b]	5.2 [b]	28.2 [b]	40-50 [a]
	Um *et al.* 2004	-	15.6	98% formic acid	methanol	2	103.8 [a,b]	40 [a,b]	4.1 [a,b]	38 [a,b]	189 [b]
		-	15.6	98% formic acid	methanol	5	257.5 [a,b]	16.4 [a,b]	5.5 [a,b]	30.6 [a,b]	119 [b]
	Marsano *et al.* 2005	-	13	aqueous NMMO monohydrate + 0.7% n-propyl gallate	ethanol	2.7	120	35	7.2	38.9 [b]	18.5 ± 0.8
	Ha *et al.* 2005	-	13	formic acid	methanol	3	1077.3 ± 173 [a]	29.3 ± 11.9 [a]	39.9 ± 6.1[a]	257.8 [b]	35 [a]
		-	13	trifluoroacetic acid (TFA)	methanol	3	959.0 ± 149.1[a]	18.1 ± 6.8 [a]	43.2 [a]	156.7 [b]	21 [a]
	Lee *et al.* 2007	-	15.6	98% formic acid	methanol	4.5	269.4 [a,b]	19.5 [a,b]	4.9 [a,b]	38.7 [a,b]	220-270
	Corsini *et al.* 2007	-	17	aqueous NMMO monohydrate + 0.7% n-propyl gallate	ethanol	2	127 ± 8	12.7 ± 1.9	5.3 ± 0.2	20.3 [b]	73 ± 8
	Zuo *et al.* 2007	-	10	hexafluoro-iso-propanol (HFIP)	ethanol / methanol	n.a.	109.7 [a]	25	n.a.	n.a.	68 [a]
	Ki *et al.* 2007	-	12.3	98% formic acid	methanol	5	285.1 ± 10.7 [a]	14.0 ± 1.7	7.2 [a,b]	30.4 [a,b]	100 [b]
	Zhu *et al.* 2008	-	12 (w/v)	hexafluoro-iso-propanol (HFIP)	methanol	3	400.5 [b]	20.7 [b]	4.3 [b]	51.3 [b]	40 [b]
	Sohn *et al.* 2009	-	29	PEG / LiBr	methanol/water	1.1	128.8 [a,b]	7.6 [a]	6 [a]	6.8 [a,b]	20-50
	Plaza *et al.* 2009	-	17	aqueous NMMO monohydrate + 0.7% n-propyl gallate	methanol	n.a.	313.6 [c]	8.5 [c]	13.4 [c]	20.5 [c]	41

RSF wet spinning	Plaza *et al.* 2009	-	17	aqueous NMMO monohydrate + 0.7% n-propyl gallate	methanol	7.2	172.4 [c]	48.4 [c]	5.1 [c]	55.5 [c]	47
	Zhou *et al.* 2009	-	15	water	aqueous ammonium sulfate	6	450 ± 20	27.7 ± 4.2	12.5 [b]	100.6 ± 6.3 [a]	10.8 ± 2.4
	Zhu *et al.* 2010	-	15	hexafluoro-iso-propanol (HFIP)	methanol	3	408 ± 80	21 ± 3	7.3 ± 0.2	51.5 [b]	n.a.
	Yan *et al.* 2010	-	16	water	aqueous ammonium sulfate	6	390 ± 50	32.1 ± 5.8	15.2 ± 3.3	109.1 ± 18.8 [a]	n.a.
	Plaza *et al.* 2012	-	17	aqueous NMMO monohydrate + 0.7% n-propyl gallate	methanol	n.a.	336.4 [c]	7.38 [c]	18.5 [c]	20.3 [c]	n.a.
		-	17	aqueous NMMO monohydrate + 0.7% n-propyl gallate	methanol	5.3	257.6 [c]	35.3 [c]	7.4 [c]	51.9 [c]	18.4
	Ling *et al.* 2012	-	20	water	aqueous ammonium sulfate	4	221 ± 64	30 ± 4	11.2 [b]	46.4 [b]	100 [b]
	Zhou *et al.* 2014	-	15	water	aqueous ammonium sulfate	9	314 ± 19	37 ± 4	10.4 [b]	105.3 ± 10 [a]	n.a.
	Zhang *et al.* 2015	-	12	$CaCl_2$-FA	water	4	470.4 ± 53.5	38.6 ± 6.3	6.9 ± 2.1	105.3 ± 15.5 [a]	12.8 ± 4.6
	Fang *et al.* 2016	-	15	water	aqueous ammonium sulfate	9	450 ± 30	27.3 ± 4.6	18.9 ± 1.1	91.0 ± 7.4	15 ± 4.7 [a]
	Chen *et al.* 2016	-	13	water	aqueous ammonium sulfate	4	98 [b]	58.9 [b]	37.8 [b]	53.5 [b]	~25
	Madurga *et al.* 2017	-	8 and 16	water + $CaCl_2$	Isopr:Acetic acid 1M 80:20	3.5	330 ± 20	22 ± 3	11 ± 3	50 ± 10	9 ± 0.5
	Hu *et al.* 2017	-	15 (w/v)	functionalized graphene ox. + $CaCl_2$-FA	ethanol / water 3:1	4	697 ± 22	n.a.	7.6	n.a.	n.a.
	Madurga *et al.* 2017	-	8	water	PEG 30% + Acetic acid 0.2 M	n.a.	30 ± 8	10 ± 4	3.3 ± 0.8	3 ± 1	n.a.
	Yazawa *et al.* 2017	-	29	water + DMSO	THF	3	180 ± 10	67 ± 12	n.a.	n.a.	n.a.

RSF dry spinning	Wei *et al.* 2011	-	20	water + (MES)-(Tris) buffer (pH adjustment) + $CaCl_2$ (Ca^{2+} adjustment)		3	301.5 ± 70.6	35.8 ± 21.9	6.2 ± 1.7	104.8 ± 37.8 [a]	5.7
		-	20	water + (MES)-(Tris) buffer (pH adjustment) + $CaCl_2$ (Ca^{2+} adjustment)	-	n.a.	295.2 ± 92.2	74.8 ± 47.4	5.8 ± 4	100.1 ± 64[a]	6.4 ± 1.5
	Sun *et al.* 2012	-	50	water + (MES)-(Tris) buffer (pH adjustment) + $CaCl_2$ (Ca^{2+} adjustment)	-	4	337.7 [b]	24.6 [b]	11.1 [b]	55.8 [b]	10 [b]
	Jin *et al.* 2013	-	40-60	water + $CaCl_2$ (Ca^{2+} adjustment)	-	4	357.3 ± 84.3	34.1 ± 8.1	8.8 [b]	86.5 [b]	6.3 ± 2.3
	Luo *et al.* 2014	-	50	water	-	2	614	27	19	136.4 [a]	2
	Yue *et al.* 2014	-	20 and 25	formic acid + $CaCl_2$ (Ca^{2+} adjustment)	-	2	333 [b]	35.1 [b]	8.8 [b]	90.9 [b]	20-30
	Peng *et al.* 2015	-	44	water + $CaCl_2$ (Ca^{2+} adjustment)	-	4	541.3 ± 26.1	19.3 ± 4.8	9.4 ± 1.2	76.4 ± 22.8[a]	9.0 ± 1.3
Recombinant wet spinning	Lazaris *et al.* 2002	60	>23%		methanol and water	5	269.6 [a]	43.4 [a]	13.2 [a]	101.4 [a]	20 [a]
	Teulé *et al.* 2007	62	25-30 (w/v)	hexafluoro-iso-propanol (HFIP)	90% isopropanol	n.a.	49.6 ± 19.4	15.8 ± 6.1	1.1 ± 1.0	10.6 ± 10.2	15.8 ± 6.1
	Brooks *et al.* 2008	71	10 to 12%	hexafluoro-iso-propanol (HFIP)	isopropanol	0	49.5 ± 7.8	3.6 ± 2.6	0.4 ± 0.3	4.7 [b]	74.1 ± 33.9
	Xia *et al.* 2010	284.9	20 (w/v)	hexafluoro-iso-propanol (HFIP)	90 vol% methanol in water	5	508 ± 108	15 ± 5	21 ± 4	81.5 [b]	n.a.
	Ellices *et al.* 2011	appr. 50	n.a.	hexafluoro-iso-propanol (HFIP)	isopropanol	5	246.7 [c]	50.6 [c]	4.5 [c]	91.7 [c]	46 ± 2
	An *et al.* 2011	70	30 (w/v)	hexafluoro-iso-propanol (HFIP)	isopropanol	n.a.	132.5 ± 49.2	22.8 ± 19.1	5.7 ± 2.4	23.7 ± 18.5	17.4 ± 5
	Teulé *et al.* 2012	58	26-27 (w/v)	hexafluoro-iso-propanol (HFIP)	90 % isopropanol / 10 % water	2-2.5	127.5 ± 23.0	52.3 ± 23.6	4.4 ± 1.0	54.6 ± 23.6	28.3 ± 6
		62	26-27 (w/v)	hexafluoro-iso-propanol (HFIP)	90 % isopropanol / 10 % water	2-2.5	96.2 ± 28.8	29.6 ± 20.5	3.8 ± 2.1	22.6 ± 15.7	14.0 ± 8.7
	An *et al.* 2012	66/48	30 (w/v)	hexafluoro-iso-propanol (HFIP)	isopropanol	3	37.6 ± 20.4	53.9 ± 68.0	3.4 ± 1.1	17.4 ± 20.1	29.1 ± 5.4
		66/48	30 (w/v)	hexafluoro-iso-propanol (HFIP)	isopropanol	3	59.6 ± 19.2	4.8 ± 8.6	4.3 ± 0.9	2.5 ± 5.4	29.1 ± 5.4

Recombinant wet spinning	Gnesa *et al.* 2012	45	20 (w/v)	hexafluoro-iso-propanol (HFIP)	95 % isopropanol	6	121.9 ± 5	18 ± 1	3.9 [2]	17.4 ± 1,2	24.5 ± 0.3
		45	20 (w/v)	hexafluoro-iso-propanol (HFIP)	95 % isopropanol	3.5	95.1 ± 3.3	25 ± 4	2.6 [b]	20.7 ± 3.8	30.5 ± 0.5
	Adrianos *et al.* 2013	66	15 (w/v)	hexafluoro-iso-propanol (HFIP)	isopropanol	3	150.6 ± 31.3	84.5 ± 37.8	4 [b]	89.1 ± 23.9	15.1 ± 1.3
	Lin *et al.* 2013	378 dimer	8 to 10 %	hexafluoro-iso-propanol (HFIP)	$ZnCl_2$ and $FeCl_3$ in water	5	308 ± 57	9.6 ± 3	9.3 ± 3	24.4 [b]	10
	Albertson *et al.* 2014	86.5	45-60 (w/v)	hexafluoro-iso-propanol (HFIP)	isopropanol	4	53.5 ± 18.0	18.0 ± 21.6	2.90 ± 1.1	9.3 ± 10.9	31.5 ± 4.5
		8.6	45-60 (w/v)	hexafluoro-iso-propanol (HFIP)	isopropanol	4	39.0 ± 7.4	181.3 ± 103.5	1.6 ± 0.4	59.3 ± 37.2	36.0 ± 5.9
	Copeland *et al.* 2015	65	25 (w/v)	hexafluoro-iso-propanol (HFIP) + >88% formic acid in 4:1 ratio	isopropanol	1.5/2	221.7 ± 11	56 ± 6.6	n.a.	102.46 ± 13.6	29.0 ± 1.1
	Jones *et al.* 2015	50-75	12 (w/v)	water	isopropanol	2-2.5	192.2 ± 51.5	28.1 ± 26	8.3 [b]	33.8 ± 33.6	n.a.
	Heidebrecht *et al.* 2015	286	10-17 (w/v)	water + Tris/HCl or Na-phosphate buffer	water + isopropanol	6	370 ± 59	110 ± 25	4 ± 1	189 ± 33	27 ± 10
	Peng *et al.* 2016	47	12 (w/v)	NaCl/water	ethanol	n.a.	62.3 ± 17.2	3.5 ± 1.2	4 ± 2.8	1.6 ± 0.9	34 [b]
		47	10-17 (w/v)	NaCl/water	ethanol	n.a.	286.2 ± 137.7	18.3 ± 12.8	8.4 ± 4.3	37.7 ± 28.8	14 [b]
	Thamm *et al.* 2016	76	10-12 (w/v)	water + Tris/HCl or Na-phosphate buffer	water + isopropanol	6	316 ± 103	93 ± 18	1 ± 0.4	142 ± 50	36 ± 9
	Bowen *et al.* 2018	556	17 (w/v)	HFIP	95% methanol	6	1030 ± 111	18 ± 6	13.7 ± 3	114 ± 51	8

[a] Units converted. The density of silk was assumed to be 1.35 g/cm^3. A circular cross-section was assumed for conversion of fineness values into diameter.
[b] Values extracted from graphs/images
[c] Values converted from true stress/strain into engineering stress/strain.

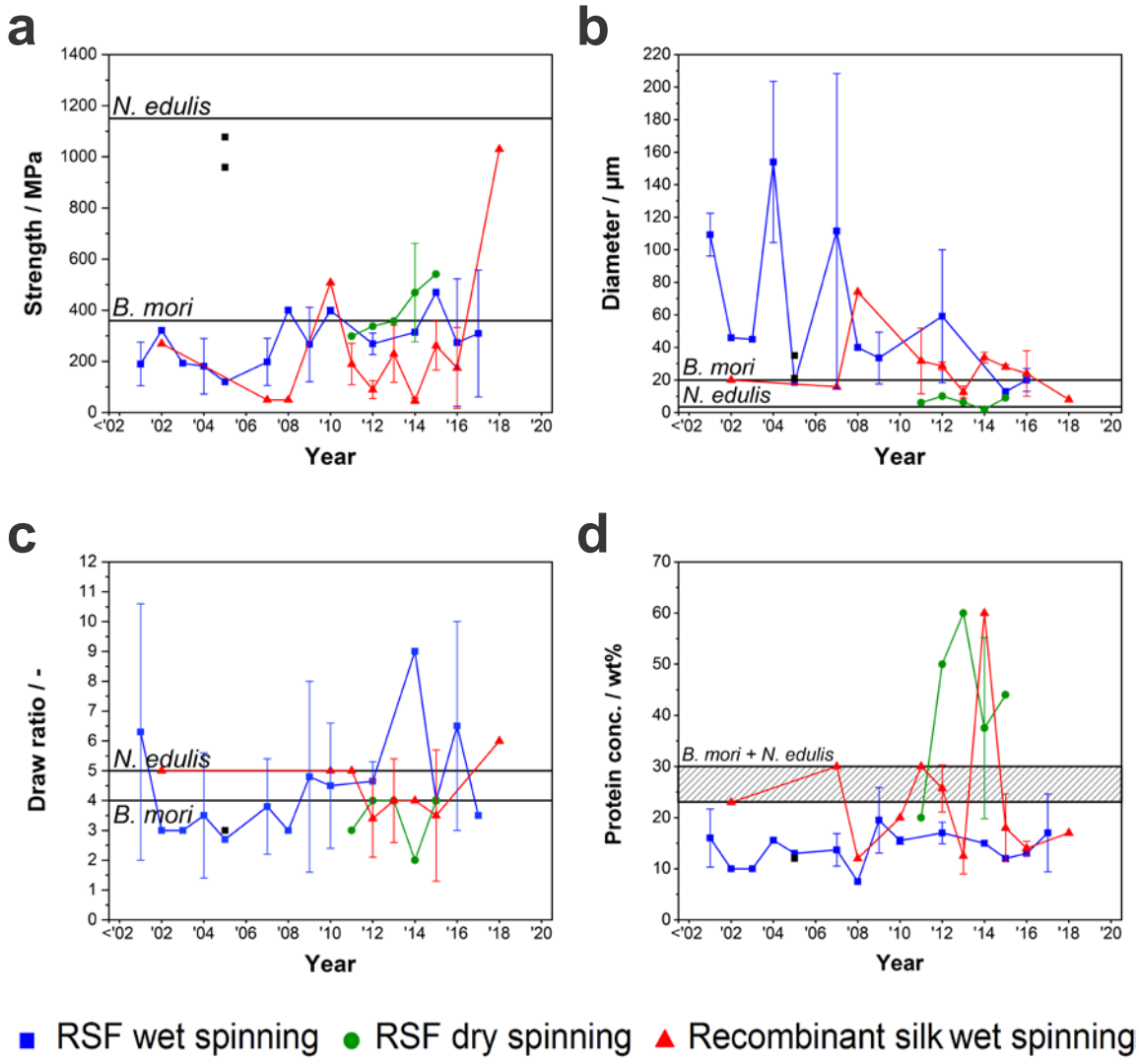

Figure 8: Fibre properties and processing parameters of different artificial silk spinning approaches over time. **The analysis is based on the papers listed in Table 2. Further information on how the data was obtained can also be found in Appendix A1.** The fibre properties of Ha *et al.*[110] are shown as black squares to demonstrate overall trends in fibre development as these findings have not yet been repeated. Fibre properties and processing parameters of *B. mori* and *N. edulis* are shown as references where strength and diameter values are extracted from Vollrath *et al.*[16] and Mortimer *et al.*[15], the natural draw ratio was calculated by Zhou *et al.*[121] and the natural protein concentrations are given between 23 and 30 wt%. The error bars represent the standard deviation from the average values for each year. No standard deviation is shown for years with only one publication.

For ease of discussion the field has been divided into regenerated silk fibroin (RSF) wet spinning, RSF dry spinning and recombinant wet spinning.

1.5.1 Regenerated silk fibroin wet spinning

The first mention of wet spinning of silk fibres may be found in patents from German and Japanese researchers in the 1920s where silk was dissolved in $ZnCl_2$, $Mg(NO_3)_2$, and orthophosphoric acid and spun in various coagulation baths.[10] Another patent by Esselen in 1933 highlights that in the early days of silk fibre wet spinning it was difficult to find an appropriate solvent/coagulant system.[155] Therefore, Esselen began using those developed for cellulose fibre spinning. He found that silk fibroin is insoluble in typical cellulose solvents and therefore used a solution of blue copper hydroxide, ammonia and sodium hydroxide to dissolve the silk fibroin before spinning it into sodium bisulphate. Yet whilst fibres were clearly produced by this process, to the best of my knowledge no mechanical property data exists. The first published journal article with mechanical properties of an artificially spun silk fibre was published a quarter of a century later in the year 1960.[103] Yazawa, like Esselen, took inspiration from cellulose spinning, and dissolved natural silkworm fibres in magnesium nitrate before extruding the dialysed solution into saturated ammonium sulphate. The fibres produced had a tenacity of 2.5 g/den and an extensibility of 20-25%. From then until the turn of the century, artificial silk fibres showed little improvement,[82, 104] which may be attributed to large fibre diameters (> 100 μm), around five times that of a natural *B. mori* fibre (Figure 8a).[156-157]

In 2002, Yao *et al.* reported promising results by spinning fibres with a performance close to silkworm silk.[83] This was achieved by using hexafluoroacetone hydrate (HFA) as a solvent for the spinning dope which has been shown to possess very good solubility for silk proteins[83] and then spinning into a methanol bath to increase the degree of molecular order

via further protein crystallisation.[158] After drawing, their fibres were then steam-annealed at 125°C for 30 min, resulting in a reduction of internal stresses and potentially a further increase in order via annealing of the disordered regions.[15, 159-160] The resulting fibres exhibited a significantly reduced fibre diameter of 46 μm and a strength of 321.2 MPa (Figure 8a and b).

In subsequent years, researchers continued to use methanol as a coagulant and examined alternative solvents for spinning.[84, 107-117] Until 2007, the properties reported by Yao *et al.* were unsurpassed, most likely because the solvents used either heavily degraded the silk proteins, had low silk solubility[107-109, 114, 117] or the spinning technique employed insufficient post-processing[111] (as evidenced by the improved properties achieved by Lee *et al.*[84] and Ki *et al.*[115] by using higher draw ratios that year).

Post 2007, a clear upward trend in fibre strength can be observed (Figure 8a). Zhu *et al.*[118] was the first to report fibre properties exceeding those of natural silkworm silk and from then onwards most studies reported fibres that were either better or close to the natural *B. mori* fibre.[121, 123-124, 127, 130-131] From my analysis, concurrent with this improvement was both a decrease in fibre diameter (Figure 8b) and an increase in post-processing draw ratio (Figure 8c). However, despite the artificial silk's material properties bearing a closer resemblance to the natural fibre, the concentration of the spinning dopes were generally lower than the natural dope protein concentration (Figure 8d), ranging from 7.5 wt%[118] to 29 wt%[120], with a mean of around 15 wt%.

To date, the most impressive properties have been reported by Ha *et al.*[110], with fibres possessing a strength, extensibility and toughness similar to a natural spider dragline silk but with four times higher stiffness (Figure 8, black squares). However, these fibre

properties were based on a small number of hand-drawn fibres and as such have been difficult to replicate. Therefore it was Zhang's efforts in 2015[131], which has to date reported the best fibre properties produced by wet spinning a reconstituted fibroin dope (Figure 9).

1.5.2 Regenerated silk fibroin dry spinning

Dry spinning of regenerated silk fibroin is a relatively recent innovation, with the first reports appearing in 2011, some 50 years after silk wet spinning began.[94-95, 103] This area is dominated by the Zhang group with 6 of the 7 publications and as they use the same degumming and dissolving conditions it is much easier to directly compare fibre properties (Figure 8). From their first paper, fibres were produced that exhibited similar strengths to silkworm silk but had twice the toughness.[94-95] Wei et al.[94-95] used a 20 wt% aqueous solution of regenerated silk fibroin, adjusted the pH to different values by a buffer and added $CaCl_2$ to adjust the calcium ion concentration to 0.3 M. The as-spun fibres had poor mechanical properties and were therefore drawn and immersed in ethanol. Since then, reports continued to show an improvement in fibre properties along with an increase in feedstock concentration from 20 to more than 50 wt.%[94-97], and a decrease in diameter to ~2 μm which is close to *Nephila edulis* dragline silk (Figure 8b), resulting in the best reported mechanical properties to date (Figure 9).[99]

Refinement of the process has been recently reported by Yue *et al.*[100] from another group. They reported similar properties to Jin *et al.*[97], although using a much lower protein concentration for spinning. They spun fibres with a concentration of 20-25 wt% silk proteins into a calcium chloride/formic acid mixture. The natural silk proteins could be dissolved directly in this solvent and immediately be processed, eliminating the dissolution and dialysing steps which could significantly reduce the processing time. This time-saving way

of using formic acid in silk regeneration seems to be a recent trend and was also used by Zhang and co-workers.[116, 131]

1.5.3 Recombinant silk wet spinning

In contrast to regenerated silk fibres, recombinant wet spun fibres do not show the same rate of improvement over time (Figure 8a). Starting in 2002, the widely publicised work by Lazaris *et al.*[70] reported fibres spun from spider silk inspired proteins expressed from mammalian cell lines that had an elongation, stiffness and toughness akin to *B. mori*. However, despite several attempts over the years[67, 72, 135-141], a comparable strength to the fibres reported by Lazaris *et al.*[70] was not achieved until 2010.[67] Surprisingly this improvement is not correlated with a reduction in diameter (like regenerated silk fibres), with fibres being generally larger than natural silks (Figure 8b). Thus, the primary improvement in properties from recombinant fibres is most likely due to an increase in molecular weight. Whilst Lazaris *et al.* spun fibres from proteins of 60-140 kDa[70], Xia and co-workers used multimerization of their gene construct to increase the molecular weight to 284.9 kDa[67] and reported improved properties. Furthermore, later reports from Lin *et al.*[142] and Heidebrecht *et al.*[143] reported a further increase in molecular weight to 286[143] and 378 kDa[142], respectively by using SUMO (small ubiquitin-like modifier) fusion technology and via disulphide bonding. Recently, a further increase in molecular weight to 556 kDa was achieved by combining standardized DNA part assembly and split intein-mediated ligation.[75] Fibres from these synthetic spidroins are very close to fully replicate the mechanical performance of native spider dragline silk which marks a huge step forward in the field of artificially spun silk fibres.

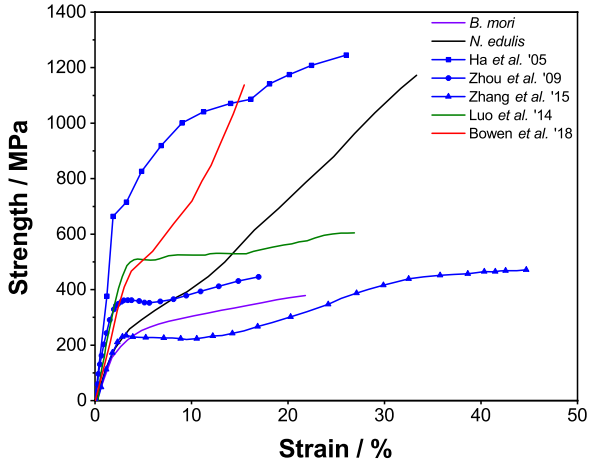

Fibre	*E* GPa	σ MPa	ε %	W_{break} MJ/m³
B. mori	8.5	360	18.5	50.5
N. edulis	7.9	1150	39	214.5
Ha *et al.* '05	39.9	1077	29.3	257.8
Zhou *et al.* '09	12.5	450	27.7	100.6
Zhang *et al.* '15	6.9	470	38.6	105.3
Luo *et al.* '14	19	614	27	136.4
Bowen *et al.* '18	13.7	1030	18	114
Regenerated Wet	Regenerated Dry	Recombinant Wet		

Figure 9: Comparison of the best performing artificial silk fibres to date. The fibres created by regenerated wet (blue), recombinant wet (red) and regenerated dry spinning (green) are compared with natural *B. mori* (violet) and *N. edulis* silk fibres (black). The stress-strain graph shows curves that are closest to the average properties reported in each paper.

1.6 Development of the fibre property space over time

Above we have seen single viewpoints on individual fibres, but we have not been able to see the *overall* development, i.e. “performance space” of the field. Here I introduce a new means for comparing the most common fibre properties to enable us to understand the material property trade-offs in fibre development and determine possible areas for further improvement. As a result, a performance space is therefore derived from the best achieved fibre properties across all studies within a time period, and not necessarily from an individual fibre (visualized as “web plots” in Figure 10). That means the interplay of all properties reported has not been achieved by a single fibre and therefore the performance space plots give an overview how the property space developed over time for the different spinning methods.

Until 2005, the best properties from any wet spun fibres from regenerated feedstocks show a performance close to the natural *B. mori* fibre (Figure 10a). However, it is worth mentioning that it was not possible to spin an individual fibre that combines *all* of these

properties. Of note is that the study from Ha *et al.* which reports fibre properties outperforming the performance of *N. edulis* dragline silk, were set aside for discussion as they still remain to be reproduced.[110] During this time period, only one publication reported the spinning of fibres from recombinant silk proteins.[70] Those fibres possessed a higher stiffness and toughness compared to fibres from regenerated silk proteins, whilst the strength, diameter and extensibility were comparable.

From 2006 to 2010, all regenerated silk fibres saw improvements (Figure 10b). For the first time, individual fibres with properties exceeding those of natural *B. mori* silk could be spun from regenerated feedstocks.[67, 118] As discussed above, this is attributed to improved processing parameters that also account for the decrease in fibre diameter. This is in contrast to recombinant fibres, which do not show an overall improvement, but rather a shift of properties: stiffness and strength were improved, albeit at the expense of extensibility and toughness.

From 2011 to 2016, only the stiffness of regenerated silk fibres increased whilst other properties plateaued (Figure 10c). Recombinant fibres, however, saw a significant improvement with a toughness reported that was close to natural spider silk; a product of increased extensibility but at the expense of fibre strength and stiffness. Bowen *et al.* report the best mechanical performance of fibres spun in a controlled spinning process by increasing the molecular weight of recombinant silk proteins and decreasing the fibre diameter.[75] This time period also saw the emergence of dry spun fibres, with properties reported that outperform regenerated wet spun silks and importantly show the highest strength of all fibres (alongside a very small diameter for dry spun fibres).

In summary, regenerated silk fibres have shown a gradual improvement in all properties over time, but upon closer inspection it appears that the wet spinning approach has reached a limit in strength and toughness although a very high stiffness was recently reported by Chen and co-workers.[132] However, it has been the innovation in dry spinning that has led

to improved properties in the field. On the other hand, the field of recombinant dope spinning appears to be currently making huge improvements as Andersson and co-workers[145] have reported impressive mechanical properties of as-spun fibres from chimeric recombinant spider silk proteins without any post-spinning modification. Moreover Bowen *et al.*[75] found new ways to increase the molecular weight which has a huge impact on the mechanical performance of artificial silk fibres (Figure 10d).

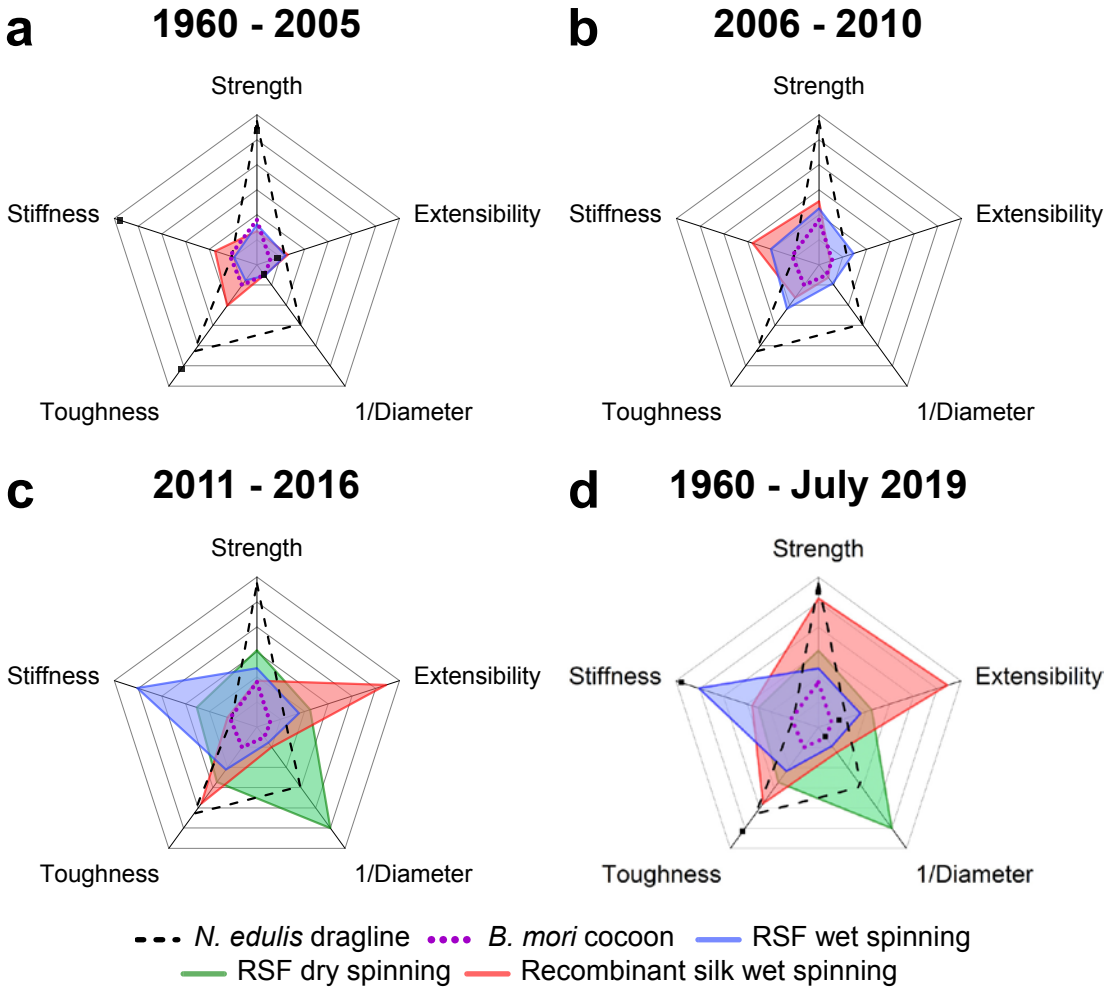

Figure 10: The performance space of artificial silk fibres for different time periods. The area of each pentagon represents a performance space and is defined by the collective (not individual) best fibre properties that were achieved during each time period. In other words, all RSF wet spun fibres reported in literature from 2011-2016 (see Table 2) lie within the blue pentagon area in image c). The single data points of *N. edulis*[16] dragline silk and *B. mori*[15] cocoon fibres represented by the dashed/dotted lines are included for reference. The fibre properties of Ha *et al.*[110] are shown as black squares as they were hand-drawn.

1.7 Why can artificial silk fibres not yet compete with natural silk?

Whilst the field has seen significant improvements in the production of artificial silks, it is arguable that the most significant challenges are still to come. In an effort to identify the general challenges faced, it is important to highlight that a fibre's mechanical properties are a product of both the feedstock *and* the means by which it is processed.

Feedstock:

I propose one of the key problems leading to difficulties in replicating the properties of the higher performing silk fibres is the use of spinning dopes that may be considered unnatural, i.e. their protein constituents differ in both structure and function compared to the native proteins. For example reconstituted and recombinant silk dopes have been shown to have either completely different mechanical/rheological properties, structure and/or a lower molecular weight compared to natural silk proteins.[66, 70, 76, 88-90, 93, 104, 111, 117, 126, 129, 161] Furthermore it is worth noting that reconstituted silk proteins typically originate from silkworms and hence are inherently different from spider silks and thus may not be able to be processed into a spider silk at all.[162] While spider silk inspired synthetic proteins with a molecular weight of 556 kDa were produced and spun into fibres with similar properties to dragline silk, the upscaling of such processes is the next challenge that has to be overcome alongside a more natural processing.[75]

Processing:

As shown in section 1.4 of this chapter, the current fibre forming processes for artificial silk fibre spinning are very different from the natural one. In nature, silk proteins are transformed into solid, insoluble fibres via a stress induced phase transition accompanied by an acidification and metal ion gradient along the spinning duct.[5, 47, 52] However, during wet spinning artificial fibre formation occurs via precipitation in a coagulant and without the

presence of an anisotropic stress (i.e. shear or post drawing under tension), which leads to a more isotropic molecular arrangement of the proteins. Even dry spun fibres formed by solvent evaporation require immersion and drawing in ethanol to get an acceptable mechanical performance. Yet there are currently several efforts to spin silk fibres in a more biomimetic fashion and move away from the more traditional means of spinning polymeric fibres.[99, 102, 163-167]

Fibre properties:

From my analysis, the ability to produce thinner fibres appears to be linked to increased fibre strength for wet spun RSF fibres. This hypothesis is supported by fracture mechanics calculations performed by Porter *et al.*[157], who proposed that natural silks are strong simply because they are thin. However, after plotting the data presented here for artificial silk fibres using the relationship for fracture strength provided by Porter *et al.*[157], it can be observed that despite being thin, dry spun fibres and most wet spun fibres do not follow the trend line for the generic energy release rate for polymers (Figure 11). The majority of the fibres follow a fit that has a lower slope, meaning artificial silk fibres exhibit either a lower strength, a higher stiffness or a smaller diameter compared to natural fibres. This suggests that apart from the external fibre structure (i.e. diameter and fibre surface), the internal structure (i.e. hierarchical structures, skin/core and micro/nanofibrils, alongside control of the ordered and disordered regions) plays a vital part in defining the mechanical performance of silk fibres and is an area for future research.

Therefore, if further developments are to be made, we now have to go back to the beginning of my discussion and understand *all* properties of the best performing individual fibres (Figure 9) by looking at the complete regime of a stress-strain graph. When comparing the best performing fibres for every spinning approach to natural *B. mori* and *N. edulis* silk, some interesting differences can be observed (Figure 9). For example, all artificial fibres

show very distinct yield points with clearly different pre- and post-yield moduli that appear to be absent in natural silk fibres. Natural silks show a homogeneous, rubber like deformation to rupture whereas the stress-strain behaviour of the artificial silk fibres suggests that a previously less ordered structure is converted into more ordered areas by cold-drawing.[168]

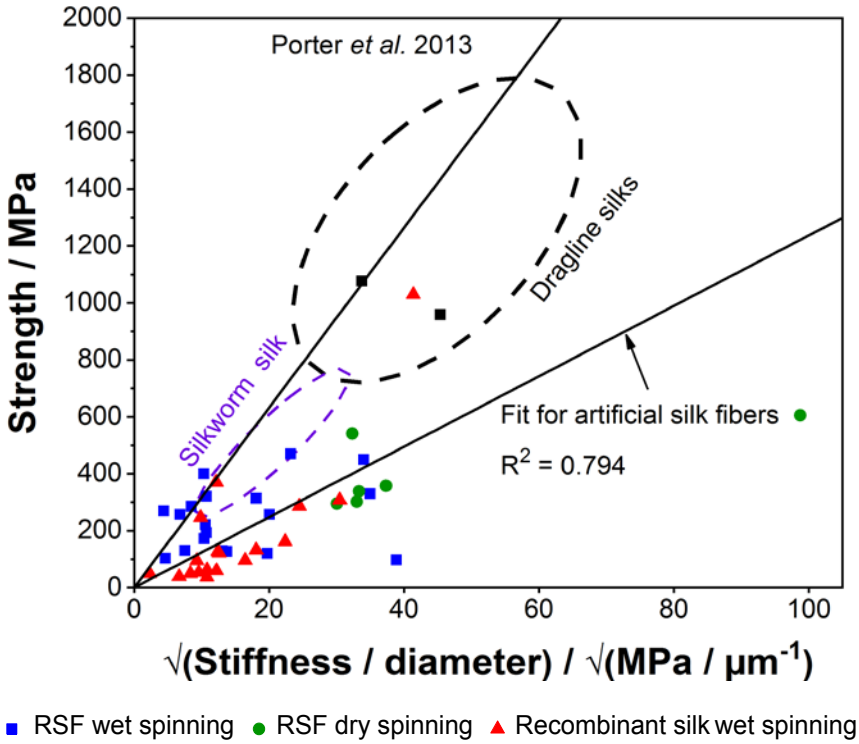

Figure 11: Fracture-strength relation for artificial silk fibres. This graph was originally developed by Porter *et al.*[157] for synthetic polymers. While natural silkworm and spider dragline silk follow the trendline for the generic energy release rate as synthetic polymers, most artificially spun silk fibres, tend to follow a different fit, indicating more disordered regions compared to natural silks. The black squares represent the values from Ha *et al.*[110].

Beyond the nanoscale, another factor that negatively influences the mechanical properties of artificially spun silks was previously discussed by Peng and co-workers.[144] They suggested impurities enclosed within the fibre inhibit fibril assembly and lead to a porous structure affecting the fibre performance. Such impurities are proposed to be either be very

short protein fragments from highly degraded proteins[91], remaining chaotropic salts[169] from insufficient dialysis or entrapped air-bubbles during processing.

In conclusion, it appears that the key to producing fibres with enhanced properties is to spin silk proteins as inherently thin fibres without impurities and at the same time develop molecular orientation *during* processing rather than by post-drawing as it is currently done.

1.8 Conclusions

This chapter give an introduction spider and silkworm silk and describes how silk fibres are spun in Nature. Subsequently, various artificial silk fibre spinning approaches are summarized and the improvements in processing conditions and mechanical properties over time are analysed. The decrease in fibre diameter being associated with an increase in post-draw ratio alongside the usage of suitable solvents successfully improved the mechanical performance of RSF wet spun fibres. For dry spinning, the use of a highly concentrated protein solution and a microfluidic device are beneficial for the final properties of the fibres. Fibres produced by recombinant wet spinning could mainly be improved by increasing the molecular weight of the protein sequences. The detailed analysis of the mechanical properties of artificial silk fibres reveals that fibres outperforming the natural *Bombyx mori* silk can be produced by all spinning methods. Nevertheless, these are non-biomimetic spinning approaches that cannot mimic spider dragline silk. The problems limiting a better fibre performance are the degraded and unnatural spinning dopes and the challenges in forming the fibre structure *during* spinning which leads to more disordered regions and a worse fibre performance. In the future, further improvements can be achieved if we get a deeper understanding of the mechanisms behind the natural fibre forming process and manage to transform this knowledge into new biomimetic spinning devices that can imitate the way how silkworms and spiders spin their outstanding fibres.

1.9 Thesis aim

The literature review above has outlined that natural silk spinning in silkworms and spiders yields fibres with a remarkable property-processing relationship. The silk fibres have a comparable mechanical performance to synthetic polymeric fibres yet have the advantage of being spun 1000 times more energy-efficient which makes natural silk spinning a paragon for environmentally friendly production of high-performance materials.[14] Understanding and replicating silk spinning can hopefully help us design new and greener materials with less environmental impact. However, copying this process via artificial routes has proven challenging to date, especially for spider silk. While the mechanical properties of silkworm silk can now constantly be exceeded by using reconstituted or recombinant silk feedstocks, the processing still uses harsh chemicals and intensive off-line post-treatments that negate the benefits of natural silk spinning. Current problems that prevent the move towards a more environmentally beneficial processing of artificial silks, are the quality of the feedstocks as well as the incomplete understanding of how the hierarchical structure in silk fibres forms during spinning. While it is understood that extensional flow, pH change and metal ions play a major role in silk spinning, the exact interplay of these mechanisms is not fully conceived yet. This knowledge, however, is essential when trying to spin artificial silk fibres with similar properties akin to their natural counterparts under environmentally-friendly processing conditions.

Therefore, to bridge this gap in our knowledge, the aim of this thesis is to investigate and understand how native silk proteins behave when subjected to extensional flow and changes in their pH and metal ion environment and under what conditions they can self-assemble into fibres with hierarchical structures that guarantee outstanding mechanical performance.

1.10 Chapter introduction

This thesis comprises seven chapters followed by the appendix. All chapters are in chronological order and a short introduction to each one is given below with a more detailed abstract at the beginning of each experimental results chapter.

Chapter 2: Experimental Techniques and Theory

In chapter 2 the preparation of native silk proteins as well as the theory behind the most important characterisation techniques is explained. In this thesis *Bombyx mori* silk proteins are being used as the silk proteins are accessible in a higher quantity compared to spider silk proteins whilst being processed in a similar way.[42] The description of the experimental techniques helps the reader to better understand and interpret the data in the following chapters.

Chapter 3: Preliminary Experiments and Results

Chapter 3 describes initial experiments that where conducted with the aim to understand how silk proteins assemble into their hierarchical structure. Although no quantifiable data was generated, these experiments provided me with useful insight that lays the foundation for the following chapters.

Chapter 4: Extensional Flow Behaviour and Spinnability of Native Silk

This chapter reports for the first time the behaviour of native silk proteins when subjected to extensional flow fields. By operating a conventional tensile tester as a filament stretching rheometer and determining the surface tension of native silk, the transient extensional viscosity could be determined. The results show that silk is intrinsically suited for fibre spinning as the proteins strain harden in uniaxial extension. Additionally, it was found that

fibre formation under extensional forces only occurs due to dehydration at low extension rates.

Chapter 5: Spinning Beta Silks Requires Both pH Activation and Extensional Stress

This work is based on the results and observations made in chapter 4. Both the influence of extensional flow and pH change on fibre formation and the mechanical properties are investigated. It is shown that extensional flow and pH change are required to spin silk fibres and that their properties depend on the rate of work input during fibre spinning.

Chapter 6: The influence of metal ions on native silk rheology

In chapter 6 the influence of metal ions on the flow properties of native silk is investigated. It was found, that the addition of metal ions changes the sensitivity of the silk feedstock for alignment and aggregation. By adding Ca^{2+} ions the silk proteins show a lower tendency towards alignment and aggregation and therefore provide ideal storage conditions in the silk gland.

Chapter 7: Summary and Future Outlook

Chapter 7 gives a short summary of the thesis and provides some ideas how the impact of this work can contribute towards the development of environmentally friendly bio-inspired materials.

CHAPTER 2:

Experimental Techniques and Theory

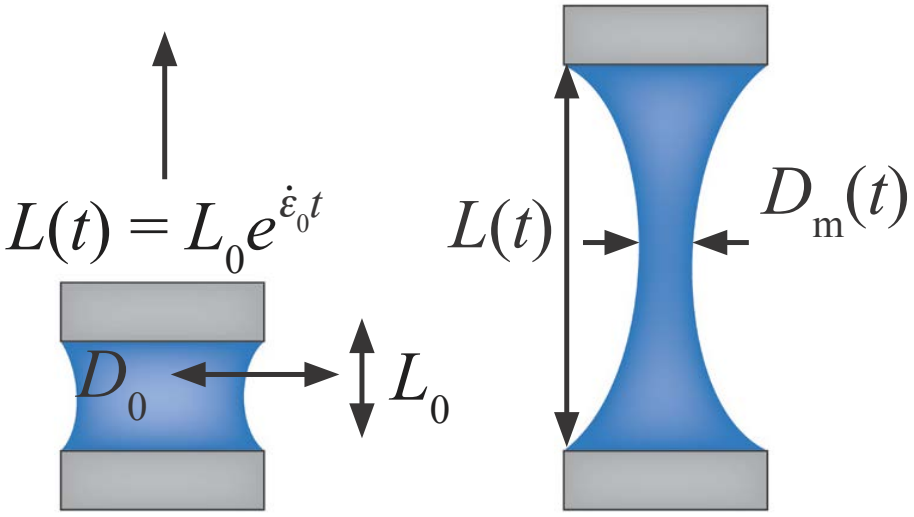

This chapter describes the theory and experimental techniques used in this thesis which helps the reader to better understand and interpret the results presented in the following chapters.

2.1 Native silk protein preparation

Bombyx mori silkworms in the 5th instar and about to spin a cocoon were stored in an incubator at 9 °C to slow down their metabolism and prevent them from spinning. Native silk proteins were obtained by dissecting the silkworms based on a protocol developed by Dr. Chris Holland.[170]

In summary, after taking the silkworms from the incubator they were left in a petri dish for around 10 minutes to acclimatise to the lab environment which was found to facilitate dissection. The head of the silkworm was then cut off with scissors and the glands were carefully removed by slightly pushing from the rear end of the worm. The glands were then transferred into a petri dish filled with deionised (Type II) water. After washing, the glands were carefully cut with tweezers at the end of the posterior gland and before the first S-shape. This section of both glands was then transferred to another petri dish to remove the epithelium layer with fine tweezers under a dissection microscope (SZ40, Olympus, Japan). All experiments were conducted using the native silk proteins extracted from the posterior part of the middle section of the silk gland which have a concentration of 24.0 $\pm$ 2.5 wt.%[64] and are predominantly free of sericin, ensuring that silk fibroin is the main component tested.[171-172]

2.2 Reconstituted silk preparation

The silk reconstitution process is based on a protocol published by Rockwood and co-workers.[80] In general, silk reconstitution consists of three major steps which are 1) degumming, which is the removal of the sericin coating of the fibres. 2) dissolution of the

fibres in LiBr. 3) dialysis to remove the metal ions and obtain a silk/water solution. The exact procedure is as follows:

Step 1: Degumming

Around 20 g of dry *B. mori* cocoons were cut into small pieces (< 5mm diameter) using scissors. The finely cut cocoons were then added into a food processor (Kenwood Mulit-Pro) with 500 ml of Type II water (deionised water with a resistivity higher than 1 MΩ.cm) to be washed for 15 minutes at maximum speed. Afterwards, the water was drained through a mesh in the blender cover, the fibres rinsed, and fresh water added to repeat this procedure for another two times. Then, 500 ml of a 0.047 M sodium carbonate solution were heated to 70 °C and added to the fibres. Then, the food processor was turned on to full speed for 20 minutes. Afterwards the sodium carbonate solution was drained and another 500 ml of 0.047 M sodium carbonate solution at 70 °C was added. This step was repeated for three times. After the final drain, the fibres were washed for 10 minutes in fresh Type II water. After washing the fibres were dried in a vacuum oven overnight at 50 °C.

Step 2: Dissolution in LiBr

The dried fibre “clumps” were blended in the spice grinder setup of the food processor for several seconds (longer times should be avoided due to heat degradation) until they became fluffy. The fibres were then transferred into a 500 ml glass beaker and dissolved in a 9 M LiBr solution (70 °C) for 60 minutes so that the ratio of silk fibres to LiBr solution was 1:15 w/v. The glass beaker was kept in a water bath which was set to 70 °C. Most of the fibres were dissolved after 60 minutes but some remaining bits of undissolved silk were filtered out after dialysis.

Step 3: Dialysis

The silk/LiBr solution was then added to a dialysis tube (Spectra/Por 4 Dialysis Membrane, molecular weight cut-off: 12-14 kDa) sealed with plastic clamps which was then submerged in Type I water (ultrapure water with a resistivity higher than 18 MΩ.cm) and kept in a refrigerator at 4 °C to avoid gelation. The water was changed four times every 2 hours and then kept overnight. The resistivity of the water was measured using a Mettler Toledo handheld conductivity meter after each change to ensure successful removal of LiBr. In a final step the silk water solution was filtered with Whatman filter paper No 1 with a pore size of 11 μm to get rid of undissolved silk.

2.3 Surface tension of native silk proteins

For an accurate calculation of the extensional viscosity of silk in chapter 4, it is required to determine the surface tension of silk fibroin.

Generally, the surface tension of a liquid (also called surface energy) describes the energy that is required to increase the surface area of the liquid by a unit of area. Surface tension results from an imbalance of intermolecular attractive forces, also called cohesive forces, between molecules on the surface of the liquid.[173] While molecules in the bulk experience cohesive forces in all directions, on a free surface the molecules experience inward cohesive forces as they are not entirely surrounded by molecules.[173] The energy to create a new surface has to be taken into account when silk proteins are stretched into filaments. The surface tension of liquid can be determined with various techniques such as the pendent drop method, Wilhelmy plate, Du Noüy ring, capillary rise or the maximum bubble pressure method.[174] However, all of these methods are only suitable for low viscosity liquids and therefore cannot be used for a very viscous solution such as native silk proteins. Therefore, I determined the surface tension of native silk proteins according to the captive bubble method based on a previous publication by Andrade and Nakamura.[175-176] This

method is specifically used for polymer gels of a high viscosity and therefore ideal for the calculation of the surface tension of silk fibroin. In brief, native silk proteins were very gently spread on the flat surface of an aluminium stub with the help of a glass slide. Special care was taken to apply as little shearing to the silk proteins as possible and to obtain an even surface. The aluminium stub was then submerged in Type II water and an air bubble was instantly placed on the silk surface with the help of a micro glass capillary (Figure 12). After taking images of the air bubble on the silk surface it was replaced by a droplet of rapeseed oil which was also photographed. Then, the silk proteins were removed from the aluminium stub and the water replaced. This procedure was then repeated 10 times to get enough statistical data for the calculation of the surface tension of silk proteins.

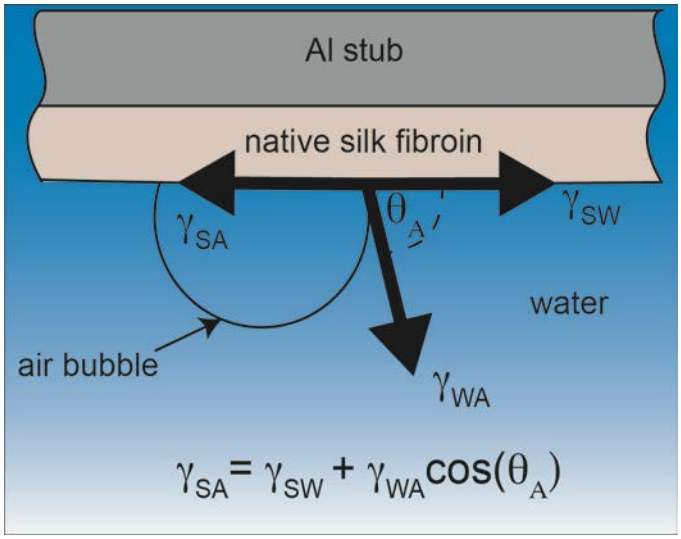

Figure 12: Surface tension measurement with the captive bubble method. An air bubble is placed on a silk surface which was carefully spread on an Al stub and submerged in water. The equilibrium state between the surface tension of water (γ_{WA}), silk (γ_{SA}) and their interfacial tension (γ_{SW}) allows the formulation of the Young's equation.

All three phases (silk, water and air) are in equilibrium and therefore the Young's equation for the surface tension of silk can be formulated as:

$$\gamma_{SA} = \gamma_{SW} + \gamma_{WA}\cos(\theta_A) \quad (1)$$

where γ_{SA}, γ_{SW} and γ_{WA} are the surface tension of silk, interfacial tension of silk with water and the surface tension of water, respectively. θ_A is the contact angles of the air bubble to the native silk protein layer. Accordingly, the interfacial tension between silk and water can be calculated from their polar and dispersive surface tension components by applying the harmonic mean approximation:

$$\gamma_{SW} = \gamma_{SA} + \gamma_{WA} - 4\left(\frac{\gamma_{SA}^{d}\gamma_{WA}^{d}}{\gamma_{SA}^{d} + \gamma_{WA}^{d}}\right) - 4\left(\frac{\gamma_{SA}^{p}\gamma_{WA}^{p}}{\gamma_{SA}^{p} + \gamma_{WA}^{p}}\right) \quad (2)$$

The superscripts *d* and *p* refer to the dispersive and polar surface tension components.

By replacing the air bubble with an oil droplet which is not soluble in water and silk, two further equations characterising the silk-oil interfacial properties can be formulated:

$$\gamma_{SO} = \gamma_{SW} + \gamma_{WO}\cos(\theta_O) \quad (3)$$

$$\gamma_{SO} = \gamma_{SA} + \gamma_{OA} - 4\left(\frac{\gamma_{SA}^{d}\gamma_{OA}^{d}}{\gamma_{SA}^{d} + \gamma_{OA}^{d}}\right) - 4\left(\frac{\gamma_{SA}^{p}\gamma_{OA}^{p}}{\gamma_{SA}^{p} + \gamma_{OA}^{p}}\right) \quad (4)$$

where γ_{SO}, γ_{SA} and γ_{OA} are the interfacial tension of silk with oil, surface tension of silk and oil, respectively. Again, the superscripts *d* and *p* refer to the dispersive and polar surface tension components.

Combining equations (1) to (4) yields two equations (5) and (6) that allow the calculation of the surface tension components of silk (γ_{SA}^{d} and γ_{SA}^{p}) and hence the total surface tension of silk ($\gamma_{SA} = \gamma_{SA}^{d} + \gamma_{SA}^{p}$). Equation 6 has been simplified as the polar component of oil is negligible so that $\gamma_{OA}^{p} = 0$.

$$\gamma_{SA}^{d}\left(\frac{\gamma_{WA}^{d}}{\gamma_{SA}^{d} + \gamma_{WA}^{d}}\right) - \left(\frac{\gamma_{OA}^{d}}{\gamma_{SA}^{d} + \gamma_{OA}^{d}}\right) + \gamma_{SA}^{p}\left(\frac{\gamma_{WA}^{p}}{\gamma_{SA}^{p} + \gamma_{WA}^{p}}\right) - \left(\frac{\gamma_{OA}^{p}}{\gamma_{SA}^{p} + \gamma_{OA}^{p}}\right) = \frac{\gamma_{OW}\cos(\theta_O) + \gamma_{WA} - \gamma_{OA}}{4} \quad (5)$$

$$\gamma_{\mathrm{SA}}^{d}\frac{\gamma_{\mathrm{WA}}^{d}}{\gamma_{\mathrm{SA}}^{d}+\gamma_{\mathrm{WA}}^{d}}+\gamma_{\mathrm{SA}}^{p}\frac{\gamma_{\mathrm{WA}}^{p}}{\gamma_{\mathrm{SA}}^{p}+\gamma_{\mathrm{WA}}^{p}}=\frac{\gamma_{\mathrm{WA}}[1\text{-}\cos(\theta_{\mathrm{A}})]}{4} \quad (6)$$

The contact angles of the oil droplet θ_{O} and air bubble θ_{A} to the silk surface were determined with an ImageJ plugin by analysing their geometric shape.[177] The surface tension of water ($\gamma_{\mathrm{WA}} = 72.8$ mN/m) and its polar and dispersive components ($\gamma_{\mathrm{WA}}^{d} = 21.8$ mN/m, $\gamma_{\mathrm{WA}}^{p} = 51$ mN/m) were taken from the literature[178] and the surface tension of oil as well as the interfacial tension of the water-oil system were determined via the pendent drop method which is reported in chapter 4.

2.4 Shear rheology

The term rheology describes the study of deformation and flow of matter. In many applications/processes fluids are exposed to shear stresses and a thorough understanding of the material's flow behaviour under such conditions is necessary, especially for complex fluids such as polymer solutions. A shear flow field is created by placing a liquid between two horizontal plates and moving one plate relative to the other. This causes adjacent liquid layers to move parallel to each other with different speeds.

The response of a fluid to shear forces can be tested with capillary rheometers which are able to generate very high shear rates (up to 10^6 s^{-1})[8] that are encountered in extrusion and injection moulding of polymer melts. Alternatively, rotational rheometers can be used which can measure shear rates up to only 10^4 s^{-1} but are more versatile as they also allow dynamic oscillatory testing. In both types of rheometers, the rheological properties are derived by measuring the relationship between imposed strain/stress and resulting stress/strain. The response of the tested material can either be 1) completely elastic where strain is proportional to stress (Hookean solid) 2) completely viscous where strain rate is proportional to stress (Newtonian liquid) or 3) viscoelastic, which describes a fluid response that lies between the two ideal cases described above.

For rotational rheometers, which are used in this thesis, the measuring setup for medium to high viscosity liquids are the cone/plate and plate/plate geometries (Figure 13). In both cases the lower plate is stationary with a rotatable upper geometry. Following is a description of the two most common tests for characterising the shear flow properties of a material, constant shear and dynamic oscillation.

2.4.1 Constant shear tests

In constant shear tests the sample is sandwiched between the two plates (cone/plate or plate/plate) and usually the upper plate is rotated at a given angular velocity Ω while the torque T is measured. From both variables the stress τ and shear rate $\dot{\gamma}$ can be calculated with the exact dimensions of the geometry as shown in Figure 13. Dividing the stress by the shear rate gives the viscosity η which is a measure of resistance to flow of a material.

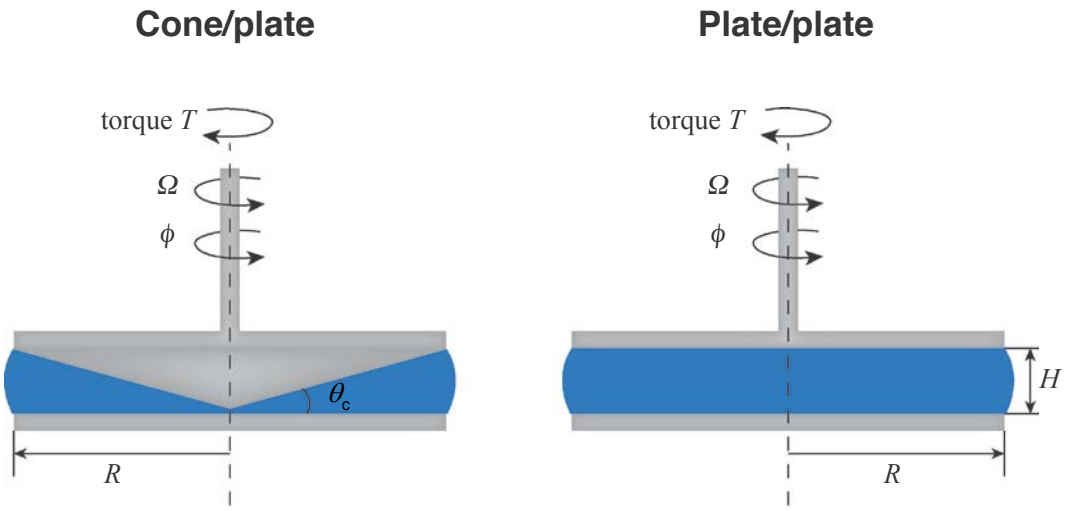

$\gamma = \frac{\phi}{\theta_c}$	**shear strain**	$\gamma(r) = \frac{r \cdot \phi}{H},\ \gamma_R = \frac{R \cdot \phi}{H}$
$\dot{\gamma} = \frac{\Omega}{\theta_c}$	**shear rate**	$\dot{\gamma}(r) = \frac{r \cdot \Omega}{H},\ \dot{\gamma}_R = \frac{R \cdot \Omega}{H}$
$\tau = \frac{3T}{2\pi R^3}$	**shear stress**	$\tau(\dot{\gamma}_R) = \frac{T}{\pi R^3}\left[3 + \frac{\partial \log T}{\partial \log \dot{\gamma}_R}\right]$
$\eta = \frac{\tau}{\dot{\gamma}} = \frac{3T}{2\pi R^3} \cdot \frac{\theta_c}{\Omega}$	**shear viscosity**	$\eta(\dot{\gamma}_R) = \frac{T}{2\pi R^3 \dot{\gamma}_R}\left[3 + \frac{\partial \log T}{\partial \log \dot{\gamma}_R}\right]$

with:

γ ... shear strain	r ... radius	Ω ... angular velocity
$\dot{\gamma}$ ... shear rate	R ... rim radius	ϕ ... angular defelction
τ ... shear stress	H ... plate separation	$\dot{\gamma}_R$ ... shear rate at rim
η ... shear viscosity	θ_c ... cone angle	T ... motor torque

Figure 13: The most common measuring geometries for rotational rheometers. The respective formula to calculate the shear viscosity of medium to high viscosity liquids are shown for each measuring geometry.

Measuring the viscosity for a series of shear rates yields a viscosity curve which provides useful information about how a material responds when exposed to a range of different processing conditions. Materials with a viscosity independent of shear rate are called Newtonian fluids and typical examples are water or oil. Polymer melts or solutions are shear thinning materials as the viscosity starts to decrease at higher shear rates due to the alignment of the long macromolecular chains which can then easily slide past each other decreasing the resistance to flow. In contrast, dilatant or shear thickening materials show an increasing viscosity with higher shear rates which can be observed in colloidal suspensions (Figure 14).

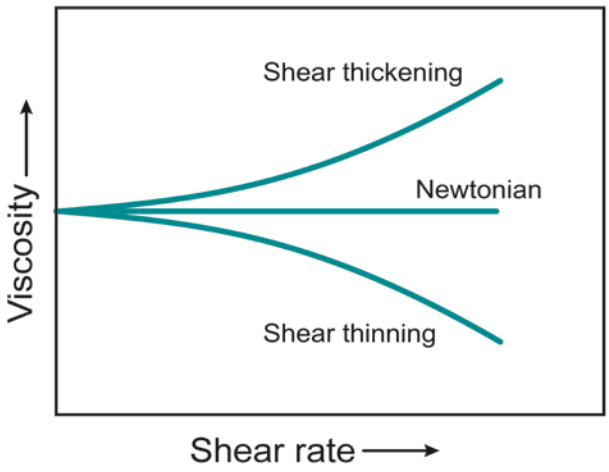

Figure 14: Viscosity curves of different material behaviours at constant shear. Newtonian (e.g. water and oil), shear thinning (e.g. polymer melts and solutions) and shear thickening fluids (e.g. colloidal suspensions).

2.4.2 Oscillatory tests

In oscillatory or dynamic shear tests a sample is excited with a sinusoidal strain $\gamma(t) = \gamma_0 \sin \omega t$ within the linear viscoelastic region of the material while the stress $\tau(t) = \tau_0 \sin(\omega t - \delta)$ is being measured (Figure 15). Dynamic tests can be performed at different frequencies and temperatures and provide useful information about the mechanical properties of a material at these conditions. Depending on the phase angle δ or lag between the imposed sinusoidal strain and measured stress, the storage and loss moduli G' and

G'' can be determined. The storage modulus G', a measure of the stored energy during the deformation, and the loss modulus G'', characteristic for the lost dissipated energy, provide useful information about the viscoelastic properties of the tested material. For a completely elastic (Hookean) solid the strain and stress are in phase ($\delta = 0$) and the loss modulus G'' equals to zero as all the energy during the deformation is recovered. In contrast, the phase angle δ is $\pi/2$ when the material behaves like a viscous (Newtonian) liquid with the storage modulus being 0. Most materials, however, show a combination of both elastic and viscous behaviour ($0 < \delta < \pi/2$) which strongly depends on the testing frequency and temperature and can be characterised by oscillatory tests.

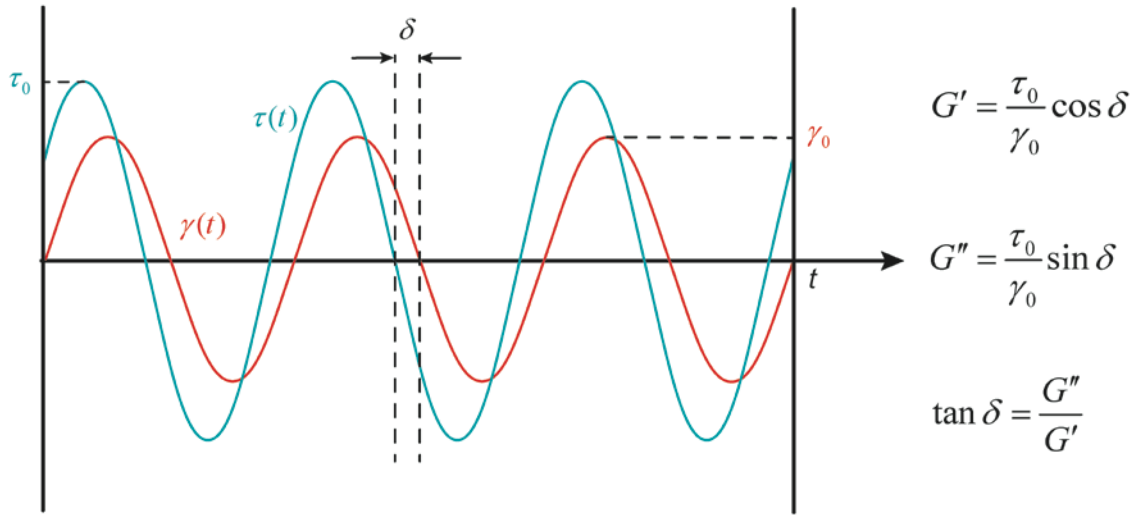

Figure 15: Oscillatory test signals. A sinusoidal strain (blue) is applied during the test and the respective stress (red) is measured.

2.5 Extensional rheology

Extensional flow which mainly occurs in processes such as fibre spinning, melt blowing, calendaring and thermo-forming is inherently different to shear flow fields and invokes a material response that cannot be described by common shear rheology experiments.[179] In an extensional flow field, a material is subjected to a homogeneous extension which is spatially uniform with a constant extension rate. Pure extensional flow fields are shear free. Despite the need to better understand the extensional behaviour of fluids to improve and optimise production processes, little experimental work has been done in the field of extensional rheometry until the 1970s due to the difficulties in creating a homogeneous extensional flow field.[180-181] The improvement of force transducers and new motion control technology at this time ultimately started the development of first techniques that allowed the extensional characterisation of high viscosity polymer melts.[182]

Instrumentation for medium to low viscosity fluids progressed more slowly and the challenges associated in creating instruments to measure extensional flow properties became evident in the M1 study in 1990 where various methods for measuring the extensional properties of a standardised test fluid were compared (including a spinline rheometer[183], opposing jets[184-185] and a converging flow rheometer[186] as shown in Figure 16).[187] The different setups revealed huge differences in measuring extensional properties of the M1 fluid as they suffered from drawbacks such as unknown pre-shear history, inability to measure steady state conditions and non-ideal extensional flow fields.[187-188] With native silk in mind, a high viscosity and shear-sensitive fluid which is available in only small amounts, the most promising method for testing this type of material was developed by Matta and Tytus who used a falling cylinder device which achieved the best approximation to ideal extensional deformation.[187, 189] This setup was later developed into the widely used filament stretching device by Sridhar and Tirtaatmadja which allows a nearly ideal uniaxial

extension.[190-191] Another widely used method akin to this is the capillary break-up extensional rheometer (CaBER) which is based on works by Entov and co-workers.[192-193] Both filament stretching and CaBER methods are now well established and have been applied primarily to characterise dilute and semi-dilute polymer[180, 194-209] as well as worm-like micelle solutions[206, 210-212] and other biopolymers such as cellulose which are relevant for fibre spinning.[213-215] However, whilst the CaBER setup lends itself very well to more dilute polymer solutions and Newtonian fluids,[203, 216] filament stretching offers the potential to obtain extensional properties of higher viscosity fluids such as polymer melts[217], making it more suitable for testing native silks.

Extensional rheometers	Shear viscosity range	Limitations
Converging flow 	>1 Pa.s	non-uniform strain rates, pre-shear history
Opposing jets 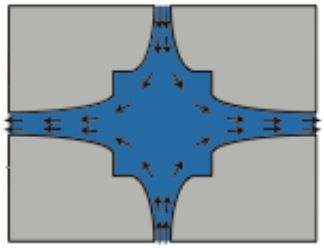	0.01-1 Pa.s	Variable strain rates and strain histories, shear components present
Filament stretching 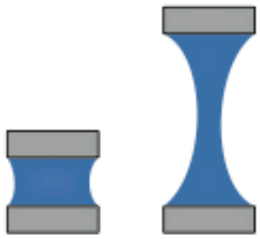	1-1000 Pa.s	Sample gripping might be problematic, high viscosity samples, elastic instabilities
Capillary break-up 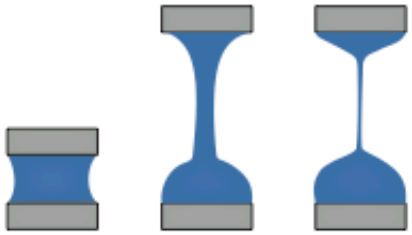	0.01-1 Pa.s	Intertial and surface tension dominate at very low viscosities
Spinline rheometer 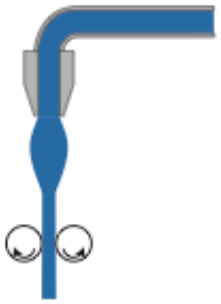	>1 Pa.s	non-uniform strain rates, pre-shear history

Figure 16: Extensional rheometers for characterising low to high viscosity fluids. The overview is based on a schematic published by Tropea and co-workers.[181]

2.5.1 Filament stretching rheometer

In the filament stretching experiment (see schematic in Figure 17) a fluid which is sandwiched between two plates has to be stretched in such a manner that it is exposed to uniaxial extension which is described by the following velocity field:

$$v_x = \dot{\varepsilon}_0 \cdot x \tag{7}$$

$$v_y = \frac{-\dot{\varepsilon}_0 \cdot y}{2} \tag{8}$$

$$v_z = \frac{-\dot{\varepsilon}_0 \cdot z}{2} \tag{9}$$

where v_x v_y and v_z are the velocities in the respective directions and $\dot{\varepsilon}_0$ is the constant extension rate. Therefore, for ideal uniaxial extension in x-direction the plates have to be separated exponentially from their initial gap L_0 according to the following equation:

$$L(t) = L_0 e^{\dot{\varepsilon}_0 t} \tag{10}$$

Theoretically, during stretching, the diameter in y-direction will then ideally decrease in the following way:

$$D(t) = D_0 e^{-\frac{1}{2}\dot{\varepsilon}_0 t} \tag{11}$$

However, due to the fluid sticking to the plates (non-slip boundary condition) additional shear forces arise near the endplates which result in a deviating diameter profile along the filament.[180, 218]

These inhomogeneities in the extensional flow field can be corrected by calculating the effective extension rate $\dot{\varepsilon}_{\text{eff}}$ (equation 12) based on the filament mid-diameter $D_{\text{m},0}$ as there is almost ideal shear free extension near the midplane.

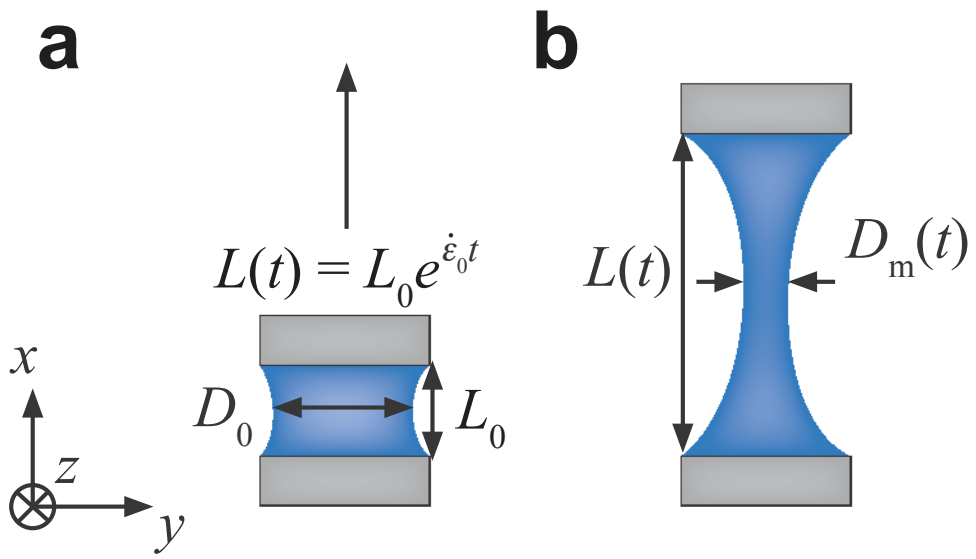

Figure 17: Setup of a filament stretching experiment. **a** A fluid is sandwiched between two parallel plates and the upper plate is lifted according to an exponential profile to realise a constant extension rate $\dot{\varepsilon}_0$. **b** The mid-diameter for each plate separation is recorded which can be used to calculate the transient extensional viscosity.

$$\dot{\varepsilon}_{\text{eff}} = \frac{-2}{D_{\text{m},0}} \frac{\mathrm{d}D_{\text{m}}(t)}{\mathrm{d}t} \tag{12}$$

With the help of a force balance derived by Szabo, the tensile stress difference of the filament can be determined.[219] In case of silk, gravitational and inertial effects can be negated due to the high viscosity of the native proteins, the low amount of sample used and the short stretching length at low extension rates.[191] This simplification does not hold for low viscosity fluids stretched at high extension rates which is not the case in my experiments. The tensile stress difference in the filament can therefore be simplified and calculated in the following way:

$$\langle \tau_{zz}\text{-}\tau_{rr} \rangle = \frac{F(t)}{\left(\pi D_m^2(t)/4\right)} - \frac{\sigma}{(D_m(t)/2)} \tag{13}$$

where $F(t)$ is the force required for stretching the filament, $D_m(t)$ is the mid-diameter of the filament and σ is the surface tension of the fluid. Dividing the tensile stress difference by the effective extension rate yields the transient extensional viscosity η_E^+:

$$\eta_E^+ = \frac{\langle \tau_{zz}\text{-}\tau_{rr} \rangle}{\dot{\varepsilon}_{eff}} \tag{14}$$

where $\langle \tau_{zz}\text{-}\tau_{rr} \rangle$ is the tensile stress difference acting on the filament and $\dot{\varepsilon}_{eff}$ the effective extension rate. Another important parameter for characterising the extensional properties is the effective Hencky strain ε_{eff} which can then be calculated with the help of the mid-diameter $D_m(t)$:

$$\varepsilon_{eff} = -2\ln\left(\frac{D_m(t)}{D_{m,0}}\right) \tag{15}$$

The Hencky or logarithmic strain is a dimensionless number describing the total strain the fluid undergoes during stretching. It offers the additional advantage that the extensional behaviour of the tested sample can be compared for different extension rates as the time factor can be eliminated.

2.6 Infrared spectroscopy

2.6.1 Theory and instrumentation

Infrared (IR) spectroscopy is a non-destructive analytical technique studying the interaction of matter with infrared light. The absorption of infrared radiation excites vibrational modes in molecules which provide information about the chemical structure and composition of the tested material.[220]

Nowadays, experiments are most commonly performed with Fourier transform infrared spectrometers (FTIR) which work as described in the following: Inside the spectrometer, polychromatic infrared radiation in the range from 14000-400 cm^{-1} wavenumbers (equivalent wavelength: 0.7-25 μm) is emitted from an electrically heated source (Figure 18). The infrared beam is then guided into a Michelson interferometer, where it is split into two beams which are reflected on a stationary or on a moveable mirror to create a defined optical path difference Δ. Both beams then recombine to form either constructive or destructive interference depending on the path difference Δ. After passing through the sample, the light reaches the detector and the instrument evaluates the light intensity relative to the initial optical path difference Δ which is plotted as an interferogram. A computer then applies a Fourier transformation to the interferogram to obtain the absorbance-wavelength spectrum.

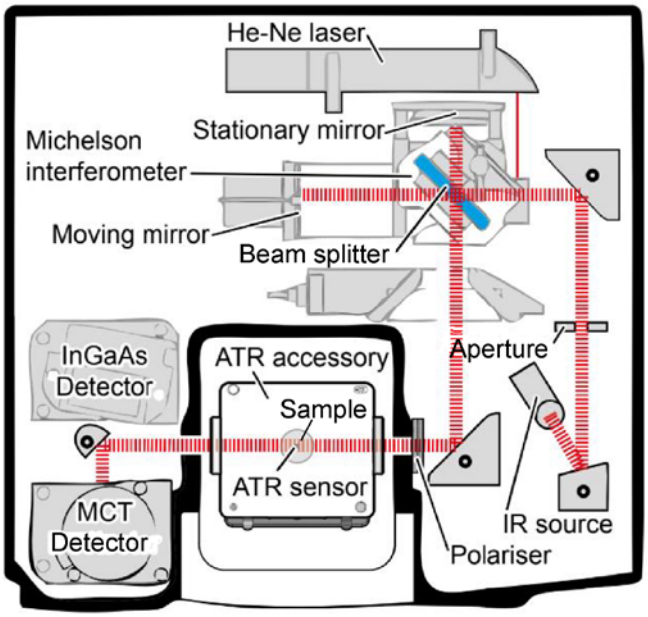

Figure 18: Schematic of the beam path of a Fourier Infrared spectrometer. The model is a Thermo Nicolet 6700 with ATR accessory attached.[221]

A common sampling technique is the attenuated total reflectance (ATR) setup which can be used for characterising samples in various kinds of shapes such as films, fibres as well as liquids and gels. The sample is placed on an ATR sensor, a crystal with a high refractive index and excellent properties for transmitting infrared radiation. The infrared light emerging from the Michelson interferometer is then coupled into the crystal at an angle of incidence so that total reflection occurs at the interface between the crystal and the sample. The total internal reflection results in an evanescent wave which is absorbed by the sample. The reflected light beam which is evaluated by the detector therefore carries the information about the absorbance spectrum of the sample. The sampling depth of ATR is approximately 2-15 μm and depends on the ratio of the refractive indices of the sample and the crystal as well as on the wavelength of the light (the sampling depth increases with decreasing wavenumber).[222]

2.6.2 Structural characterisation of silk

In the literature FTIR is one of the main methods to characterise the composition and secondary structure of proteins and therefore silk.[158, 223-224] The most common secondary structures in proteins are α-helices as well as β-sheets which can be found in a parallel or antiparallel configuration.[225] Another form of secondary structure is β-turns which reverse the direction of the protein chain and thus enable compact folding of the protein.[225] These three types of secondary structures consist of a large network of hydrogen bonds and contribute to the overall stabilisation of the protein. In contrast, areas with little or no specific structural features are referred to as random coil or amorphous configuration.

FTIR is a powerful tool to obtain structural information about proteins in general and especially silk as it can directly measure the strength of hydrogen bonds.[226] Generally, hydrogen bonding lowers the restoring force of stretching vibrations which leads to a peak shift towards lower frequencies. The exact opposite happens for bending vibrations where the restoring force is increased resulting in a higher vibration frequency.[227]

In case of silk, the position of the amide I peak (~1650 cm^{-1} for unspun silk proteins) depends on the secondary structure of the protein backbone and is therefore commonly used for secondary structure analysis.[158, 228-229] The amide I peak arises mainly due to C=O stretching vibrations with minor contributions from out-of-phase CN stretching and NH in-plane bending.[220] A high amount of hydrogen bonding (α-helices and β-sheet structures) which is synonymous for structural order in silk will therefore result in a right shift of the amide I peak as can be seen for spun silk where the position is shifted towards 1620 cm^{-1}. Hence, a right shift of the amide I peak position indicates a more ordered structure while a left-shift is characteristic for less ordered samples.[220] Consequently, by analysing the amide I peak location for different silk samples a direct comparison of the amount of hydrogen bonding structure can be deduced. A high amount of hydrogen bonding means a high molecular order in silk is present which is due to the high amounts of α-helices and β-sheet

structures. In contrast, molecular disorder refers to the random coil configurations within silk which do not show hydrogen bonding.

By using polarized FTIR, additional information about the molecular alignment in silk fibres, which are highly anisotropic, can be obtained.[23, 30-32] Commonly used polarizers that are made from an IR-transparent substrate such as BaF_2, CaF_2 or ZnSe, have metal deposited on linearly space grooves to form a wire grid. Only the infrared radiation perpendicular to the wire grids gets transmitted and the other radiation is absorbed or reflected. With the help of the polarizer, the electric field of the infrared beam is polarized perpendicularly to the plane of incidence (*s*-polarized) (see Figure 19). Two different spectra are then recorded ($A_\perp$ and $A_\parallel$) where the silk fibre is placed on the ATR crystal so that it is oriented parallel ($A_\parallel$) and perpendicular ($A_\perp$) to the s-polarized infrared light. The bond orientation within the fibre can be analysed by the comparison of the amide I peak in the $A_\parallel$ and $A_\perp$ spectra. If the molecular bonds in the fibre are highly aligned along the axis, the Amide I peak at 1620 cm^{-1} in the $A_\perp$ spectra is shifted towards 1649 cm^{-1} in the $A_\parallel$ spectra and appears with a much lower intensity.[230-231] However, if the molecular bonds in the fibre are not aligned at all, the peak at 1620 cm^{-1} in the $A_\perp$ has the same location and similar intensity in the $A_\parallel$ spectra. Consequently, the ratio of both amide I peak intensities ($A_\perp/A_\parallel$) gives a qualitative measure to compare the molecular alignment of artificial and native silk fibres (see Figure 20). Another indication of oriented β-sheet structure is the 1698 cm^{-1} peak in the $A_\parallel$ spectra.[231]

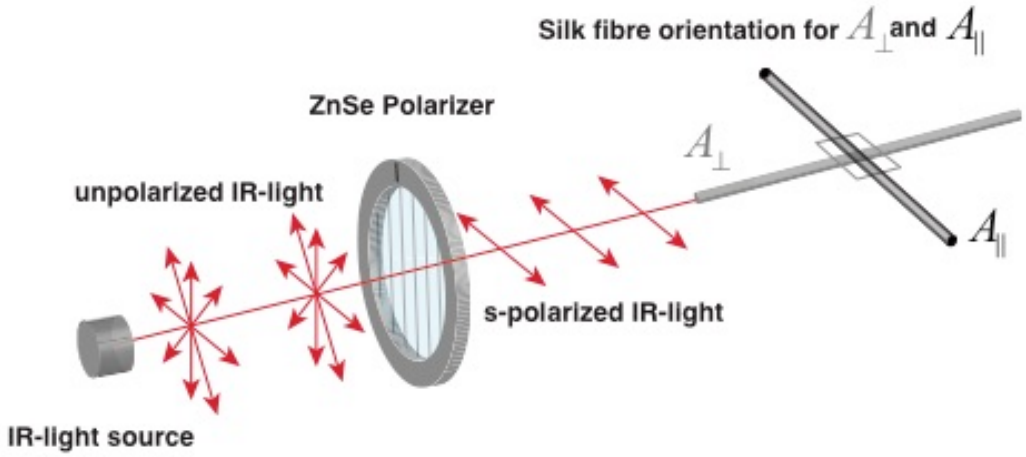

Figure 19: The principle of polarized FTIR. S-polarized light is created by a ZnSe polarizer which then interacts with the silk fibre. Depending on how the silk fibre is oriented to the s-polarised light, either a parallel ($A_\parallel$) or perpendicular ($A_\perp$) spectra is obtained.

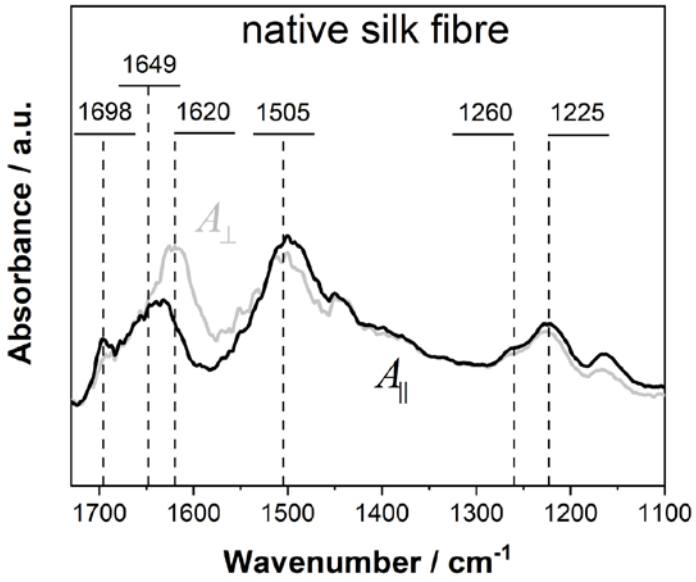

Position in cm^{-1}	Assignment	Preferential orientation
1698	Amide I, β-sheets	∥
1649	Amide I, unordered	
1620	Amide I, β-sheets	⊥

Figure 20: Parallel and perpendicular spectra for a native silk fibre. The ratio of the amide I peak intensities ($A_\perp/A_\parallel$) provides information about the molecular alignment while the location of the amide I peak in the perpendicular spectrum determines the order/disorder in the fibre. Additionally, the assignment and orientation dependence of the Amide I bonds is given.[231]

2.7 Optical Birefringence

The molecular structure of silk fibres on a macroscale can be qualitatively characterised by birefringence measurements using an optical microscope with polarized light. With this method it is possible to see whether the silk fibres exhibit structural features (β-sheet structures) and molecular alignment. Birefringence, an optical phenomenon, means the double refraction of light in an anisotropic material which is caused by differences in the orientation of the refractive indices within the material.[232] For birefringence measurements, a silk fibre is oriented at a 45° angle between crossed polarizers in an optical microscope. The light that enters the polarizer is linearly polarized and gets refracted by the silk fibre which splits the incoming light into separate components. The next polarizer, also called analyser, blocks all light waves perpendicular to the wire grid and therefore allows analysis of the retardation between the light waves.

Generally, there are two different forms of birefringence which can be either caused by structural features (structural birefringence) or external forces that lead to alignment or deformation of a material that is not naturally birefringent (stress and strain birefringence).[232] In silk fibres, birefringence is caused by the difference in refractive indices between the crystalline β-sheet and the amorphous regions as well as by the highly aligned molecular chain within the fibre. Additionally, flow birefringence can be observed for the liquid silk feedstock when the proteins are subjected to shear and extensional flow. These flow fields cause molecular alignment which can also result in flow-induced crystallisation when aligned molecular chains come in close proximity, interact with each other and eventually form crystalline structures.

2.8 Dynamic light scattering (DLS)

Dynamic light scattering (DLS) is a technique for measuring the size, number and distribution of sub-micron molecules/particles dispersed in a liquid based on their molecular diffusion rate. Due to collisions with solvent molecules, the molecules/particles undergo constant random movements (Brownian motion) which can be analysed by shining a monochromatic laser on the sample in a cuvette (Figure 21a).

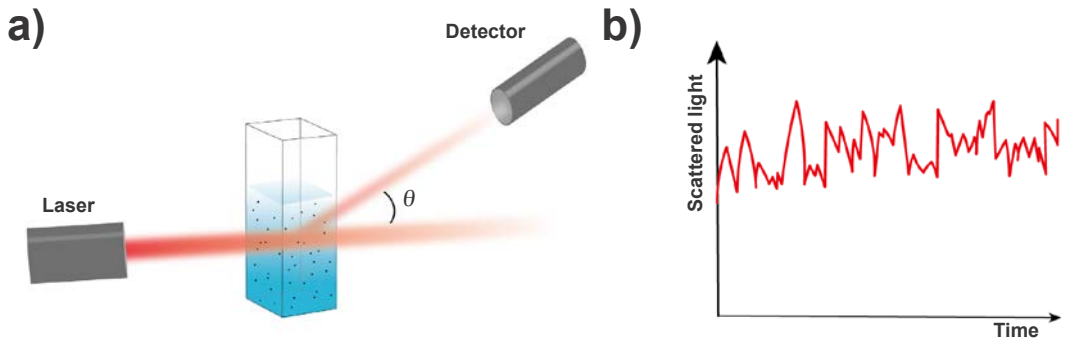

Figure 21: The principle of dynamic light scattering. **a** Schematic of the DLS setup. **b** The scattered light intensity is recorded over time a fixed angle θ.

The moving particles scatter the light which is detected over time at a fixed angle θ (Figure 21b). Intensity fluctuations in the signal caused by the different sizes and shapes of the particles are analysed to derive a correlation function which is a mathematical description of the intensity fluctuations and allows the determination of the translational diffusion coefficient of the particles. Larger molecules move slower than smaller ones and therefore show slower fluctuations and a less rapid decay of the correlation function (Figure 22).[233]

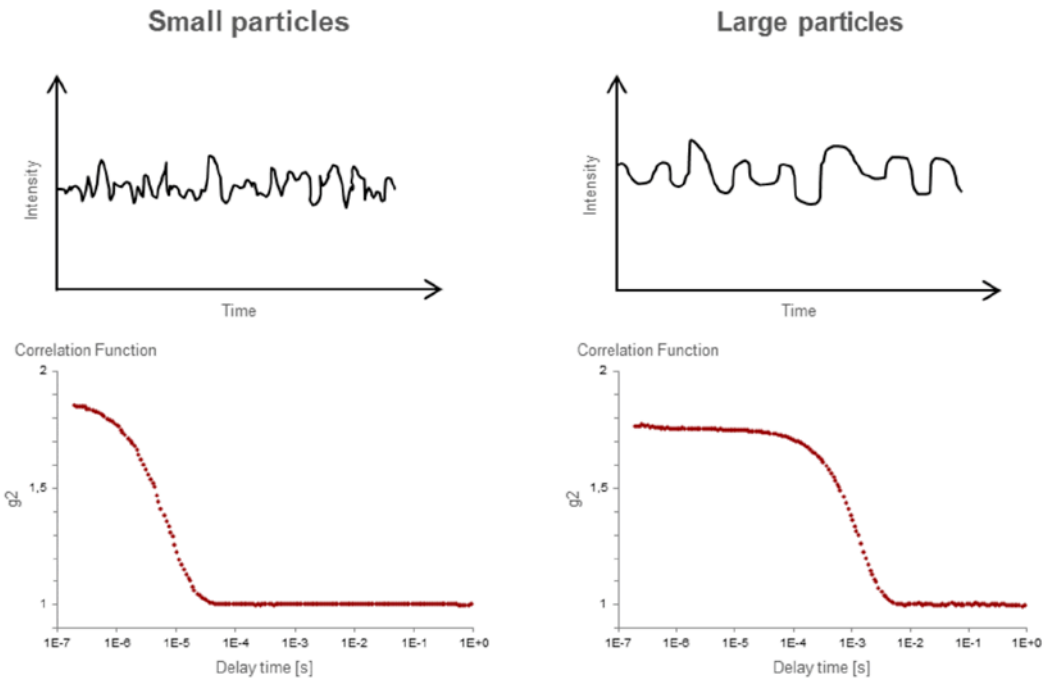

Figure 22: Light intensity fluctuations for small and large particles. Small particles show a much faster decrease in the correlation function compared to larger particles. Image taken from Anton Paar website.[234]

With the help of the diffusion coefficient D the particle size (hydrodynamic radius R_{H}) can be calculated via the Stokes-Einstein equation.[235]

$$D = \frac{k_{\mathrm{B}} T}{6\pi\eta R_{\mathrm{H}}} \tag{16}$$

where k_{B} is the Boltzmann constant, T the temperature, η the viscosity of the liquid and R_{H} the hydrodynamic radius which is the radius of a sphere that has the same translational diffusion coefficient as the particle.

From the correlation function different size information can be determined. By fitting a single exponential to the correlation function, the mean particle size (z-average) and an estimate of the polydispersity can be determined. When fitting multiple exponential functions, the intensity distribution of particles sizes can be calculated from which the number and volume distribution can be derived (Figure 23). The intensity distribution emphasises larger

particles as they scatter more light than smaller ones while the number and volume distribution represent small particle fractions more strongly.

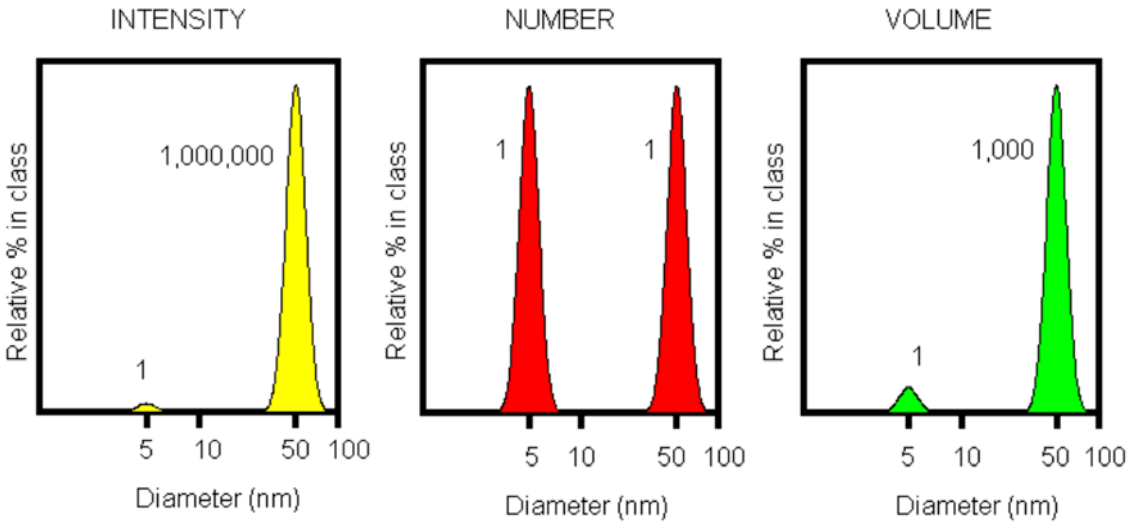

Figure 23: Intensity, number and volume distribution for DLS experiments. The intensity distribution can be determined by fitting multiple exponential functions to the correlation function. The number and volume distributions can be calculated from the intensity distribution. This image was taken from a technical note by Malvern Instruments.[236]

CHAPTER 3:

Preliminary Experiments and Results

This chapter describes initial experiments that were carried out with the aim to get a better understanding how silk proteins can assemble into strong and tough fibres under natural conditions. As outlined in the literature review, such knowledge is not only necessary for improving the production of artificial silk fibres but can also inspire the development of a new class of materials that can be processed under very benign conditions in a similar way to silk.

The results and observations described in this chapter provided me with helpful insights into silk processing and this is why I find it important to mention. This knowledge laid the foundation for the following main part of this thesis that significantly contributes to a better understanding of how silk is spun.

One overlooked aspect of silk spinning to date is extensional flow which has only been partially addressed for silk although it is critical for structural development in the final fibre. Therefore, the plan was to replicate silk spinning with a flow visualisation device that has a similar geometry to the natural silkworm duct. Such a device can help to shed new light on how and under what conditions silk proteins assemble into hierarchical structures within the duct.

In the literature, most devices for silk spinning are based on syringe needles or other simplified spinnerets for protein extrusion that are unable to mimic the silk duct geometry and do not allow flow visualisation.[94-98, 100, 125, 127-131] Additionally, they lack a tapering part which induces elongational flow, the most important flow field for molecular alignment.[5] Recently, microfluidic devices have gained a lot of popularity in silk spinning as they can be manufactured in various geometries and only require small amounts of feedstock.[99, 102, 163-166] However, the devices that were used to date still do not manage to mimic the flow conditions in the silkworm duct as they lack either a tapering geometry or a circular cross section.

Martel et al. [164-165] for example introduced a tube-in-square-pipe microfluidic cell made from borosilicate glass to study the fibre formation of regenerated silk. With their cell they could realise a concentric flow profile of silk proteins and buffer solution but only in a non-tapering geometry. Kinahan[163] also presented a rectangular device and introduced an elongational flow field by two polyethylene oxide (PEO) cross flow channels. Other devices with a tapering geometry were implemented by Rammensee[166] and Yaopeng Zhang's group[99, 102]. While Rammensee does not specify the geometry, the devices manufactured by Zhang's group only have a rectangular cross section.

Therefore, in order to be able to mimic the silkworm gland geometry and allow flow visualisation I consider pulled glass capillaries to be a promising option as they can be easily and repeatedly tapered to a required geometry.[237] Moreover, glass is transparent for visual and microscopic inspection and the inside surface can be treated with chemicals to achieve different surface properties such as hydrophobicity.

3.1 Developing a flow visualisation device for silk proteins

A Narishige PB-7 glass capillary puller (Figure 24) was used to produce glass capillaries with differently tapered geometries by varying the heater settings. For different heater settings (6, 7, 8 and 10) at least two glass capillaries were pulled and their shape characterised.

Figure 24: Narishige PB-7 glass capillary puller.

The inner diameter of the tapering part of the capillary was analysed using a Leica MZ6 modular stereomicroscope (Leica Microsystems GmbH, Germany) and the tip region was measured with a Diaphot-TMD inverted microscope (Nikon Corp., Japan).

For a better visualisation of the inner diameter, the glass capillaries were submerged in vegetable oil to match the refractive index of glass and filled with a red food colour/water mixture (see Figure 25).

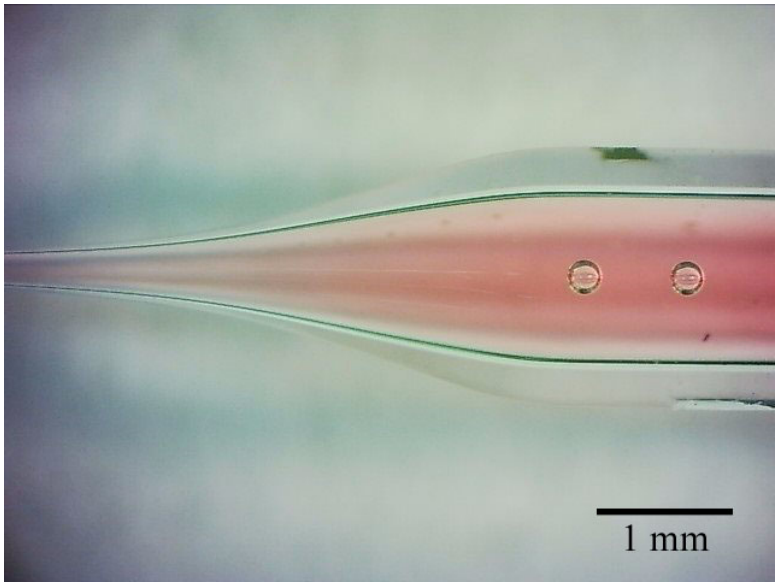

Figure 25: Pulled glass capillary. The analysis of the glass capillaries' tapered region was done with a Leica MZ6 stereomicroscope. Scalebar:1 mm.

The inner diameters of the capillaries produced with heater settings 6,7,8 and 10 were measured on merged images using the software Image J and are plotted in Figure 26. The straight capillary part has an average inner diameter of 1.22 ± 0.02 mm and the beginning of the tapering part of the capillary (length 0 mm in Figure 26) was defined as the value were the capillary's straight diameter dropped by two percent. In the tapering region the diameter decreases abruptly to around 250 μm within a length of 4 mm and ends in the tip region where the slope almost becomes linear. It is obvious that depending on the heating power, the shape of the tapered part and tip region can be altered. With increasing heating power (higher heater setting) the inner diameter of the tip region gets bigger. The two replicates for each heater setting show a concurring regime. The inset in graph a) depicts the final diameter for all capillaries. With a heater setting of 6 the final diameter is around 50 μm and increases to 80, 100 and 117 μm for heater setting 7, 8 and 10. In graph b) the capillaries dimensions are compared to the lumen of the *Bombyx mori* silk duct (data extracted from Asakura et al. 2007[47]). The regime of the silk duct is in good agreement with the capillary produced with heater setting 6 and only shows slight differences between 3 and 7 mm on the length scale where the capillary shows a less steep transition from the tapering part to the tip. In conclusion, capillaries prepared with heater setting 6 can very accurately reproduce the geometry of the natural silkworm duct and are therefore used as flow visualisation device. The slightly steeper decline in diameter from 3-6 mm of the silkworm gland (see Figure 26b) results in different extensional forces at this point, yet the exact extensional flow field is difficult to plot.

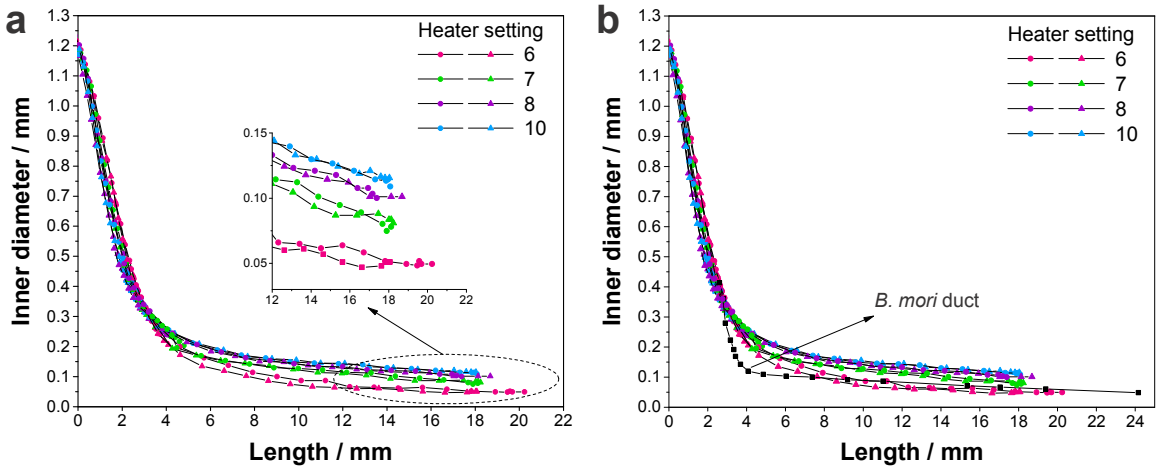

Figure 26: Dimensions of the flow visualisation device. The inner diameter of the glass capillaries produced with different heater settingsAt least two capillaries were pulled and measured for every heater setting. The inset of graph a) shows the final diameter at the very tip. Graph b) compares the different glass capillaries to the *Bombyx mori* silk duct dimensions which were extracted from Asakura et al. 2007.[47]

3.2 Realising a defined flow through the device

With the glass capillary having very similar dimensions to the *B. mori* silk duct, the next step is trying to realise a defined flow through the device. The first approach was to attach the glass capillary to a 1 ml syringe by pushing it into the opening of the syringe and fixing it with PTFE tape (see Figure 27). The PTFE tape was able to fix the capillary and also helped to prevent the syringe from leaking. The experiment was conducted with native silk proteins obtained from the posterior part of the middle gland of 5th instar *B.mori* silkworms as these proteins are mainly free of sericin. The silk proteins were loaded into the syringe and a syringe pump (AL1000-220, World Precision Instruments LLC) was used to push them through the capillary. Unfortunately, this did not work due to a build-up of pressure which ejected the capillary from the syringe. Another problem was that silk already started to form aggregates within the syringe due to the shear and extensional forces the proteins were experiencing when flowing through the syringe.

Figure 27: Silk flow visualisation setup 1. Pushing a glass capillary into the opening of a 1 ml syringe and fixing it with PTFE tape to prevent it from leaking. The syringe in this picture is filled with a red food colour/water mixture for better visualisation.

In a next step, I tried to modify the flow visualisation device to implement a vacuum system at one side of the capillary while pushing from the other with a syringe pump. This setup simulates the silkworm pulling the fibre from the gland[56] (see Setup 2 in Figure 28). For this, Luer adapters were connected to a converging-diverging glass capillary with polyurethane tubes at both sides. The capillary is then glued to a petri dish with a glass window (microscope cover slide) to allow for flow visualisation under a microscope with polarized light. Again, with this setup it was not possible to flow silk proteins through the glass capillary as the required forces were too high. In a later study by our group we have shown that it is not possible to push silk through a capillary with similar dimensions to the silkworm duct.[56]

Figure 28: Silk flow visualisation setup 2. A glass capillary with a tapered middle part was accessed at both ends to push and suck the proteins through the duct. A glass cover slip is glued to a petri dish with hot melt glue to allow visualisation under polarized light.

In an attempt to reduce the pressure build-up and further facilitate the flow of the silk proteins through the glass capillary, the capillary tip was shortened from 20 mm to around 10 mm in setup 3 (Figure 29). This time a flow rate of 0.2 μl/min could be realised with a syringe pump which was calculated to be the flow rate of silk proteins inside the gland of a silkworm. The flow rate inside a silkworm can be estimated via the principle of conservation of mass. The silkworm spins fibres with a diameter of 20 μm (0.020mm) at a speed of around 10 mm/s. This is a total fibre volume of 0.003 mm^3 which is spun per second. The same amount has to flow inside the duct due to conversation of mass and is therefore equal to the flow rate $\dot{Q}$ of silk proteins inside the silkworm gland (0.003 mm^3/s which is equal to 0.2 μl/min)

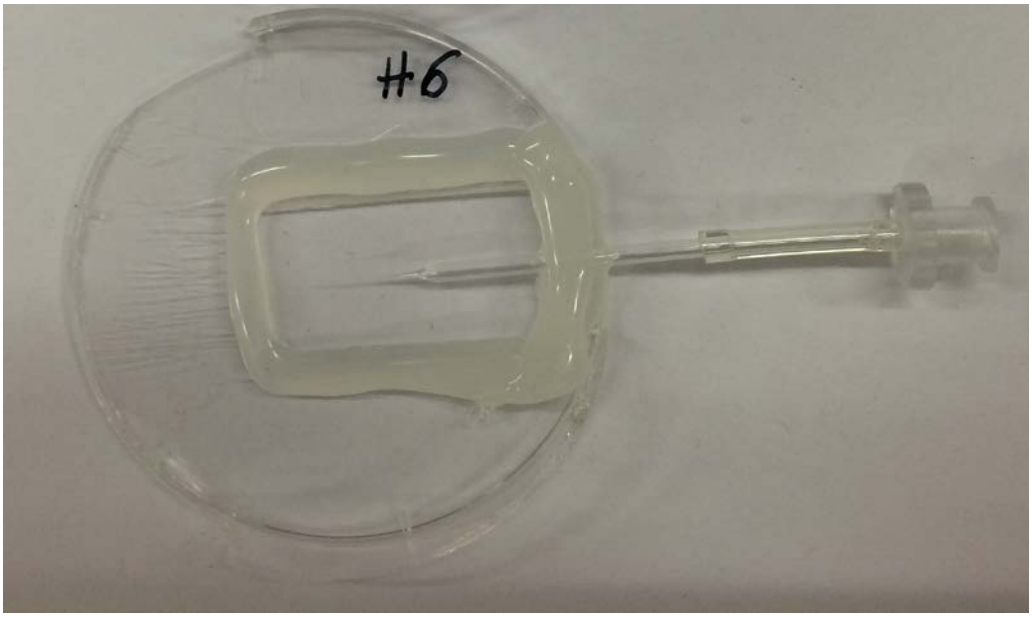

Figure 29: Silk flow visualisation setup 3. The glass capillary and a microscope cover slide are glued together on a hole in the petri dish. The capillary is connected to a Luer adapter by a polyurethane tube which can then be connection to the syringe.

3.3 Flow visualisation under a microscope

Using setup 3, the native silk proteins obtained from the posterior part of the middle gland of 5th instar *B.mori* silkworms were flown through the glass capillary and imaged using a

microscope with polarized light to investigate whether birefringence can be detected. The experiments were carried out at standard lab conditions (23 ± 1 ˚C, 50 ± 5% RH). In order to allow for visualisation and look “inside” the capillary, I had to match the refractive index of glass with air which was done by submerging the capillary in glycerol (99% glycerol supplied by Acros Organics). Although no birefringence could be detected at a flow rate of 0.2 μl/min (flow rate of silk proteins in silk duct), flow alignment was visible when using an excessive amount of force which was supplied by pressing the syringe plunger by hand (Figure 30).

Figure 30: Silk birefringence. The proteins start to align and show birefringence when flown through a glass capillary only at very high speeds.

3.4 Spinning natural silk under unnatural conditions

In the next set of experiments setup 3 (see Figure 29) was used to spin silk fibres from native silk proteins. Just flowing silk proteins through the capillary fibre formation was not possible. Therefore, I tried to induce fibre formation under unnatural conditions (i.e. fibre

formation was cause by precipitation in a coagulation bath instead of flow-induced crystallisation). I found that glycerol which was used to match the refractive index of glass with air also served as a coagulation bath for the native silk proteins. The spinning setup in Figure 31 was operated under a Diaphot-TMD inverted microscope (Nikon Corp., Japan) with polarized light.).

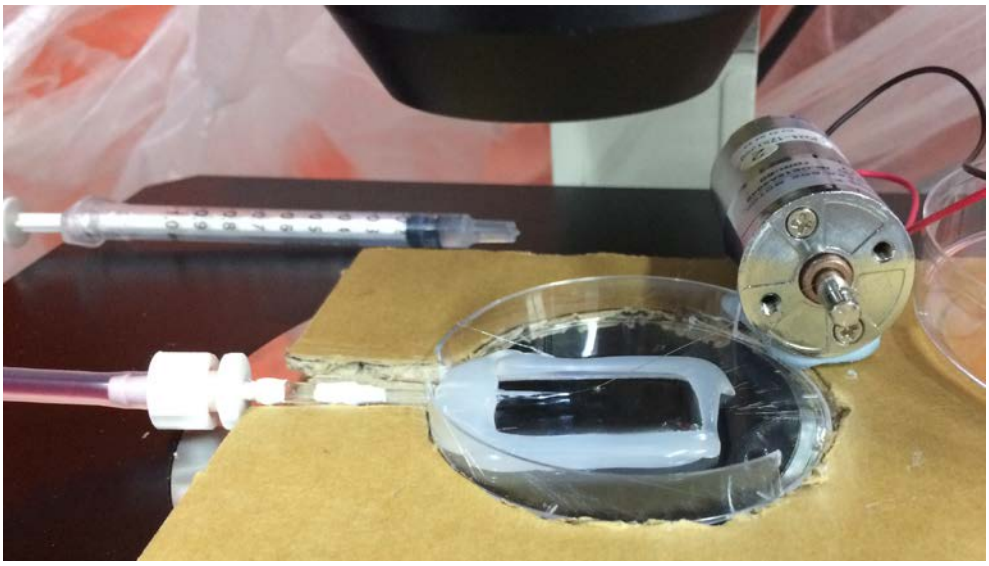

Figure 31: Silk fibre spinning setup.The glass capillary is connected to a syringe pump and a reeling motor is added so that the proteins can constantly be pulled out as a fibre. With this setup it is possible to visualise what happens at the capillary tip.

The glass capillary in this setup was produced with heater setting 7 and the syringe pump flow rate was set to 0.2 μl/min. The reeling motor was calibrated so that an electrical voltage can be related to a specific number of rotations of the motor. The voltage was set so that the motor runs at 24 rpm which is equivalent to a fibre drawing speed of 5 mm/s with a 4 mm diameter of the rotating metal stick. Due to the protein precipitation in glycerol a solid fibre could be drawn from the capillary. The fibres were not soluble in water.

The visualisation of the capillary tip under polarized light can be seen in Figure 32. The inner diameter at the very end is 200 μm. Birefringence indicating the orientation of the proteins can clearly be seen from the point where the proteins detach from the wall and

start to form a fibre. During this experiment it was possible to continuously spin fibres for 7 minutes at a spinning rate of 5 mm/s until all the loaded silk (150 mg in total) was flown through the capillary. However, characterisation of the dried, spun fibres has shown that they were very brittle and weak (strength: 52.7 ± 19.8 MPa, elongation: 1.2 ± 0.4%), similar to as-spun artificial silk fibres in literature (see chapter 1). The fibre diameter varied a lot over the length and was roughly around 56 μm in average.

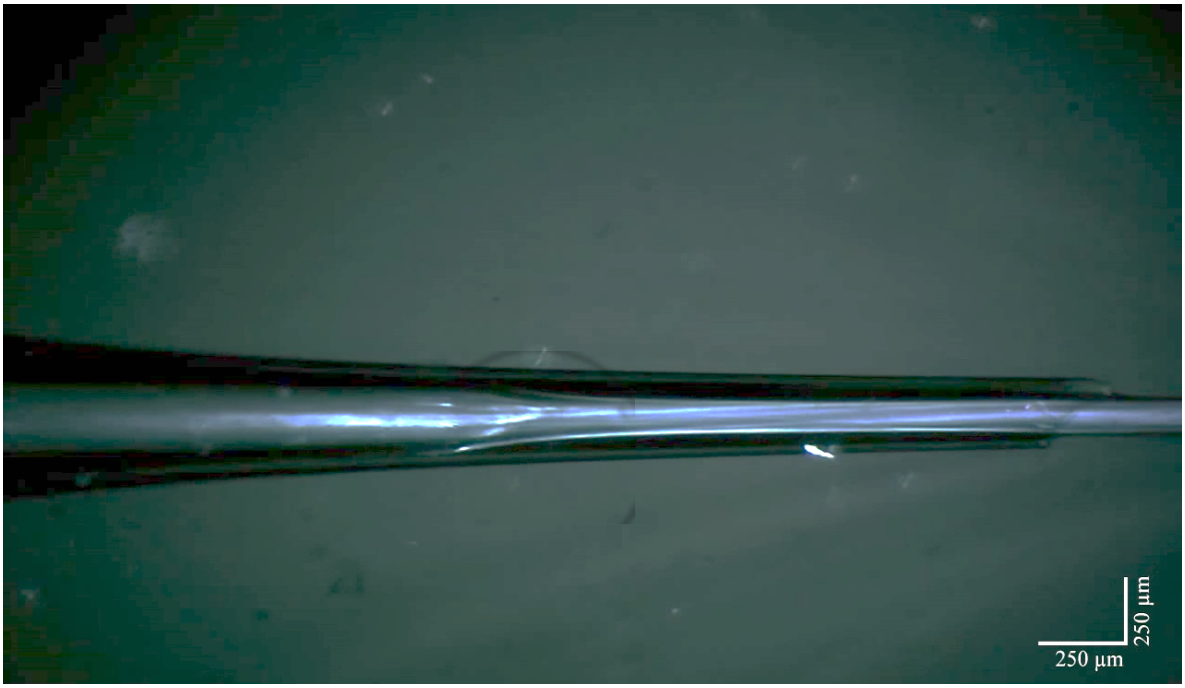

Figure 32: Spinning silk via coagulation in a glycerol bath. Native *B. mori* silk proteins flowing through a capillary with a shortened tip (see setup 3 in Figure 29) under polarized light. Due to the drawing, the proteins detach from the wall (in literature termed as draw-down taper[47], red circle) and can be pulled out. Starting from the draw-down region birefringence can be observed as the proteins orient along the fibre axis.

Despite these seemingly disappointing results, the following lessons were learned from the above-mentioned experiments that were important for my understanding of silk processing and the design of the experiments in the following chapters:

1) It was not possible to flow native *B. mori* silk proteins through a glass capillary with similar dimensions to the natural silk gland. While in this thesis the conclusion is based on observations for this specific geometry, the modelling and experimental

verification for the silkworm duct geometry was addressed and discussed later in a paper by Sparkes and Holland.[56]

2) Silk fibre formation is not possible by flowing silk proteins through short, tapered geometry as in setup 3 in Figure 29. This suggests that metal ions and pH seem to play an important role in structure formation during flow.
3) Silk proteins are able to align in flow fields, as indicated by flow birefringence in Figure 30, yet only with a huge amount of force that was supplied by pressing the syringe plunger by hand.

To conclude, native *B. mori* silk proteins could only be flown through a tapered glass capillary that is around half the length of the silkworm duct (see setup 3). During fibre spinning with the same setup 3, fibre formation only occurred via coagulation in a glycerol bath which ultimately yielded very brittle and weak fibres. This suggests that silk spinning is not only about the quality of the protein feedstock but also the correct processing where pH and metal ions seem to play an important role.

CHAPTER 4:

Extensional Flow Behaviour and Spinnability of Native Silk

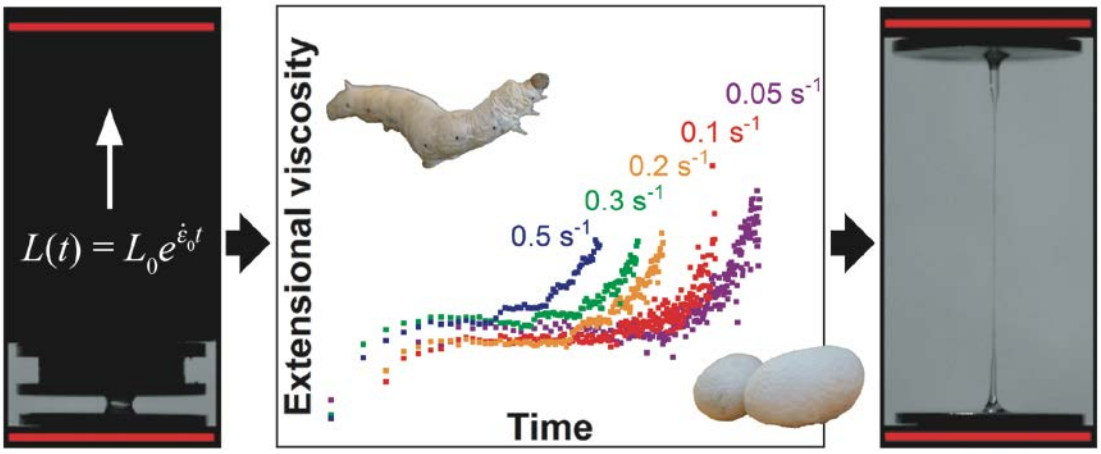

The literature review in chapter 1 has highlighted that in order to improve the processing and poor mechanical performance of current artificial silk fibres it is crucial to get a better insight into how silk assembles into strong and tough fibres in Nature. Therefore, in this chapter, I investigate the currently unknown extensional flow behaviour of native silk proteins. Extensional flow is the main flow field in fibre spinning and responsible for structure formation and studying it can provide us with new insight into how native silk fibres are formed. Additionally, the surface tension of native silk proteins is determined which is required for calculating the transient extensional viscosity. This chapter is based on the manuscript “Extensional flow behaviour and spinnability of native silk” published in the journal Soft Matter.[238]

4.1 Abstract

Silk fibres are assembled via flow. While changes in the physiological environment of the gland as well as the shear rheology of silk are largely understood, the effect of extensional flow fields on native silk proteins is almost completely unknown. Here I demonstrate that filament stretching on a conventional tensile tester is a suitable technique to assess silk’s extensional flow properties and its ability to form fibres under extensional conditions characteristic of natural spinning. I report that native *Bombyx mori* silk responds differently to extensional flow fields when compared to synthetic linear polymers, as evidenced by a higher Trouton ratio which I attribute to silk’s increased interchain interactions. Finally, I show that native silk proteins can only be spun into stable fibres at low extension rates as a result of dehydration, suggesting that extensional fields alone are unable to induce natural fibre formation.

4.2 Introduction

Natural silk spinning is a highly energy efficient process, creating protein fibres with an impressive combination of stiffness, strength and elasticity comparable to, and often exceeding, that of synthetic polymers.[11-12, 17-19] These properties are attributed to the self-assembly of hierarchical structures present in silk fibres[13, 239] which are not only the result of protein sequence but also the way the feedstock is processed[42, 240], i.e. spun[2].

Understanding and successfully replicating natural silk spinning can hopefully pave the way for a new generation of high performance, low energy materials.[14] My systematic analysis of 49 studies over the past 70 years in chapter 1 revealed that current artificial spinning approaches are yet to match as-spun natural fibres and in order to do so require non-natural spinning conditions (i.e. harsh solvents) or significant post-processing (i.e. post spin draw).[1, 67, 99, 121, 131] I concluded that to produce a truly biomimetic silk requires the field to both develop improved (i.e. higher molecular weight)[75] artificial feedstocks and in tandem, spinning systems that replicate the flow conditions and chemistry present in the natural spinning duct.

Natural silk spinning begins with an aqueous native protein feedstock secreted at high concentration (~400 kDa at ~250 mg/ml or 25% dry weight) into specialised glands.[2, 47] As the feedstock is pulled through the gland[56], the silk proteins in both spiders and silkworms experience changes in pH[46, 48, 241-242], metal ion content[42, 49, 243], and become aligned due to flow stress[5, 58] before finally forming a solid fibre as they undergo extensional flow and dehydration.[5, 56, 59]. While the physiological changes during natural spinning are well understood, little is known about how silk proteins respond to a purely extensional flow field.

This is an important gap in our knowledge as control of extensional flow fields has been shown to be crucial in successfully designing fibre spinning devices in both polymer and biopolymer-based systems.[99, 180, 244-246] This was first seen by Chappel and co-workers[247] in

1964 when they were trying to spin Nylon 6.6 and today with a range of groups across the world who are looking at how extensional flow imparts orientation and structure development during melt processing and especially in fibre spinning.[248-253]

In the case of silk, whilst the shear flow behaviour is largely understood, its extensional flow is not, having only begun to be addressed in a single study by Kojic and co-workers over a decade ago.[254] In that study they reported extensional properties by stretching a native spider silk protein sample extracted from the major ampullate gland in a customised microscale capillary break-up extensional rheometer. However, due to limited sample availability and an estimation of surface tension, the resulting extensional properties may not be entirely representative of the natural system.

This chapter seeks to extend this knowledge by investigating fibre formation of native silk proteins extracted from the silkworm *Bombyx mori* under extensional flow fields.

To achieve this, I have developed, as suggested by Kojic *et al.*[254], a filament stretching rheometer[190] as a means to investigate the extensional properties of small sample sizes with high viscosity[188] and determined the surface tension of native silk (which is also important for other silk-water interactions[255] such as electrospinning[256] and printing[257]).

4.3 Experimental methods

4.3.1 Surface tension of native silk proteins

The surface tension of native silk proteins was determined by the captive bubble method described in detail in chapter 2.[175-176] However, firstly it is required to determine the surface tension of water and oil as well as the interfacial tension of the water-oil system which was done via the pendent drop method. Images of pendent drops were taken at standard lab conditions (23 ± 1 °C, 50 ± 5% RH) in equilibrium state (drop is about to fall off). Generally, the measurement is influenced by temperature and humidity where the surface tension decreases with increasing temperature and humidity. The influence of humidity is, however,

much less pronounced compared to a change in temperature.[258] The images were converted to greyscale and then analysed using the ImageJ plugin by Dearr and Mogne.[259] Depending on the curvature of the pendent drops and the density difference to the surrounding medium the surface tension can be calculated according to the Young-Laplace equation[174] (see equation (17)).

$$\gamma\left(\frac{1}{R_1}+\frac{1}{R_2}\right)=\Delta P \equiv \Delta P_0\text{-}\Delta\varrho g z \qquad (17)$$

where R_1 and R_2 are the radii of curvature (see **Figure** 33), ΔP is the Laplace pressure across the interface and $\Delta\varrho$ is the density difference to air in case of surface tension or another media for calculating the interfacial tension. The density of water (Type II water) and oil (rapeseed oil) was determined by weighing 10 ml of each liquid which was pipetted into a weighing boat. The average of 10 measurements was taken for the calculation of the surface tension. The gravitational acceleration g was taken as 9.81 m/s^{-2}.

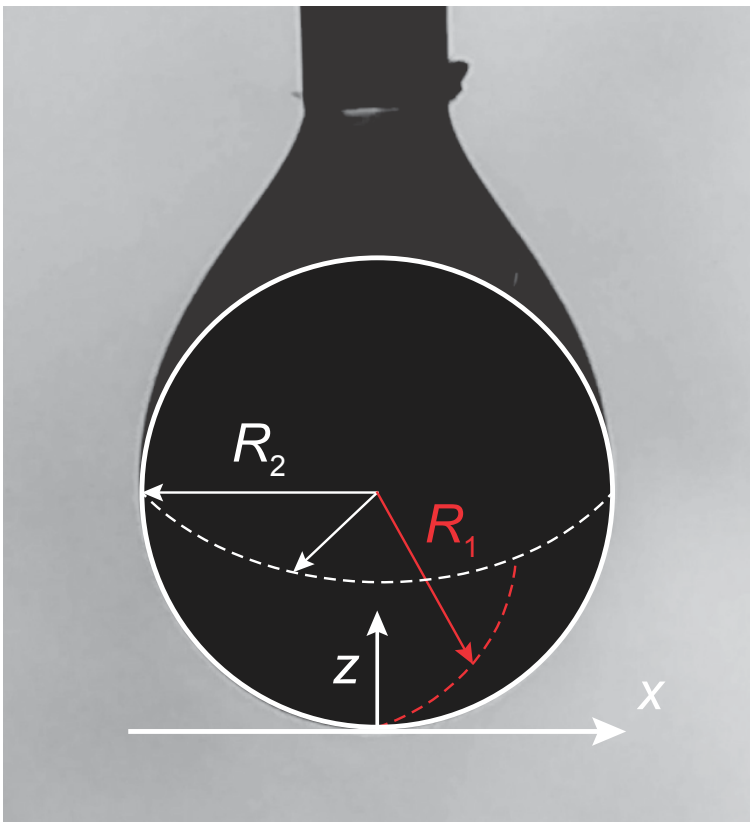

Figure 33: Schematic of a pendent drop with the radii of curvature R_1 and R_2 which are used to calculate the surface tension of a liquid.

4.3.2 Filament stretching on a tensile tester

For the extensional characterisation of native silk proteins from the silkworm *Bombyx mori* a Zwick Z0.5 TS tensile tester was modified so that it can be operated as a filament stretching rheometer (Figure 34a). The challenges are the realisation of the exponential plate separation which is required for ideal uniaxial extension and the measurement of the mid-diameter for the calculation of the effective extension rate (Figure 34b and c). The Zwick tensile tester is inherently not capable of performing an exponential plate separation but by programming several linear steps in the test sequence editor provided in the Zwick testXpert software an exponential profile can be approximated with very good accuracy. This was done for extension rates of 0.05, 0.1, 0.2, 0.3 and 0.5 s^{-1} which were identified to be characteristic for natural silk spinning (see Figure 35, **Table** 3).

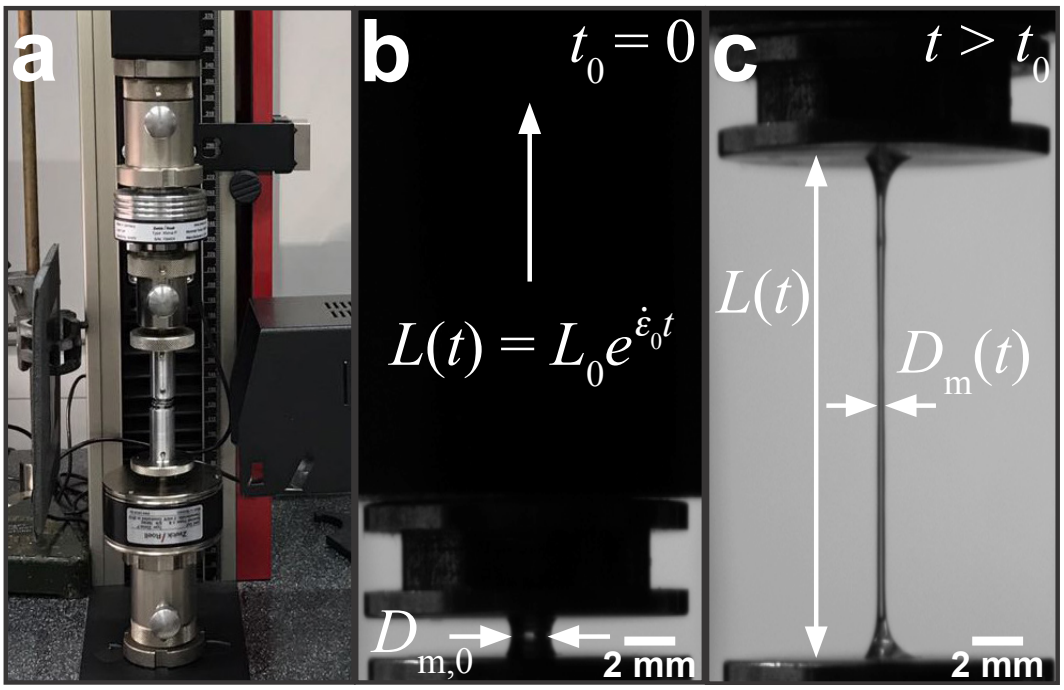

Figure 34: Setup for measuring the extensional properties of silk. **a** A conventional Zwick Z0.5 testing machine was modified for filament stretching. **b** Initial plate separation prior to starting the test. The plates were then separated according to an exponential profile which was realized with the help of the test sequence editor in the Zwick testXpert software. **c** The force and filament mid-diameter were recorded for each experiment which permits the calculation of the transient extensional viscosity with an effective extension rate (see chapter 2).

Table 3: Parameters for fitting an extensional plate separation

0.05 s^{-1}		**0.1 s^{-1}**		**0.2 s^{-1}**		**0.3 s^{-1}**		**0.5 s^{-1}**	
Plate separation in mm	Speed in mm/s	Plate separation in mm	Speed in mm/s	Plate separation in mm	Speed in mm/s	Plate separation in mm	Speed in mm/s	Plate separation in mm	Speed in mm/s
1.1	0.075	2.5	0.31	0.4	0.23	0.4	0.32	0.3	0.55
2.1	0.13	3.5	0.4	1.2	0.33	1.1	0.5	0.9	0.8
3.1	0.18	4.75	0.5	2.6	0.56	2.7	0.84	3	1.5
5	0.25	6.25	0.66	4.4	0.9	4.8	1.4	6	3.1
8	0.37	8	0.83	7.2	1.37	8.8	2.5	12	4.9
11.5	0.53	10	1.10	11.2	2.1	13.6	3.8	20	9.3
15.75	0.73	12	1.2	16.8	3	20	5.8		
20	0.95	14.25	1.4	20	4.3				
		18	1.7						
		20	2.3						

The lowest and highest extension rates during natural silk spinning in the silkworm were estimated the following equation.[254]

$$\dot{\varepsilon} = \frac{4\dot{Q}}{\pi L}\left(\frac{1}{d^2} - \frac{1}{D^2}\right) \quad (18)$$

where $\dot{Q}$ is the flow rate of the silk proteins within the silkworm duct, L is the length of the converging duct, D and d are the duct diameters before and after the converging section, respectively.

The natural spinning speeds in silkworms range from around 5-15 mm/s and the dimensions of the spinning duct were taken from Asakura and co-workers.[34, 47]

The lowest extension rates during silk spinning occur in the tapering part of the silk gland. At the lowest spinning speed (5 mm/s), a fibre volume of 0.0016 mm^3/s (fibre diameter 20 μm) is spun which is equal to the flow rate $\dot{Q}$ due to the principle of conservation of mass. This results in a minimum extension rate of 0.036 s^{-1} for L=22 mm, D=0.4 mm and d=0.05 mm.[47] At 15 mm/s the extension rate within the duct equals to 0.11 s^{-1}.

The highest extension rates, however, occur at the draw-down taper where fibre is pulled from the silk gland. At this position the diameter converges from D=0.04 mm to d=0.02 mm over a length of L=3 mm. For the lowest and highest spinning speeds (5 and 15 mm/s) this results in extension rates of 0.625 and 1.88 s^{-1}, respectively.

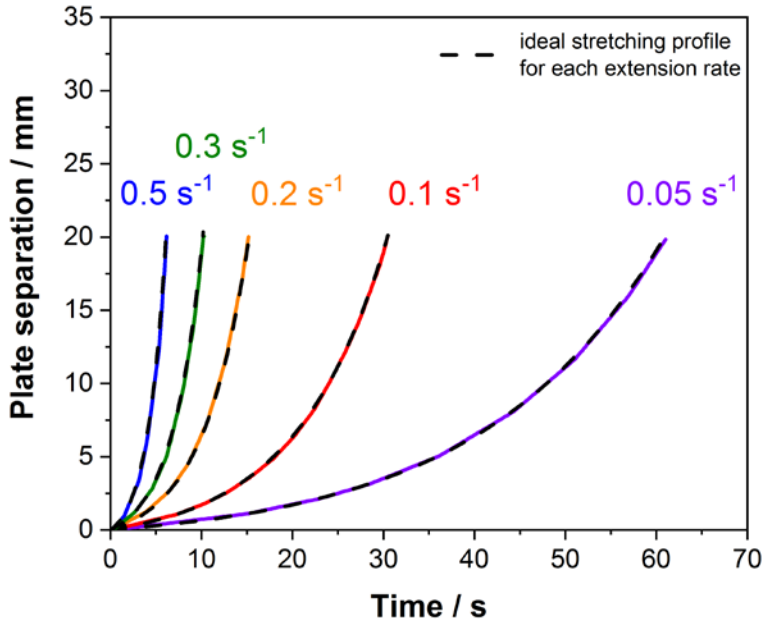

Figure 35: Exponential plate separation for ideal uniaxial extention. The dashed lines represent the ideal extensional profile and the coloured lines are the fitted profileprogrammed into the Zwick testXpert software (see Table 3).

The change in diameter of the silk filament was recorded by a 1.45MP QICAM 12-bit Mono camera (QImaging, Canada) at a rate of 10 frames per second. The mid-diameter was subsequently determined by analysing the video material in Matlab. In short, the image stacks recorded with the camera were converted to binary images with Fiji software and then loaded into Matlab. The plate separation of each image was then correlated with the values from the Zwick machine so that the exact location of the filament midpoint was known and marked for each image (Figure 36). Along this line the Matlab programme was scanning for the first and last white pixel from which it can calculate the number of pixels in between. As the scale of the image is known in mm/pixel the mid-diameter can be calculated. Unfortunately, due to the transparent nature of the silk proteins an automated measurement with Matlab was not always possible and therefore several image stacks had to be measured manually.

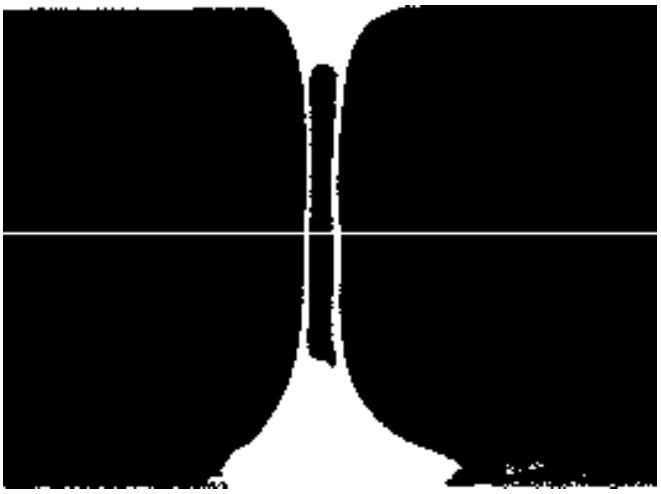

Figure 36: Automated determination of the filament's mid-diameter. The image is produced by the Matlab programme and shows where the mid diameter was determined.

The silk proteins were uniaxially stretched on a Zwick Z0.5 TS testing machine (Zwick GmbH & Co. KG, Germany) equipped with a 5 N load cell under standard lab conditions (23 ± 1 ˚C, 50 ± 5% RH) at rates varying from 0.05 to 0.5 s^{-1}. Of particular note is that the

exponential profiles of the highest rates (0.3 and 0.5 s^{-1}) are equivalent to spinning speeds between 5-10 mm/s, replicating those used by the silkworm in nature.[33-34] (see calculation above)

For extensional tests in a high humidity atmosphere, an environmental chamber was built around the sample which was then filled with saturated water vapour created by a humidifier. The humidity inside the chamber was measured with a TRH 22 hygrometer (Meterman, UK).

4.3.3 Shear rheology experiments

For the shear rheology experiments the same loading and handling protocols reported earlier by Laity and Holland were employed.[64-65] In short, the experiments were performed on a Bohlin Gemini rheometer (Malvern Instruments, UK) with a CP1/10 cone and plate geometry (10 mm diameter, 1° opening angle and 30 μm truncation) at 25 ˚C.

Experiments were performed in three stages. At first, a conditioning step was applied at a shear rate of 1 s^{-1} for 100 s to equally distribute the sample in the geometry and eliminate any residual stresses from loading. Second, oscillatory measurements were performed from 25 to 0.1 Hz at an applied strain of 0.02. Lastly, the shear viscosity was determined by applying a shear rate ramp from 0.1 s^{-1} to 100 s^{-1}. The value for the zero-shear viscosity η_0 was determined by extrapolation of the viscosity curve to 0 s^{-1}. The concentration of the native silk proteins from the posterior section of the middle gland was determined gravimetrically. Therefore, the weight of around 200 mg of proteins from an adjacent section was dried at 60 °C under vacuum until constant weight was achieved. The solid residue was then used to calculate the protein concentration.

4.4 Results and discussion

4.4.1 Surface tension

The surface tension of oil and water as well as the interfacial tension of the water/oil system, which are required for the calculation of silk's surface tension, were measured by analysing the shape of pendent drops as shown in Figure 37.

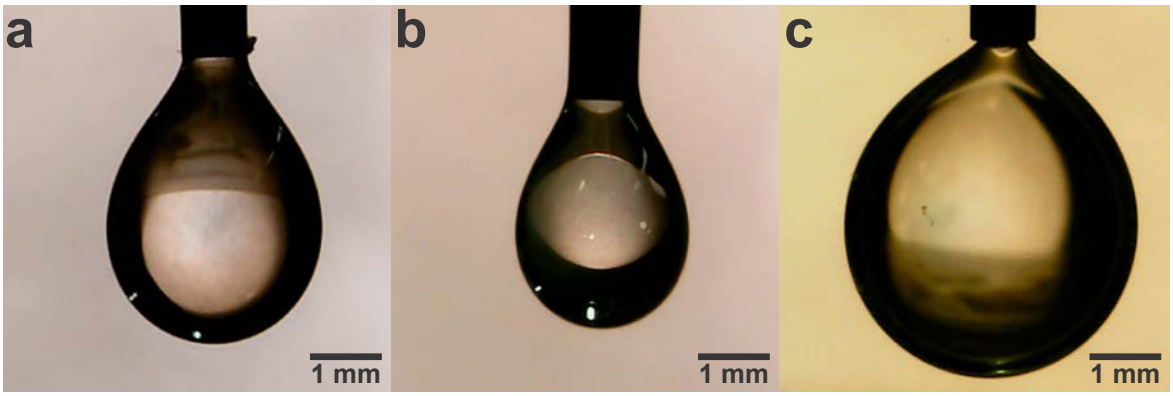

Figure 37: Determining the surface tension with the pendent drop method. **a** water in air, **b** oil in air and **c** water in oil.

The results of the measured density difference and the surface/interfacial tensions are shown in Table 4.

Table 4: Results of the surface/interfacial tension measurements.

T = 24°C	$\Delta\rho$ in g/cm^3	γ in mN/m
water-air	0.9976 ± 0.0004	71.8 ± 0.8
oil-air	0.9161 ± 0.0027	31.2 ± 1.7
oil-water	0.0815 ± 0.0031	22.4 ± 1.2

At 24°C, the surface tension of water was calculated to be 71.8 ± 0.8 mN/m which is in good agreement with the value reported in literature for 25˚C (72.0 ± 0.1 mN/m).[260] The

surface tension of rapeseed oil with 31.2 ± 1.7 mN/m and the interfacial tension of oil-water with 22.4 ± 1.2 mN/m are also in accordance with values reported in literature.[261-262]

Based on these results the contact angle measurements of an air bubble and oil droplet on a silk surface and the resulting surface tension of silk together with its polar and dispersive components can be calculated (Figure 38a-c).

The surface tension of native silk was found to range between 43.3 and 69.1 mN/m, with an average of 54.2 mN/m. Any inter-sample variability (see Table 5) was attributed to minor differences in concentration, surface roughness and measurement time. Additionally, the silk proteins get diluted in water which also contributed towards sample variability. However despite this variation, our results are based on 1o repeated experiments and are in agreement with the range from 30 to 60 mN/m that was estimated by Kojic and co-workers[254] and those measured previously for a reconstituted silk[263].

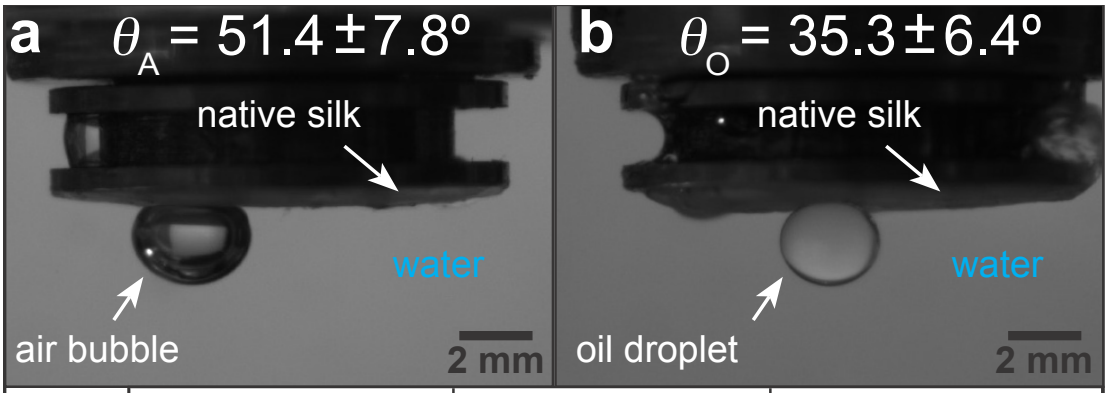

c	γ^d_{SA} in mN/m	γ^p_{SA} in mN/m	γ_{SA} in mN/m
n=10	27.8±6.1	26.4±1.8	54.2±7.8

Figure 38: Results for the surface tension of silk. **a** Contact angle of air bubbles to the silk surface. **b** Contact angle of oil droplets to the silk surface. **c** Polar and dispersive components and total surface tension of native silk. The results for all 10 measurements are shown in Table 5.

Table 5: Contact angle measurement results. The contact angle of air and oil to the silk surface as well as for the surface tension of silk and its dispersive and polar components is shown. The average was taken from 10 measurements and the standard deviation is reported.

θ_O in °	θ_A in °	γ_{SA}^{d} in mN/m	γ_{SA}^{p} in mN/m	γ_{SA} in mN/m
23.2	42.6	33.0	28.9	61.9
42.1	52.0	28.4	25.7	54.1
38.3	51.0	28.4	26.2	54.6
27.7	43.8	32.7	28.4	61.1
32.3	51.7	26.6	26.6	53.2
37.3	60.7	20.3	24.6	44.9
34.7	37.7	40.2	28.9	69.1
32.2	59.1	20.7	25.3	46.0
45.4	63.1	19.9	23.4	43.3
40.0	52.4	27.5	25.8	53.3
35.3 ± 6.7	51.4 ± 8.2	27.8 ± 6.5	26.4 ± 1.9	54.2 ± 8.2

4.4.2 Extensional flow behaviour and spinnability of native silk

Native silk proteins were stretched at different rates to evaluate their extensional flow behaviour and subsequent spinnability (ability to form fibres, see video 1 in Appendix A2). From initial observations during stretching, I found native silk proteins to be prone to necking in the middle of the fluid column. This process is initiated by shear forces acting on the fluid at small strains as a result of the material adhering to the endplates.[191, 194] Despite this necking, samples showed good spinnability at the lowest rates (0.05 s^{-1} and 0.1 s^{-1}) as they could always be stretched out into fibres up to a plate separation of 20 mm.

Upon increasing the extension rate, filament formation became less likely at 0.2 s^{-1} and impossible > 0.3 s^{-1} (video 1 in Appendix A2 and Figure 39a). From video 1 it is clear that these filaments did not fail due to continuous necking but snapped instantly due to elastic fracture. I interpret this as when subjected to higher extension rates the silk proteins cannot either relax/rearrange in time to the deformation field or lack sufficient stiffness (gel

strength) and therefore the fluid column ruptures due to the build-up of elastic stresses. This is surprising as these higher extension rates coincide with natural spinning speeds. Therefore, there may be factors other than extensional flow contributing to natural fibre formation at higher rates that are not accounted for here and will be the subject of the next chapter.

Regardless of whether fibre formation was possible, the extensional flow behaviour of the silk proteins could still be evaluated by determining the transient extensional viscosity (η_E^+). When plotted against time, three distinct regions can be identified in the viscosity curve for all extension rates (Figure 39b): after an initial transient response, the viscosity plateaus before it deviates upwards. The viscosity increase after the plateau arises from an effect called strain hardening, which is shifted to shorter times for higher extension rates. For the animal this appears fortuitous as strain hardening is an important property in polymers that improves processability during fibre spinning by stabilising the fluid column and reducing necking.[264-265] For the higher extension rates there are several pronounced steps in the viscosity data after plateau which can be explained by a shift in velocities of the tensile tester as the exponential velocity profile is fitted by a series of linear increases. Some of the sample show a slight decrease of the transient extensional viscosity in the plateau region. This could either be due to gravitational effects or molecular rearrangements during stretching which lowers the viscosity before strain hardening occurs.

Assuming the silk feedstock to be akin to an entangled polymer solution[266], I attribute the observed strain hardening and associated viscosity increase to be due to chain entanglements hindering the rearrangement of the silk proteins during flow.[197, 217 267]

The extent of strain hardening can be compared for the different extension rates by eliminating the time factor and plotting the transient extensional viscosity against the total Hencky strain ε_{eff} (Figure 39c). Starting from a Hencky strain of 1 all curves show strain hardening with similar slopes up to a value of 10^5 Pa·s, suggesting that the viscosity

increase is independent of the tested strain rates. These measurements of silkworm silk fibroin shows less pronounced strain hardening when compared to Kojic's spider silk which reaches viscosity values above 10^6 Pa·s for a Hencky strain of 3.[254]

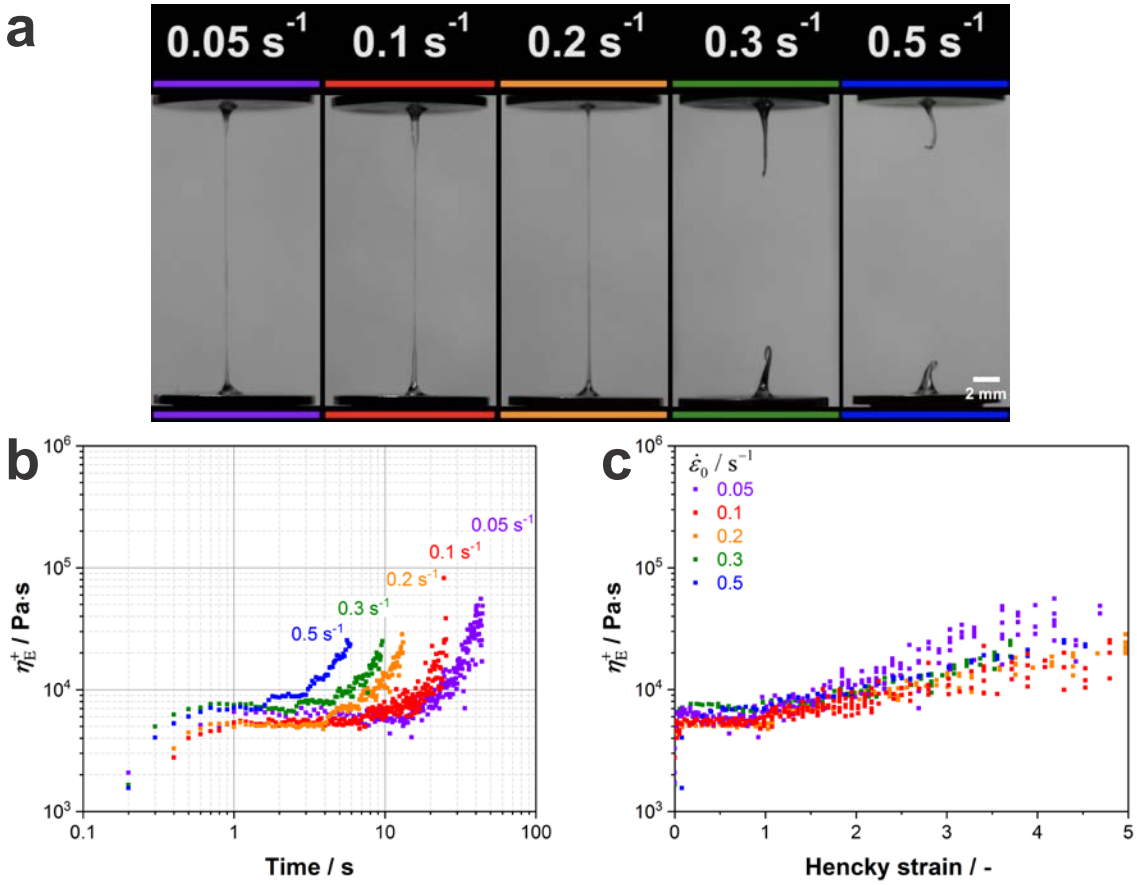

Figure 39: Extensional properties of silk. **a** Native silk proteins show a good spinnability at low extension rates while no stable fibre formation is possible at speeds which are characteristic for natural silk spinning. b Transient extensional viscosity of silk fibroin for different extension rates plotted against time. c Transient extensional viscosity plotted against the Hencky strain ε_{eff} to eliminate the time factor and compare the strain hardening behaviour for the different extension rates. It was found that η_E^+ in the plateau region is highly variable between different worms. This variability was already found in shear rheology experiments from our group.[64] As proteins from different worms were used for each extension rate, we compared curves with similar extensional viscosities in the plateau region (5000-7500 Pa·s).

Although spider and silkworm silks differ markedly in molecular structure, this order of magnitude difference may also be due to the small sample size and therefore the influence of dehydration in the previous work.[254] In order to estimate the influence of dehydration during my extensional experiments, I determined the processability parameter P, a

dimensionless number, that relates the stretching time with the time scale of water diffusion (limits water evaporation) through the native silk dope ($P=t_{stretch}/t_{diff}$).[254, 268-269] Water evaporation is negligible for $P<<1$ but becomes significant for values approaching 1. At the start of my extensional experiments where the filament diameter is around 1 mm, evaporation is certainly negligible yet might have an influence at smaller diameters towards the end of the experiment. Consequently, I analysed the influence of water evaporation starting from the point where the filament has a diameter of 100 μm. The time scale for diffusion is given by $t_{diff} = R/D_w$, where R is the initial filament radius (100 μm in my case) and D_w the diffusivity for water in silk ($D_w = 2 \cdot 10^{-5}$ mm^2/s).[254, 270]

For 0.3 and 0.5 s^{-1} the stretching time $t_{stretch}$ from a filament diameter of 100 μm to the end of the test (in this case filament rupture) is around 1s, which results in a processability parameter of $P \leq 0.008$. This suggests a negligible influence of water evaporation during stretching at high extensional rates. Towards lower extension rates, the stretching time increases and the processability value P returns values of 0.12 for 0.1s^{-1} and 0.24 for 0.05 s^{-1}. These values indicate that at low extension rates filament dehydration has to be taken into account which was checked by stretching native protein samples at 55% R.H. and in a water saturated atmosphere (98% R.H.) at 0.1 s^{-1} (see video 2, Appendix A2). Although the proteins exhibited the same transient extensional viscosity increase under both conditions, it was not possible to form a fibre in a high humidity atmosphere as the fluid column continuously necked until the filament was completely separated (see video 2 and Figure 40).

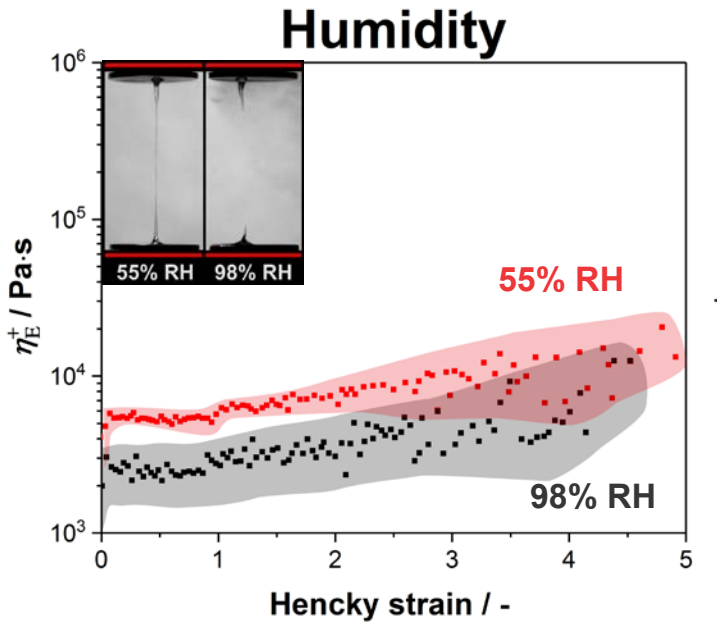

Figure 40: The extensional viscosity of native silk at different humidities. The stretching is compared at standard lab conditions (55% RH, 23 °C) and in a water saturated atmosphere (98% RH). Three samples for both conditions were measured and the curves were averaged. The coloured area around the data points shows the standard deviation.

Consequently, I conclude that the strain hardening behaviour which is evoked by the entangled structure of silk is only influenced by water evaporation starting from a Hencky strain of around 4-5. This suggests that fibre formation at low extension rates is only possible due to dehydration at the final stage of stretching, when the diameter gets smaller than ~20 μm.

Another factor thought to have considerable influence on fibre spinning is the shear viscosity of the dope.[154] It is known from previous publications that despite having a similar concentration of fibroin in the posterior middle gland (24.0 ± 2.5 wt.%), the shear viscosity of *Bombyx mori* silk is highly variable and thought to be controlled mainly by the ratio of Ca^{2+} to K^+ ions in the gland.[51, 64] Therefore, to determine the relationship between shear and extensional responses in silk, and to compare to other polymers, I performed both experiments on samples from the same silk gland and calculated the transient Trouton ratio $Tr^+ = \eta_E^+ / \eta_0$.

At the extremes of the natural zero shear viscosity range for silk (~3500 Pa·s), I found it was not possible to stretch samples in a consistent manner due to inconsistent necking. At zero shear viscosities of 2500 Pa·s and below, silk's response to stretching was markedly improved, becoming much more uniform.

The shear rheology response of the native silk protein samples with zero-shear viscosities within the natural range[64] (< 1500 Pa·s) are shown in Figure 41. All samples are taken from the posterior middle part of the *Bombyx mori* silk gland and have similar concentrations (534 Pa·s: 19.6 wt.%, 776 Pa·s: 20.2 wt.% and 1161 Pa·s: 22.1 wt.%) but show a highly variable zero-shear viscosity due to the formation of salt bridges induced by metal ions (Figure 41a).[51] All protein samples show pronounced shear-thinning similar to synthetic polymer melts. Starting from a shear rate of 1 s^{-1}, a significant increase in the normal stress can be observed due to the elastic nature of the native silk proteins. The drop in the normal stress around 4 and 5 s^{-1} for the 534 Pa·s and 1161 Pa·s sample, respectively, might indicate the occurrence of slippage which also affects the shear thinning behaviour in the viscosity curve starting from 4 s^{-1} (Figure 41b).

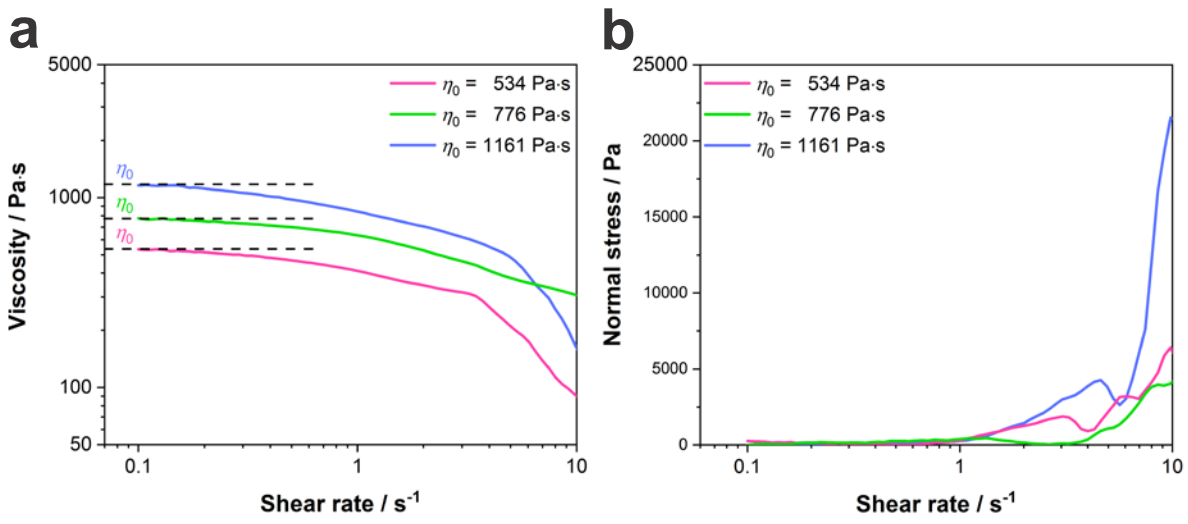

Figure 41: Shear rheology response of native silk. The protein samples were compared at different zero-shear viscosities (< 1500 Pa·s).

However, for my results, only the zero-shear viscosity is of importance for the determination of the Trouton ratios for our samples (Figure 42). All curves show three characteristic regions (transient start-up, plateau and strain hardening) as previously discussed. As seen from Figure 42, the Trouton ratio in the plateau region (Hencky strains smaller than 1) approaches values close to 3, which is consistent with the ratio Trouton found in 1906 for Newtonian fluids.[271] However, this finding also holds for viscoelastic fluids, such as silk fibroin, for very low extension rates.[272] The transient Trouton ratio further increases and reaches values of around 20 at a Hencky strain of 4, with all samples showing the same strain hardening behaviour.

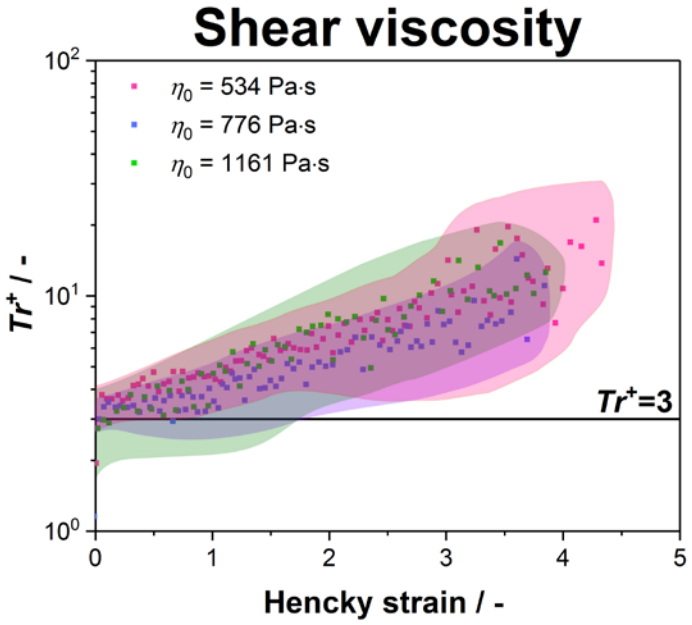

Figure 42: Transient Trouton ratio over Hencky strain. The native silk samples are compared at various zero-shear viscosities. Five samples were measured for each viscosity and the curves were averaged. The coloured area around the data points shows the standard deviation

When these numbers are compared to other polymer systems, they are much lower than dilute polymers where Trouton ratios can reach several hundred or even exceed several thousand[196, 210], but higher than entangled linear polymer melts such as high density polyethylene (HDPE) or linear low density polyethylene (LLDPE) which do not, or only marginally show, strain hardening.[197] Instead, the silk samples display Trouton ratios comparable to branched molecules such as low density polyethylene (LDPE).[217]

To explain this, one must consider the molecular structure of silk. *B. mori* silk feedstock's primarily protein component, H-fibroin, is a linear polypeptide chain consisting of highly repetitive GAGAGS domains and non-repetitive regions including the N- and C- terminals that consist mainly of charged and polar side groups.[29] Hence together with hydrogen bonding between repetitive domains and polar side groups, salt bridges between charged side groups could act as physical crosslinks that create an additional hindrance in removing molecular entanglements during extension, accounting for silk's increased strain hardening compared to other linear polymers.[51]

4.4.3 Mechanical and structural properties of fibres formed via extensional flow

Despite being strain hardening, I have shown that native silk proteins can only be stretched into fibres at low extension rates and via dehydration. To get an understanding whether structure was formed in these fibres, they were characterised, and their mechanical and structural properties compared to native silk. Mechanical testing revealed that the fibres formed via dehydration are very brittle and weak (see Figure 43a) which is likely due to a completely amorphous structure as indicated by the absence of crystalline structures by polarized light microscopy (Figure 44a). Trying to improve the mechanical properties, the fibres were submerged in methanol and acetic acid for 30 minutes. Methanol is known to induce β-sheet structure in silk and could significantly influence the properties of the fibres.[273] While the methanol treatment resulted in slightly more extensible fibres, the breaking strength decreased. Additionally, the fibres were also treated with acetic acid which resulted in highly extensible fibres with some of them having a breaking strain of up to 200%. The strength, however, remains still very low with an average strength of 45 MPa (see Figure 43b).

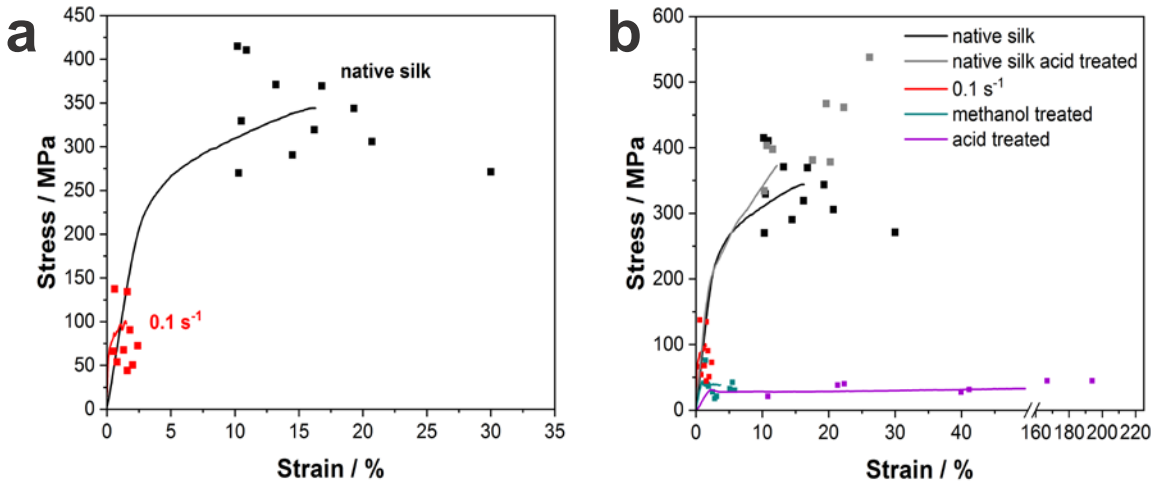

Figure 43: Mechanical properties of post-treated fibres formed via extensional flow.

The structural characterisation revealed that after treatment with methanol and acetic acid the fibres increase in diameter due to swelling and the uptake of acetic acid/methanol (Figure 44a). The swelling might result in a slightly increased mobility of the molecular chains allowing them to reorient which leads to a subtle increase in molecular alignment and decrease in disorder for both methanol and acid treated fibres (Figure 44c,d). While the methanol fibres only slightly increase in breaking strain, the treatment with acetic acid significantly increases the strain to break. The acidification may have neutralised repulsive charges between the protein chains and allow the N- and C-termini to link together which results in a chemically crosslinked network that behaves like a synthetic rubber and therefore the extensibility significantly increases.

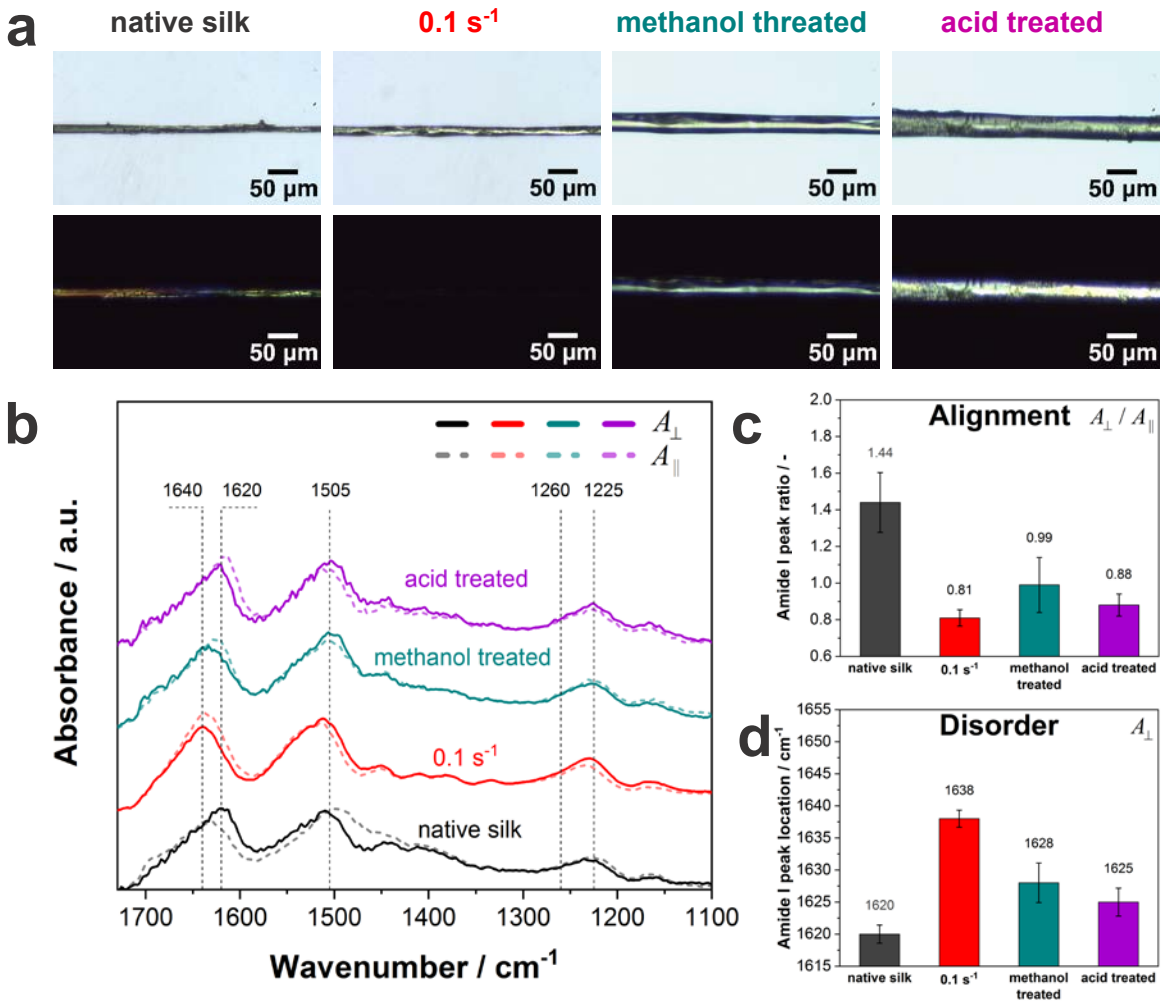

Figure 44: Structural properties of post-treated fibres formed via extensional flow.

In summary, the fibres formed via extensional flow are very weak and brittle fibres which is comparable to current as-spun artificial silk fibres.[97, 99, 131, 143] As fibre formation occurs via dehydration, instead of structural conversion as in Nature, the fibres do not have any oriented, crystalline structure. Artificial as-spun silk fibres have the same problem as they are formed via precipitation in a coagulation bath that rapidly removes the water from the proteins and does not allow structural rearrangement during processing. This results in brittle and weak as-spun fibres that have to be extensively post-processed (chapter 1). Post-treatment by soaking my fibres in methanol as well as acetic acid does not significantly improve the strength of the fibres. Therefore, in the following chapter I investigate whether

extensional flow combined with a pH change can result in structure formation *during* processing as opposed to post-processing.

4.5 Conclusions

This study investigates the extensional flow properties and spinnability of native silk feedstock. By adapting a conventional tensile tester into a filament stretching rheometer, it can be demonstrated that it is possible to test the spinnability of various high viscosity fluids, in this case silk, in a reliable way. This technique also provides new insight into the response of native silk proteins to extensional flow conditions, which to date has yet to be fully explored but is immensely important if we are to fully understand natural fibre formation.

These results show that the native silk feedstock exhibits a surprisingly high degree of strain hardening for a linear protein solution which is rather comparable to branched entangled polymers. I suggest that silk's unusual extensional behaviour may be attributed to a high degree of interchain interactions formed by salt bridges.

Yet despite strain hardening, which makes silk intrinsically suited for spinning, I found that fibre formation via extensional flow is only possible at low extension rates due to dehydration. At higher spinning speeds which are more characteristic for the natural spinning process, the fluid column ruptures and fibres cannot be formed. This suggests that extensional flow alone is not sufficient to create fibres at natural spinning speeds and physiological changes such as pH and metal ion concentration which occur during natural silk spinning have to be considered. Therefore, it is important to study the combined influence of extensional flow and pH change which will be the topic of the following chapter.

CHAPTER 5:

Spinning Beta Silks Requires Both pH Activation and Extensional Stress

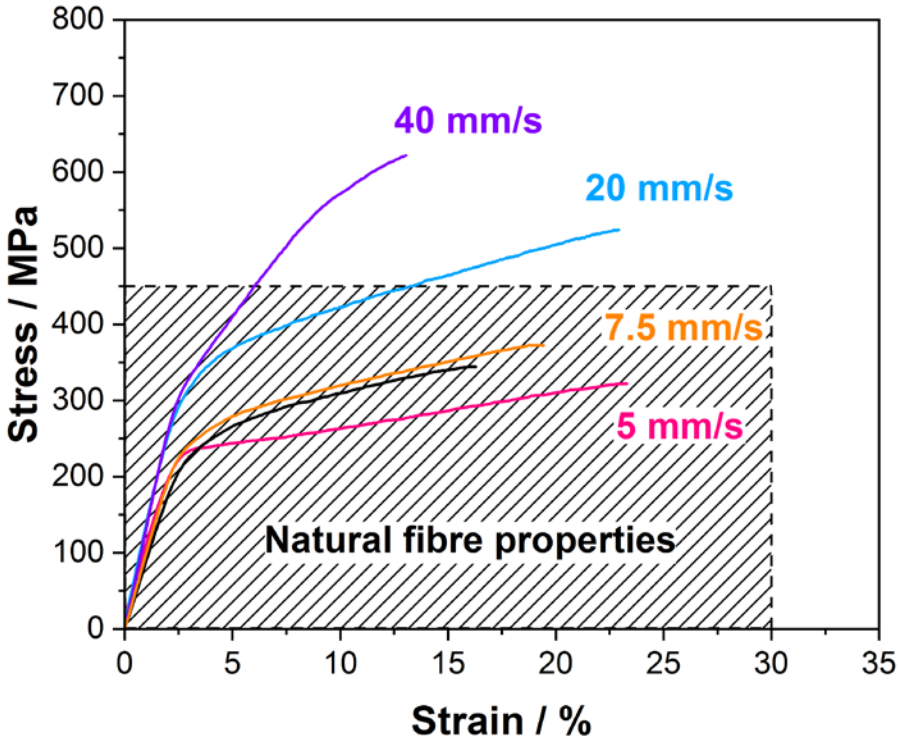

In chapter 4 I have shown that extensional flow alone is not sufficient to stretch native silk proteins into fibres with hierarchical structures. While fibre formation is not possible at extension rates comparable to natural spinning speeds (0.3 and 0.5 s^{-1}), only very weak and brittle filaments can be formed at low extension rates due to dehydration. Therefore, in this chapter, I consider the physiological changes that happen during natural silk spinning and investigate the combined influence of extensional flow and pH change on silk fibre formation. This chapter is based on the manuscript “Spinning Beta Silks Requires Both pH Activation and Extensional Stress” which has been submitted to the journal Advanced Materials.

5.1 Abstract

Synthetic silk production has undergone significant technological and commercial advances over the past 5 years, with fibres from most labs and companies now regularly matching the properties of a natural silk by one metric or another. Yet the fundamental links between silk protein processing and performance remain largely unresolved and fibre optimization is commonly achieved through non-natural methods. In an effort to address this challenge, I present data that closes this loop of processing and performance, by spinning a native silk feedstock *ex vivo* into a near-native fibre using just two naturally occurring parameters; pH activation and extensional flow (i.e. spinning rate). This allows me to link previous experimental and modelling hypotheses surrounding silk’s pH responsiveness directly to multiscale hierarchical structure development during spinning. Finally, I create fibres that match, and then exceed, natural silk’s mechanical properties and explain this by introducing the concept of rate of work input. This approach not only provides energetic insights into natural silk spinning and controlled protein denaturation but will help interpret and improve synthetic silk processing as a means to meet the current demands for high performance fibre design and upscaling.

5.2 Introduction

Natural silk spinning combines benign processing with outstanding mechanical performance, offering a means to create synthetic (bio)polymer materials with minimal energy input.[2-3, 11-12, 17-19, 274] Serving as inspiration, silk's desirable properties are a direct result of a multi-scale hierarchical structure carefully developed during spinning.[275-276] However, efforts to replicate this process have historically fallen short due to a reliance on unnatural feedstocks and processing methods as shown in chapter 1.[1]

When using the natural system as a biological blueprint, it is both necessary and important to look at the process variables involved in natural fibre formation. It is well established that during spinning, aqueous silk proteins experience chemical changes (ions[45, 48-50], pH[44, 46-47, 57]) and mechanical stress (shear, extensional[5, 43, 56, 58-59]), however the specific contributions of each variable towards fibre formation are only just beginning to be determined.[14, 238, 241, 277-279]

The current consensus is that shifts in the chemical environment in the silk gland serve to control silk protein hydration and interaction, making them more or less susceptible to denature and aggregate as a result of an applied flow field.[1, 42, 276, 280-281] For example, it has been recently shown by our group that the monovalent/divalent metal ion ratio is correlated with viscosity in the silk gland[51]; providing optimised storage conditions[49] and mediating interactions between charged side groups during spinning[45, 55].

However, a far greater body of evidence surrounds the influence of pH during spinning. Numerous studies have observed a consistent drop in pH along the gland and duct.[42, 276] This, combined with reports of pH inducing changes in silk protein conformation [48, 55, 166, 241-242, 279, 282-284] and rheological properties[53] strongly suggest that pH is also used to control silk protein stability and interactions. Specifically, small changes in pH have been shown experimentally to cause native silk proteins to refold[55] and through simulation and recombinant systems this phenomena has been attributed to the N- and C-termini

interacting and interlocking[167, 242, 279, 285]. Additionally, a more significant shift in pH induces an increase in β-sheet content and subsequent protein denaturation.[47-48, 53-55]

Whilst pH appears to alter silk protein structure, the primary energetic input for silk fibre formation is flow.[286] Although silk's response to shear has been intensively studied for over 15 years,[53, 64-65, 254, 266, 277, 287] only recently have we been able to test how silk proteins behave under extensional flow.[238] Such new insights are important, as extensional flow is by far the dominant flow field in fibre spinning and is much more efficient at aligning molecules [288-289], which may facilitate hierarchical structure development.[290-291] However, to directly counter this hypothesis, I have shown in chapter 4 that under extensional flow, native silk proteins could only form fibres at low extension rates due to dehydration, not the structural conversion typically observed during natural silk spinning.[238, 292]

This per se, is not necessarily a contradiction, as mentioned above prior to extensional flow silkworms and spiders condition the silk proteins by changing the pH along the gland. Therefore, I propose that, in order to further understand structure formation in silk, it is necessary to study the interplay of changing the pH and extensional flow as controlled energy inputs during fibre processing.

5.3 Experimental methods

5.3.1 Stretching native silk proteins in different vapour environments

Native silk proteins were stretched at an extension rate of 0.1 s^{-1} at standard lab conditions (23 ± 1 °C, 50 ± 5% RH) on the filament stretching setup used in chapter 4.[238] Starting from a plate separation of 5 mm (filament diameter ~ 100 μm), the proteins were exposed to acidic or basic vapour which was created by bringing a 2 cm x 2 cm tissue paper soaked with 40 μl of either a 3 M, 17.5 M acetic acid or a 14.8 M ammonium hydroxide solution close to the filament for 10 seconds. For the experiments at constant spinning speed the upper plate of the tensile tester was raised to reduce the filament diameter to around 50 to

100 μm after the silk proteins were loaded. This is done to recreate the conditions of the natural spinning process where the pH of the proteins drops inside the spinning duct (diameter 50 to 100 μm) prior to spinning. The proteins were then exposed to vapour from a 17.5 M acetic acid solution for 10 seconds before the stretching commenced. Fibre spinning was performed at 5, 7.5, 20 and 40 mm/s.

5.3.2 Fibre characterisation

The molecular alignment of the fibres was analysed by polarized light microscopy (Diaphot-TMD inverted microscope, Nikon Corp., Japan). The fibres were oriented at a 45° angle to the crossed polarizers and images were taken with a Moticam 2500 microscope camera (Motic Electric Group Co., Ltd, China).

Fourier-transform infrared spectroscopy measurements on single fibres were performed in attenuated total reflection (ATR) mode on a Nicolet 380 spectrometer (Thermo Scientific, USA). A polarizer with a ZnSe holographic wire grid (Thorlabs, USA) was used to polarize the electric field of the infrared beam perpendicular to the plane of incidence (*s*-polarized). Parallel and perpendicular spectra ($A_{\perp}$ and $A_{\parallel}$) were collected for each fibre from 800 cm^{-1} to 4000 cm^{-1} at a resolution of 4 cm^{-1} by averaging over 128 scans. A baseline correction was applied by subtracting the offset value at 1730 cm^{-1} and afterwards both spectra were normalized to the intensity at 1335 cm^{-1} which had been shown to be independent of orientation.[231] Both spectra were then normalised again to the amide I peak of the spectra to account for the amount of sample measured and therefore allow a comparison between different fibres. The protein chain alignment was analysed by the ratio of the amide I peak intensities ($A_{\perp}/A_{\parallel}$) and the amide I peak location in the $A_{\perp}$ spectra revealed information about the amount of order within the fibres.

Mechanical testing was performed on a Zwick Z0.5 testing machine (Zwick GmbH & Co. KG, Germany) with a 5 N load cell at standard lab conditions (23 ± 1 °C, 50 ± 5% RH). The

gauge length was set to 5 mm and tests were performed at a strain rate of 2 mm/min. The fibre diameter was determined as the average of at least 15 different measurements along the fibre axis from micrographs taken with a Diaphot-TMD inverted microscope (Nikon Corp., Japan).

5.4 Results and discussion

Upon exposing silk proteins to acidic vapour during extensional flow, the feedstock viscosity (here indicated by the extensional stress) increases (Figure 45a), supporting previous observations in shear experiments.[53] This increase in viscosity is dependent on the concentration of the acid and was not observed in the absence of acidic vapour or under basic vapour exposure. I found that if the sample was exposed to the acidic vapour for too long (>15 seconds) the proteins completely gelled, and stretching was no longer possible. The resulting fibres spun in vapour from a 17.5 M acetic acid solution reveal a significantly improved strength and elasticity (Figure 45b and Table 6), alongside a concurrent development of structural features comparable to those spun in air and lower acetic acid concentrations (Figure 46).

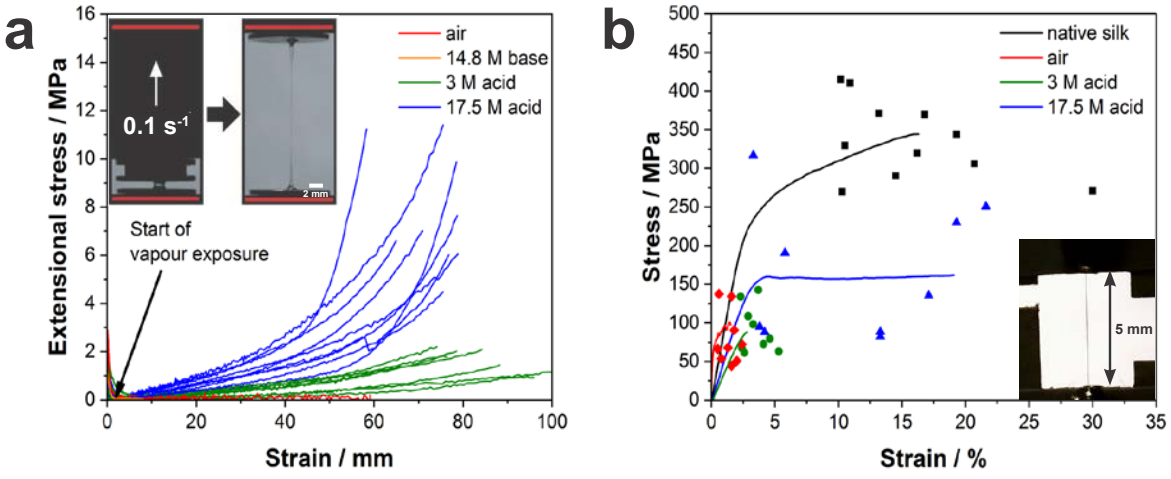

Figure 45: Mechanical characterisation of fibres created in air and acidic vapour at a constant strain rate of 0.1 s^{-1}. **a** Extensional stress of silk proteins after exposure to acidic/basic vapour. **b** Mechanical properties of fibres stretched in air and vapour from different acetic acid solutions compared to native silkworm silk.

Table 6: Mechanical properties of fibres stretched in different vapour environments at a constant strain rate of 0.1 s^{-1} compared to *Bombyx mori* silk.

	n	Breaking stress σ / MPa	Stiffness E / GPa	Elongation at break ε / %	Toughness W_{break} / MJ m^{-3}	Diameter d / µm
native silk	12	337.8 ± 46.2	7.0 ± 1.1	16.1 ± 3.9	42.1 ± 11.2	17.1 ± 3.5
air	10	81.5 ± 31.4	29.1 ± 19.3	1.4 ± 0.6	0.8 ± 0.5	14.4 ± 3.2
3 M	10	91.5 ± 27.5	3.7 ± 1.5	3.4 ± 1.0	1.9 ± 0.8	33.7 ± 2.2
17.5 M	10	163.9 ± 77.2	5.6 ± 3.8	12.1 ± 6.8	16.6 ± 13.9	48.7 ± 2.4

The high variability in strength of the 17.5 M samples is likely due to different amounts of acidic vapour taken up by the fibre which results in various degrees of crystallisation which impacts the strength. Interestingly, the samples prepared with 17.5 M acetic acid have the thickest diameter (Table 6) which can be attributed to the increased resistance towards necking due to increased gelation which counteracts the thinning of the filament during stretching. The improvement in mechanical properties can be attributed to the development of structural features in the fibre during stretching in an acetic acid atmosphere. Using polarized light microscopy (Figure 46a) and FTIR spectroscopy (Figure 46b), an increase in molecular alignment and a reduction in the amount of disorder in the pH activated feedstock fibres compared to the ones stretched in air was observed. The properties of the pH activated fibres match those of a naturally spun silk (Figure 46 c and d).

This suggests that by lowering the pH of native silk proteins and subsequent extensional stretching, fibres with structural features can be spun.

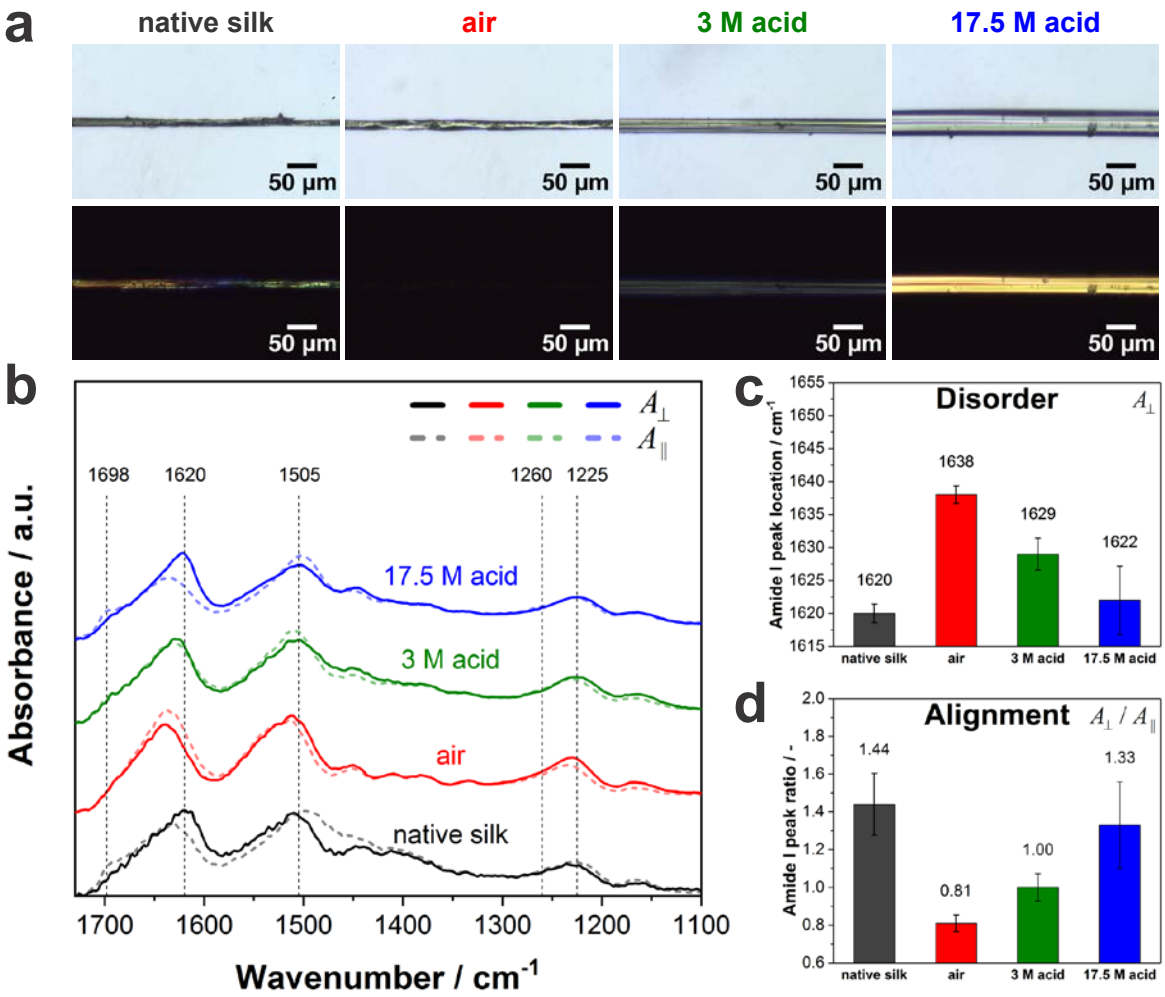

Figure 46: Structural characterisation of fibres created in air and acidic vapour at a constant strain rate of 0.1 s^{-1}. **a** Polarized optical microscopy images reveal orientation in silk fibres when stretched in an acidic environment. **b** Parallel and perpendicular FTIR spectra ($A_\perp$ and $A_\parallel$) of fibres created in different vapour environments compared to natural *Bombyx mori* silk. The most important peak assignments are 1698 cm^{-1} (Amide I, β-sheets in ∥ orientation), 1620 cm^{-1} (Amide I, β-sheets in ⊥ orientation), 1505 cm^{-1} (Amide II, β-sheets in ∥ orientation), 1260 cm^{-1} (Amide III, β-sheets), 1225 cm^{-1} (Amide III, unordered).[231] **c** The amount of disorder in the fibres can be analysed by the amide I peak location. A higher wavenumber indicates a lower hydrogen bonding density and therefore a higher amount of disorder. **d** The analysis of the Amide I peak ratio ($A_\perp/A_\parallel$) provides a qualitative measure of the molecular alignment in the fibres confirming the results from polarized microscopy.

My results above have shown that pH activation prior to extensional flow appears necessary to create structural features in silk fibres. However, in order to test whether structural features in silk can be formed solely by lowering the pH, I exposed a thin hand drawn protein filament laid upon an FTIR-ATR crystal to acidic vapour *without* stretching (Figure 47, inset image). Even after 60 seconds of vapour exposure, the FTIR spectra does not indicate any structural changes (Figure 47). In a second experiment, a protein filament was exposed to acidic vapour for 10 seconds and then stretched with tweezers and tested. This pH activated, extended, sample displayed an amide I peak shift from 1641 to 1625 cm^{-1}, confirming that only through the combination of protein acidification *followed* by extensional flow can structure formation occur.

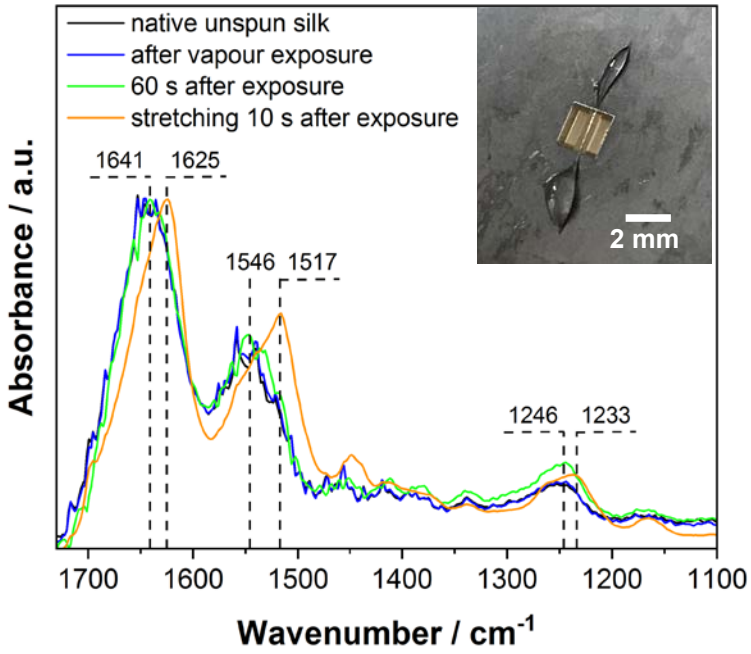

Figure 47: The influence of pH change on the structure in silk. FTIR spectra of a thin filament of native silk proteins (see inset picture) before and after exposure to vapour from a 17.5 M acetic acid solution. Structural development in the fibres can only be observed after stretching.

By means of an explanation, I hypothesise that a drop in pH initiates two pathways that prepare silk proteins for flow-induced fibre formation. Firstly, at a pH around 6, the N- and C-terminal domains of multiple silk proteins refold and entangle, increasing the effective molecular weight which manifests as an increase in feedstock stiffness (modulus and

relaxation time), and permits a more efficient uptake of a subsequently applied mechanical stress.[53, 242] Secondly, a further drop in pH close to the silk protein fibroins' isoelectric point of 4.2, reduces the negative repulsive forces of neighbouring chains by protonation of charged amino acid groups.[293] This allows chains to come closer together during flow, increasing alignment and subsequent hydrophobic interactions and reducing the stability of the protein, making it more likely to denature. Once entangled and destabilised, a subsequent extensional flow field, in excess of that which can be dissipated through relaxation of the now-gelled protein network, provides the mechanical stress input necessary to drive protein denaturation, ultimately leading to the formation of intra- and intermolecular β-sheets and a molecularly oriented, solid fibre.[53, 242]

Building upon these observations and theory, using just pH activation and extension, I was able to spin silk fibres *ex vivo* without a specialised spinning device, chemical fixation or post draw.[1] Spinning using extension rates akin to natural spinning speeds (5 and 7.5 mm/s), resulted in fibres that perform like natural silkworm silk (Figure 48a). At higher speeds (20 and 40 mm/s), fibre strength is significantly improved, supporting previous forced reeling observations.[33-34] Of particular note is that in a departure from many other artificially spun silks, the shape of the stress/strain curves produced here also closely resembles that of the natural fibre, implying that the stress dissipation mechanisms (yield and work hardening) are similar which is most likely due to the development of comparable structural hierarchies during spinning.[1, 15, 156, 160, 168, 294] Additionally, when comparing the fracture strength of the *ex vivo* spun fibres from this study to artificial silk fibres in chapter 1 (see also Figure 11, Porter *et al.*[157]), I found that *ex vivo* spun fibres follow a trendline for the generic energy release rate that is much closer to that of silkworm silk (Figure 49). A lot of the *ex vivo* spun fibres even fall directly in the area where native silkworm fibres are,

indicating that the *ex vivo* spun fibres exhibit an internal, hierarchical structure that results in a strength, stiffness and diameter that is comparable to natural silkworm fibres.

Finally, the strongest *ex vivo* spun fibre has a breaking strength of 719.2 MPa (diameter of 23 μm), which is two times stronger than natural *B. mori* silk and the strongest as-spun silk fibre reported to date.[1]

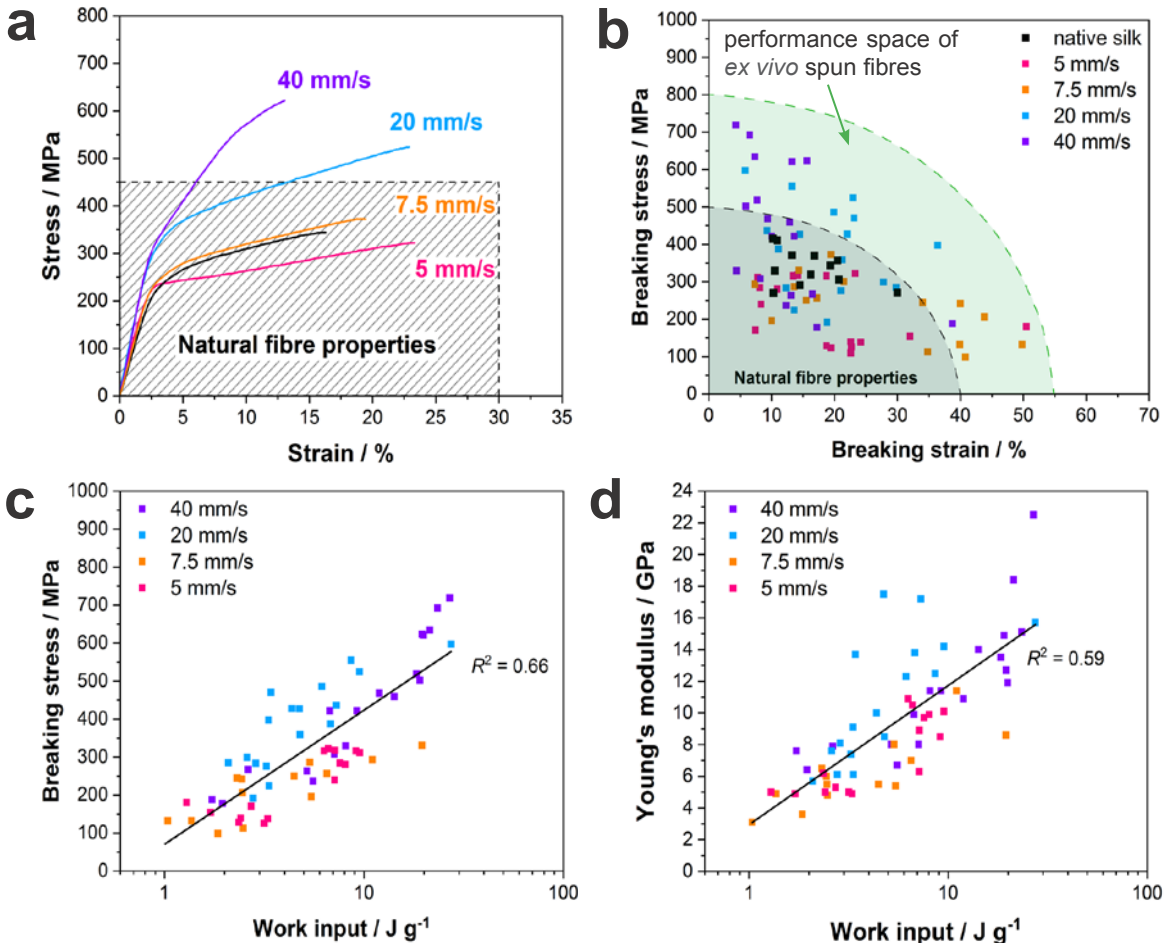

Figure 48: Spinning silk fibres ex vivo. **a** Stress/strain curves of *ex vivo* spun silk fibres with the best combination of strength and toughness compared to the natural fibre property region of *Bombyx mori* silk. **b** Breaking stress/strain points of all spun fibres spun at different extension speeds. The green area indicates a performance space of properties that can be achieved with *ex vivo* spun fibres depending on protein gelation and extension speed. **c** Breaking stress plotted against work input required for fibre formation. The work input is a qualitative measure of the degree of protein gelation. **d** Young's modulus plotted against work input required for fibre formation which shows a similar trend as the breaking stress.

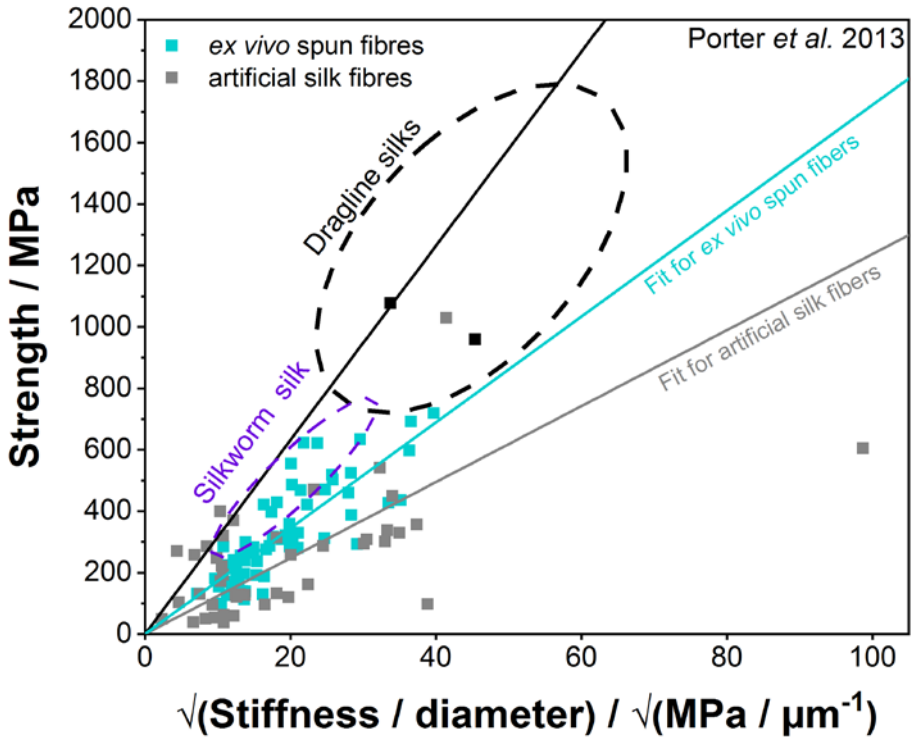

Figure 49: Comparison of the fracture-strength relation of *ex vivo* spun and artificial silk fibres. Compared to the artificial silk fibres in chapter 1, *ex vivo* spun fibres follow a fit that is closer to the trendline for the generic energy release rate of natural silk fibres. The black squares represent the values from Ha *et al.*[110].

However, despite impressive individual fibre performance, collectively the mechanical properties of *ex vivo* spun fibres appear to display a significant degree of variation (Figure 48b). I hypothesise this could be related to the different amounts of acid absorbed by the feedstock and therefore its degree of gelation prior to spinning, which will in turn affect its ability to absorb and respond to mechanical stress input.[53] In light of previous work from our group investigating the role of silk denaturation and solidification via shear, it is known that silk feedstocks require a critical shear stress threshold to be surpassed[266] and more recently a certain degree of mechanical work[295]. Hence to verify this, I compared the work input to form a fibre, as defined by the area under each fibre's stretching curve (as shown as an example in Figure 50 for fibres spun at 20 mm/s) to its breaking stress (Figure 48c) and Young's modulus (Figure 48d).

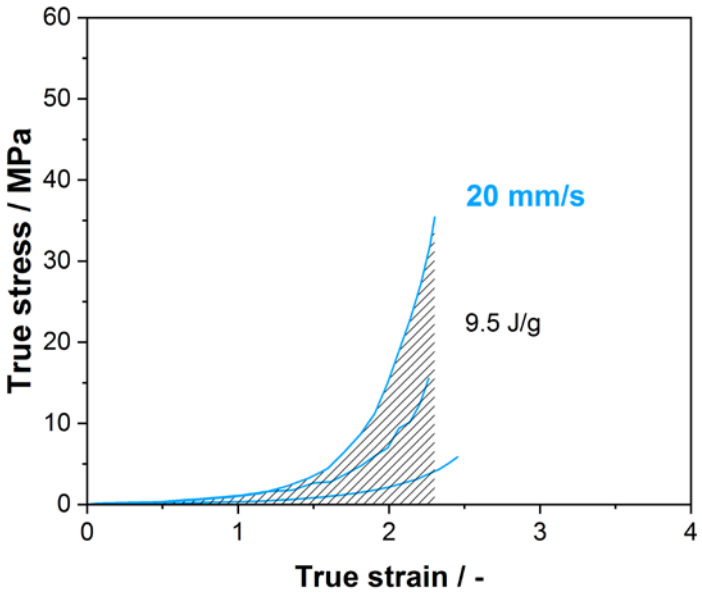

Figure 50: Calculation of the work input required for fibre formation. The stretching graphs for all fibres (similar to Figure 45a) were transformed into true stress/true strain graphs and then integrated to calculate the work input during fibre formation. Here, one example is shown for a fibre created at 20 mm/s. The work input for fibre stretching is an indication of the protein gelation prior to stretching.

Mostly the work required for feedstock solidification, centring around 7.48 ± 6.57 J g^{-1} agrees well with recent DSC (1.78 ± 0.25 J g^{-1})[296] and shear rheology (2.75 ± 1.37 J g^{-1})[295] studies[295-296]. Moving beyond an average, when plotting breaking stress against work input for each individual fibre, a correlation is observed (Figure 48c and d). Such a correlation indicates that the degree of gelation prior to processing affects fibre performance and by adjusting the feedstock pH as well as the spinning speed, fibre properties can be tuned to be very strong and stiff (high work input) or weaker but more extensible (low work input) (Figure 48c and d).

However, the use of a cumulative work input parameter has limitations as it does not account for the time period in which the work was applied. Therefore, in Figure 51 the *rate* of work input (work input divided by total extension time, Figure 51a) was calculated for all *ex vivo* spun fibres from Figure 48b. In Figure 51b and c the resulting fibre's structural and mechanical properties are displayed in dependence of the rate of work input.

In general, fibre mechanical and structural properties improve with rate of work input (Figure 51a and b) with the results suggesting that a rate of work input of 2 J/(g s) $^{-1}$ is required to spin fibres with properties similar to native *Bombyx mori* silk. By comparison fibres spun with a low rate of work input (< 0.3 J (g s)$^{-1}$) tend to have less molecular alignment (Figure 51c) and a high amount of disorder, which explains their high extensibility and toughness but low strength. Feedstocks subjected to a medium rate of work input (0.3 to 8 J (g s)$^{-1}$) exhibit alignment under polarised light (micron scale) but still possess a certain degree of disorder under FTIR (nano scale), indicating that the mechanical stress applied during processing may be sufficient to align the proteins, but insufficient to generate complete protein denaturation and β-sheet conversion. Under a high rate of work input (> 8 J (g s)$^{-1}$) fibre strength increases further, while the breaking strain and also toughness are decreased as the amount of amorphous disordered regions responsible for the extensibility is reduced.[297]

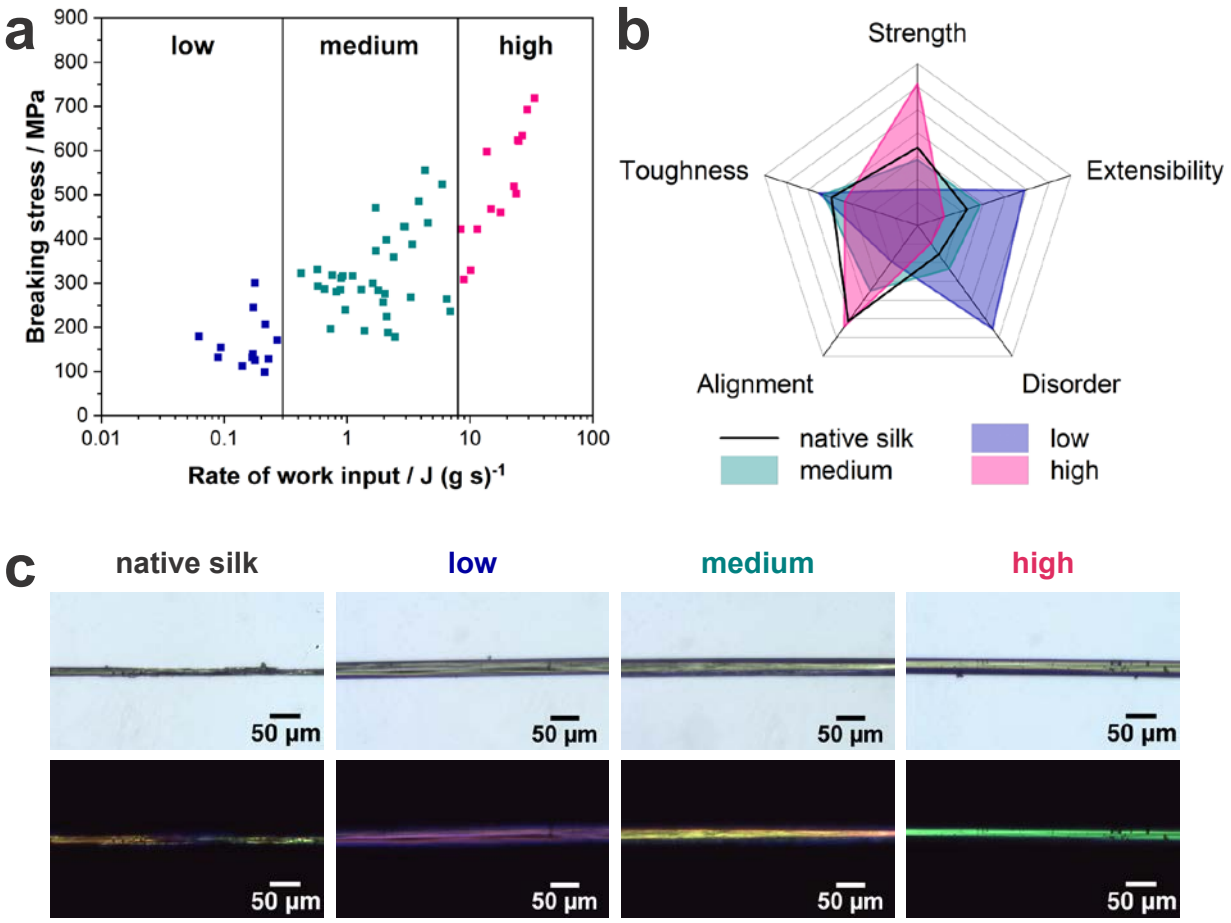

Figure 51: Silk's properties in dependence of the rate of work input. **a** Breaking stress plotted against the rate of work input which is separated into low (< 0.3 J (g s)$^{-1}$), medium (0.3 to 8 J (g s)$^{-1}$) and high (> 8 J (g s)$^{-1}$). **b** Mechanical and structural properties of fibres spun with low, medium and high rates of work inputs. **c** Polarized light micrographs of native silk as well as silk fibres spun with a low, medium and high rate of work input.

These results indicate that apart from spinning speed, which up to now was the main lever to change a silk fibre's properties,[33-34] the protein gelation prior to spinning also affects the mechanical performance. The influence of both parameters can be described by the concept of rate of work input. Therefore, in order to produce silk fibres with good mechanical properties, the rate of work input during spinning has to be high. This can be achieved by gelling the feedstock by pH activation to such a high degree that it can afterwards still be stretched at a high spinning speed. In the context artificial silk spinning, this means that feedstocks have to be developed that are able to absorb enough work input that contributes towards structure formation.

5.5 Conclusions

To conclude, this study draws clear links between processing and performance in native silk proteins through two key variables, pH activation followed by extensional flow, connecting both together through the concept of rate of work input. From a scientific perspective, the results presented have supported and validated previous observations and simulations surrounding hierarchical structure development in silk which in the future may facilitate new insights into silk evolution (i.e. the interaction between animal behaviour and physiology). From an engineering perspective, I have successfully spun fibres without the need for complex spinning devices, chemical fixation or post draw, with properties that meet, and exceed, natural *B. mori* silk, including ones that are the strongest and toughest reported to date. Taken together I hope my results may lead to new bio-inspired energy efficient processing strategies that are driven by work input optimization and where excellent mechanical properties are self-emergent. For such bio-inspired processes it is also important to understand the influence of metal ion composition on the native silk feedstock to develop optimised spinning dopes. The influence of different metal ion (KCl, $CaCl_2$, LiBr and LiCl) on the flow properties of native silk will therefore be addressed in the following chapter.

CHAPTER 6:

The influence of metal ions on native silk rheology

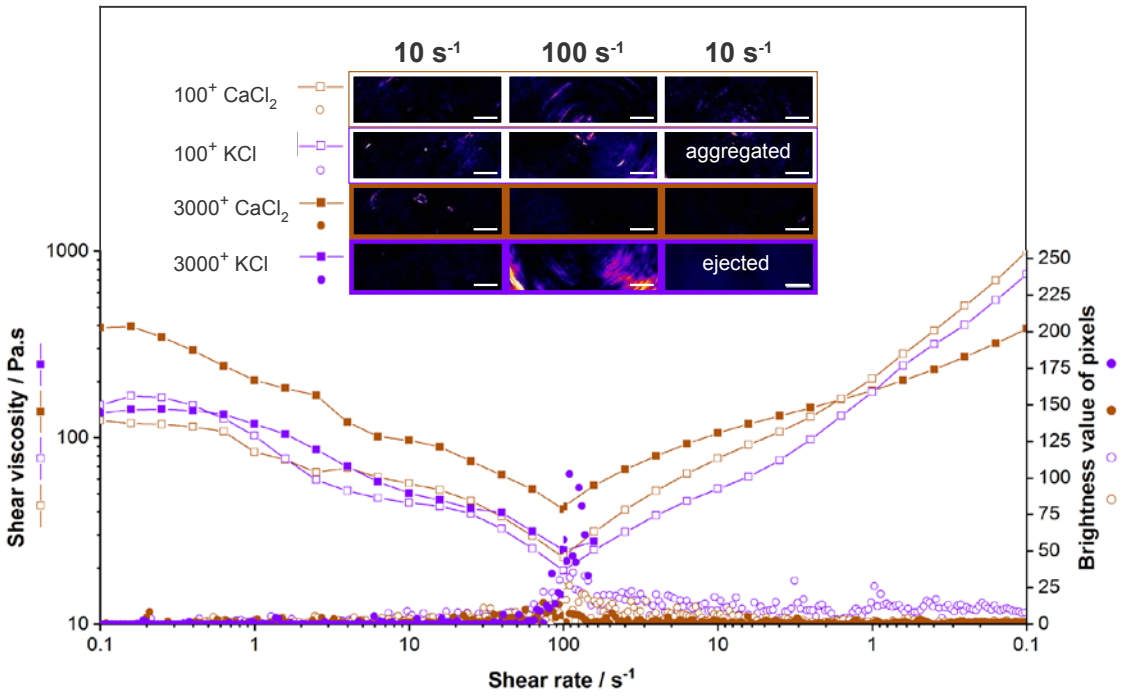

In previous chapters I have studied the effect of extensional flow and pH change on native silk proteins and shown how both mechanisms can be used to spin fibres *ex vivo* with structural and mechanical properties that resemble those of native silk fibres. However, looking back to the natural spinning process, there is a third mechanism, metal ion composition, that is hypothesised to plays a major role in modifying the flow properties of the silk feedstock during spinning. This understanding is important for the development of bio-inspired feedstocks for artificial silk spinning and will therefore be investigated in this chapter.

6.1 Abstract

Silk fibres are spun from a liquid protein feedstock that is processed into a solid fibre with remarkable properties. During this transition the silk proteins undergo changes in the chemical environment as they flow along a specialised silk gland including a pH drop and shift in metal ion composition. While the effect of pH change on the silk feedstock is largely understood, the influence of metal ions has only been manifested by correlative work and observations.

Therefore, here I provide a causative study of how the most abundant metal ions in the silk feedstock, Ca^{2+} and K^{+}, affect its flow properties. My results show that Ca^{2+} ions are involved in providing ideal storage conditions for the native silk feedstock by forming a stable salt bridge network between protein side chains which increases the viscosity and prevents molecular alignment and aggregation. In contrast, the addition of K^{+} ions promotes molecular alignment and aggregation and therefore seems to transfer the silk feedstock into a spinning state. Additionally, I characterised the influence of LiBr and LiCl on silk's flow properties which are solvents that are often used to prepare regenerated silk solutions. Both salts promote molecular alignment and prevent aggregation by reducing hydrogen bonding between the protein side chains.

My results provide a clearer picture what role metal ions play in providing ideal conditions that allow silk proteins assemble into highly hierarchical structures that are responsible for the remarkable fibre properties.

6.2 Introduction

Silk spinning in Nature is a sophisticated process that ultimately results in strong and tough fibres in a benign environment that can easily compete against synthetic alternatives.[5, 17] The secret behind such remarkable properties lies in the self-assembly of protein chains into hierarchical structures under carefully controlled conditions. It is known that such conditions include a change in pH and the ionic environment as well as a defined mechanical energy input via flow.[47, 275-276] While recently a much clearer picture has been drawn about the influence of shear, extensional flow[238, 298] and pH change[44, 46-47, 57] on native silk feedstocks, the final processing parameter, the role of metal ions, is not fully understood.

Several previous studies have shown the influence of externally introduced metal ions on the properties of the spun fibre through altering the interchain bonding type, [299] or the secondary structure of the silk proteins.[299-301] However, there is little evidence to directly link the presence of metal ions to changes in the flow properties of the unspun silk feedstock before silk is spun, despite several studies into the natural system indicating that metal ions are regulated in the spinning duct.[48-49, 243, 302]

Recent evidence of the causative influence of metal ions on the structure and properties of silk fibres has been provided by genetic modification of the metal ion channels in the silk duct.[303] By suppressing the amount of K^+ ions in the fibre, fibres were weaker and had more random coil structures, whereas overexpression of Ca^{2+} increases the amount of helical

and β-sheet structures and fibre strength.[303] Hence the role of metal ions clearly has an impact on the spinning process, and thus is an important factor to understand and potentially control during any attempt at artificial silk spinning.[1]

Generally the Hofmeister series[304] is used to describe and understand the interactions between metal ions and protein solutions. Yet, this is just a phenomenological description of how cations and anions interact with the peptide bond and therefore hardly applicable to silk which consists of a huge amount of charged, polar and hydrophobic amino acids that can interact differently with metal ions. Metal ions, for example, can form or suppress salt bridges, which are non-covalent, pH-dependent bonds, due to electrostatic interactions with negatively (Asp, Glu, Tyr, Cys and C-terminal carboxylate groups) and/or positively (His, Lys, Arg, and N-terminal amino groups) charged amino acid groups that are in close proximity.[305-308] Salt bridges can induce constraints in the mobility of molecular chains which affects protein structure and interaction, potentially manifesting as changes in solution flow properties.[45, 48-50, 309]

For silk solutions, the effect of metal ions on silk protein structure has largely been limited to studies focussing on dilute[45, 55] and regenerated silk solutions.[49] For dilute spider silk solutions it has been shown that metal ions such as Al^{3+}, K^{+}, and Na^{+} induce structural changes towards a more oriented structure while divalent ions such as Ca^{2+} and Mg^{2+} were found to stabilize a disordered state. Cs^{+} and Li^{+} on the other hand did not any significant effect.[55, 310] However in contrast, for silkworm silk solutions Ca^{2+} and Mg^{2+} ions were found to induce network formation with carboxylic groups in dilute fibroin solutions that are broken down when small shear forces are applied.[45]

When switching focus to the natural system, for native *B. mori* silk feedstock it has been suggested that metal ions are involved in providing optimised storage/spinning conditions for the silk proteins in the gland prior to spinning.[45, 49, 55] Ca^{2+} and K^{+} are the most abundant metal ions in the silkworm feedstock and it was found that the amount of K^{+} along with other ions (Mg^{2+}, Cu^{2+}, Zn^{2+}, Na^{+}) increases from the posterior to the anterior gland section whereas the amount of Ca^{2+} was shown to either decrease or stay constant.[49, 51] This led to the hypothesis that Ca^{2+} ions induce salt bridge formation between negatively charges amino acids while other divalent ions such as Mg^{2+}, Cu^{2+} are thought to induce transition from a helical structure to β-sheets.[311-312] Other studies have suggested that K^{+} ions help to break down the protein network as they have been shown to accelerate the dissolution of the native silk feedstock.[49] These findings are in good agreement with most recent findings that suggest that the increase in K^{+} ions in the silk feedstock is linked to a decrease in viscosity and therefore a break down in intermolecular forces.[51]

Therefore, based on this body of previously correlative work and observations, I conducted a causative study that shows how metal ions affect the flow properties of native silk. One major challenge is that direct mixing of metal ions into silk is not possible due to its high viscosity and shear sensitivity. Therefore, the native silk feedstock has to be diluted and reconcentrated after the metal ions are added. I show that reconcentration does not change the flow properties of native silk and thus was able to investigate the influence of Ca^{2+} and K^{+}, the most abundant metal ions in the *Bombyx mori* silk feedstock, on the flow properties of native silk proteins. I found that Ca^{2+} ions do not only increase the viscosity of the silk feedstock by salt bridge formation, but also make the proteins less sensitive to shear alignment and aggregation and therefore provide ideal storage conditions for silk. In contrast, K^{+} ions provide optimised spinning conditions by breaking down the salt bridge network and allowing the proteins to rearrange, align and aggregate.

Finally, I investigated the effect of Li cations on the flow properties of silk. Li^+ does not naturally occur in the silkworm but plays a crucial role in dissolving already spun silk in a process called regeneration. I found that by changing the cation from KCl to LiCl the silk feedstock does not aggregate when sheared. Thus, I also provide helpful insight into how residual Li cations can affect the properties of regenerated silk feedstocks.

6.3 Experimental Methods

6.3.1 Silk sample preparation

Native silk proteins were obtained from fifth instar *Bombyx mori* silkworms as reported in chapter 2. As mixing silk with metal ions cannot be achieved in its native state due to its high viscosity and shear sensitivity, the native silk proteins were dissolved in Type I water (ultrapure water with a resistivity higher than 18 MΩ.cm) to prepare a 2 wt.% batch solution. Around 10 ml from this batch solution was then used and in addition to a control solution, metal ions (KCl, $CaCl_2$, LiBr and LiCl) were added in such amounts to obtain a solution with 100 and 3000 positive charges per fibroin chain, respectively. 100 positive charges per fibroin chain is similar to the concentration of naturally occurring metal ions in the silk gland and 3000 charges was chosen to have saturated conditions.[51] Afterwards each of the solutions were concentrated in separate petri dishes by water evaporation to around 20 wt%. The concentration was done at standard lab conditions (23 ± 1 ˚C, 50 ± 5% RH) and the petri dishes were placed on a laboratory shaker which kept moving very gently. As a further set of controls native silk samples from an early and late cocoon stage were taken directly from the silk gland and characterised. The pH of all silk samples was measured using a glass free micro-electrode pH sensor (CupFET 3200-010 pH probe) with a SI600 pH meter (Sentron, The Netherlands). The concentration of the native silk proteins was determined gravimetrically. Therefore, the weight of around 200 mg of proteins from an

adjacent section was dried at 60 °C under vacuum until constant weight was achieved. The solid residue was then used to calculate the protein concentration.

6.3.2 Rheological characterisation

Rheological characterisation was performed on a Discovery Hybrid Rheometer (DHR 2, TA Instruments, USA) equipped with an 8 mm parallel plate geometry. A modular microscope accessory was attached to the rheometer which allows flow visualisation under polarized light with a 1x magnification objective. To prevent the samples from drying out, water droplets were placed around the geometry. Flow experiments were conducted in three steps: First, the sample was sheared at a constant rate of 1 s^{-1} for 100 seconds to remove any residual stresses that occur due to sample handling and loading as well as to evenly distribute the sample between the plates. Afterwards, oscillatory measurements were performed from 100 to 0.1 rad/s at a strain of 0.02. Lastly, all samples were subjected to a flow sweep test from 0.1 s^{-1} to 100 s^{-1} and then from 100 back to 0.1 s^{-1}.

The pixel brightness value was determined from the micrographs via ImageJ. Firstly, the brightness of the pictures was normalized to a gap height of 500 μm and a background image of the loaded sample prior to shearing was subtracted. The images where then converted to greyscale with the same threshold setting before false colouring was applied.

6.3.3 DLS measurements

At first, 1ml of the native 2% silk batch solution was added into a DLS Standard cell with the help of a pipette. The solution was then measured with a Zetasizer Nano ZS (Malvern Panalytical Ltd., UK) at 25°C after a 60 s equilibration time. Afterwards, the same sample was remeasured after metal ions were added from a 6 wt.% solution to adjust the amount to 100 positive charges per fibroin chain. Subsequently, more salt solution was added to reach 3000 positive charges and samples retested. This allowed a comparison of both

levels of salt concentrations using the same initial silk solution. This procedure was repeated for KCl, $CaCl_2$, LiBr and LiCl with 1ml of native silk proteins from the same 2% batch solution.

6.4 Results and discussion

6.4.1 Influence of silk preparation and natural variation comparison

Before the influence of individual ions are considered, as an important control, the flow behaviour of reconcentrated and native silk was compared to investigate whether our preparation process significantly altered silk's rheological properties. Furthermore, to ensure the entire natural range of silk's rheological properties were accounted for, native silk was extracted directly from the gland of *B. mori* silkworms both at an early and late stage during cocoon construction.[51] Reassuringly, our oscillatory data show that reconcentration does not significantly alter silk's rheological properties (Figure 52).[65] Both, storage (G') and loss (G'') moduli , as well as the angular frequency were normalised to the cross-over point (G_x/ ω_x) for a better comparison of the data as it removes the influence of concentration of the rheological properties.

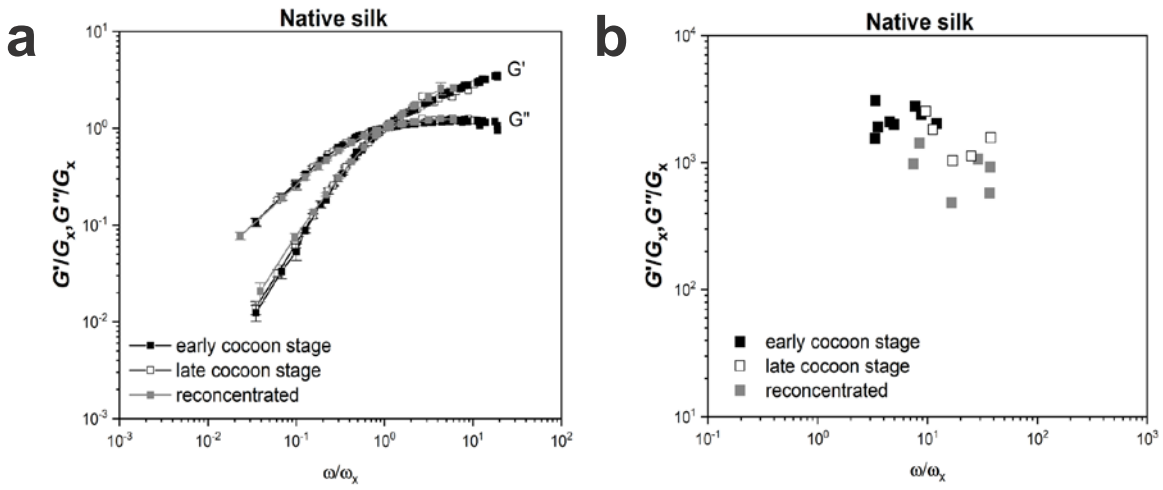

Figure 52: Oscillatory test for early and late cocoon as well as reconcentrated silk. **a** The storage (*G'*) and loss (*G''*) moduli for all three samples against the normalised angular frequency (ω/ω_x). **b** The cross-over modulus value G_x is plotted against the cross-over frequency ω_x for reconcentrated, early and late cocoon silk.

However, differences were observed when comparing the flow curves of all three samples (Figure 53). Native silk from an early cocoon stage shows very high viscosities at low shear rates compared late cocoon silk. This phenomenon has been previously observed and discussed by our group.[51] In short, Ca^{2+} ions are hypothesised to form inter-protein salt bridges between charged amino acid groups which increase the feedstock viscosity in the early cocoon stage. An increase of K^+ ions in the feedstock towards the end of cocoon construction displaces the Ca^{2+} ions in this physical network which reduces the protein chain interactions and therefore also the viscosity.[51] Recently this hypothesis has been extended to incorporate predictions from a “sticky reptation” model of silk rheological behaviour.[313]

In Figure 53, when the early cocoon stage samples are sheared, the network formed by the salt bridging Ca^{2+} ions appears to break down, as indicated by a sharp drop in viscosity not seen in the other samples. It also appears that over the timescale of this experiment (5 min), this network breakdown is not able to recover, as the viscosity only goes back to around 10% of its initial value after shearing ceases.

In addition, I found that not only the viscosity, but also the feedstocks' sensitivity for molecular alignment and aggregation changes between different cocoon stages (Figure 53). In the early cocoon stage there appears to be little molecular alignment under flow as indicated by the absence of birefringence during shearing. In contrast, silk from a late cocoon stage shows strong birefringence which ultimately leads to premature aggregation and silk gelation. I hypothesise that this behaviour is caused by the increased amount of K^+ ions in the silk feedstock at the late cocoon stage, weakening the network and allowing proteins to move, rearrange, align and interact with each other which results in a higher susceptibility for registration and subsequent aggregation.[51] Of particular note is that the flow behaviour of our reconcentrated silk lies in between these two extremes, thus making it a representative native silk sample.

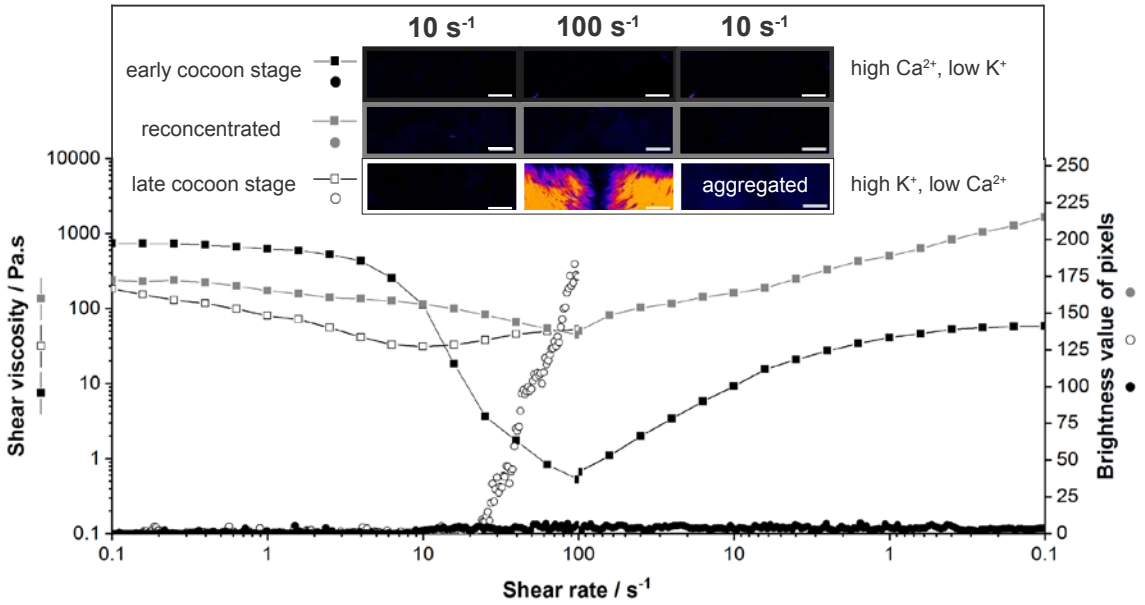

Figure 53: Shear viscosity and pixel brightness values for early and late coccon silk as well as reconcentrated silk. Both, viscosity and pixel brightness, are plotted against shear rate from 0.1 s^{-1} to 100 s^{-1} and back to 0.1 s^{-1}. The inset pictures show micrographs at 10 s^{-1}, 100 s^{-1} and again 10 s^{-1}. For better visualisation, each micrograph shows only half of the area of the 8 mm parallel plate. The scale bar is 1 mm and the flow direction is clockwise.

6.4.2 Effect of adding various metal ions on the properties of reconcentrated native silk

After adding metal ions to the dilute silk solutions in different amounts (100 and 3000 positive charges per fibroin chain) the samples were reconcentrated to natural silk concentrations which is around 21% protein dry weight[64] (see Table 7). It was also found that the pH of the silk solutions slightly decreased upon addition of KCl and $CaCl_2$ and increased when LiBr and LiCl were added.

Table 7: pH value and concentration of the different samples with metal ions.

Material	pH at 24 °C (when at 2% concentration)	Tested protein concentration in WT % (±SD, n=3)
Native silk (early cocoon)	6.96	21.1 ± 1.3
Native silk (late cocoon)	6.87	21.8 ± 0.8
Native silk reconcentrated	6.74	20.2 ± 1.8
Native silk + KCl 100	6.61	20.4 ± 2.2
Native silk + KCl 3000	6.72	21.2 ± 1.9
Native silk + $CaCl_2$ 100	6.48	18.7 ± 1.6
Native silk + $CaCl_2$ 3000	6.63	22.3 ± 2.1
Native silk + LiCl 100	7.13	19.5 ± 0.7
Native silk + LiCl 3000	7.11	20.7 ± 0.6
Native silk + LiBr100	7.27	19.5 ± 1.3
Native silk + LiBr 3000	7.61	19.3 ± 1.5

Adding 100 positive charges per fibroin chain of K^+ and Ca^{2+} ions, equivalent to that found in the native silk feedstock, does not significantly change the viscosity profile (Figure 54). Slight molecular alignment in the sample is visible and the samples aggregate towards the end of the shearing as indicated by the increase in viscosity. Whilst a more significant

response was expected, it may be that during sample preparation the addition of the salts in a dilute solution favours intramolecular salt bridge formation which saturates the proteins and reduces the opportunities for new intermolecular associations to occur when the sample is reconcentrated.

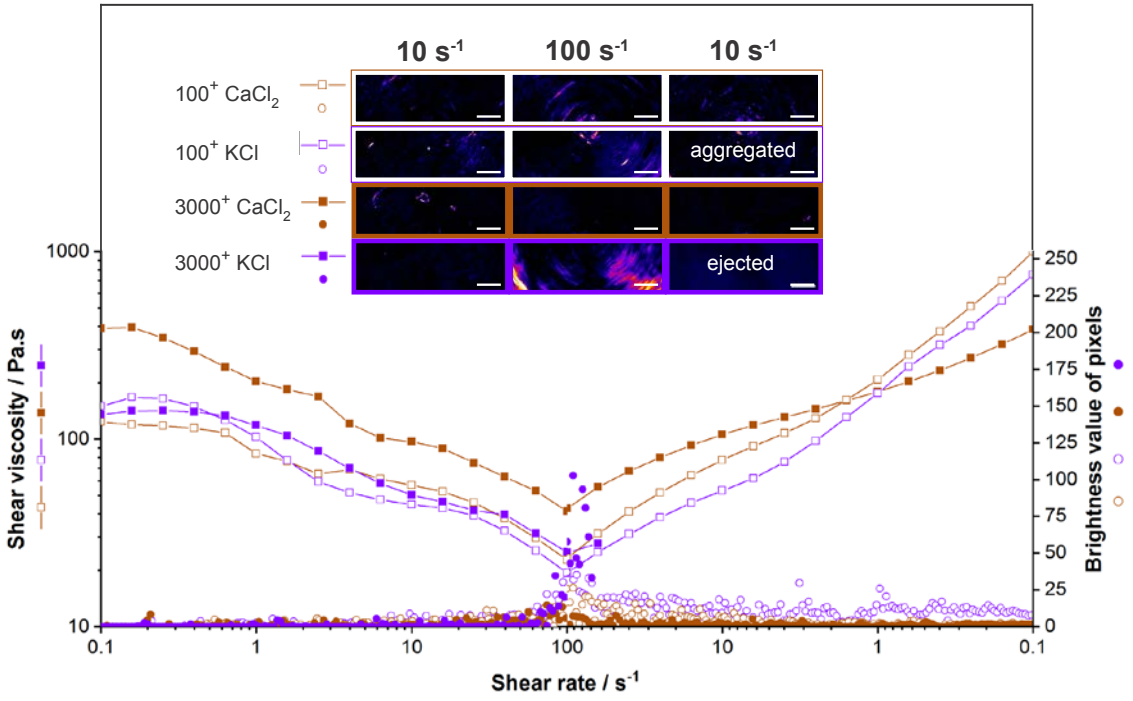

Figure 54: Shear viscosity and pixel brightness values for KCl and $CaCl_2$. The results for 100 and 3000 positive charges per fibroin chain are plotted against a shear rate from 0.1 s^{-1} to 100 s^{-1} and back to 0.1 s^{-1}. The inset pictures show the micrographs at 10 s^{-1}, 100 s^{-1} and again 10 s^{-1}. For better visualisation, each micrograph shows only half of the area of the 8 mm parallel plate. The scale bar is 1 mm and the flow direction is clockwise.

To probe this, an excess of 3000^+ charges per fibroin chain was added (Figure 54). Firstly, samples with $CaCl_2$ seem to have a much higher initial viscosity than 100^+ charges per chain and the alignment and aggregation behaviour are very similar to native silk from an early cocoon stage, suggesting intermolecular salt bridging is occurring. From the birefringence images no molecular alignment can be detected in the samples with $CaCl_2$, however in contrast, the KCl samples display alignment and aggregation similar to native silk from a late cocoon stage. This provides evidence that the differences in the flow and

aggregation behaviour of early and late cocoon native silk feedstocks are dependent on the Ca^{2+} and K^{+} ions present.

This difference in the aggregation behaviour of silk due to the presence of Ca^{+} and K^{+} ions was also observed in the dilute solutions before reconcentration (Figure 55). Subjecting samples to Dynamic Light Scattering the addition of $CaCl_2$ shows the highest hydrodynamic diameter indicating the formation of larger clusters between the silk proteins. While KCl does show slight cluster formation it is much less pronounced.

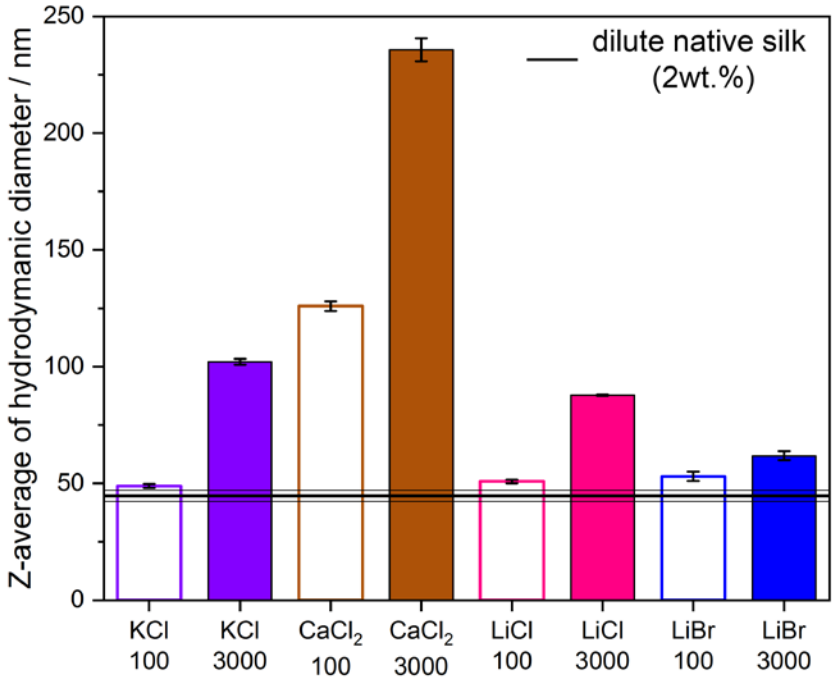

Figure 55: The Z-average of the hydrodynamic diameter determined by DLS measurements for dilute silk solutions (2 wt%) when different metal ions are added. In DLS, the Z-average is known as the cumulants mean and is an estimate of the width of the distribution (polydispersity index) which is defined in ISO13321.[236]

To probe the effect of other ions on silk feedstock's rheological properties, LiCl and LiBr were tested as both salt solutions are well known to dissolve spun silk fibres (Figure 56).[85] Unsurprisingly almost no aggregation was visible, however shear alignment is visible and the samples are aggregated at 100^{+} charges when the shearing is stopped. The pronounced alignment brings the chains closer together which facilitates aggregation.

However, at 3000⁺ charges the alignment of the chains is much more pronounced, but no aggregation happens, as the alignment is completely reversible.

I hypothesise that the increased sensitivity for alignment for both LiBr and LiCl is mainly evoked by the Li^+ cation. Li^+ is a kosmotrope which strongly binds water molecules[314], and forms a hydration shell around the cation. Previously it has been suggested that this lithium hydration sphere or the lithium cation itself bind to carbonyl groups of the proteins and therefore prevent formation of larger aggregates compared to other salt solutions which is confirmed by our DLS data in Figure 55.[315] At very high Li^+ concentrations (3000⁺ charges) the interaction between the protein chain is greatly reduced that the proteins do not aggregate when subjected to shear.

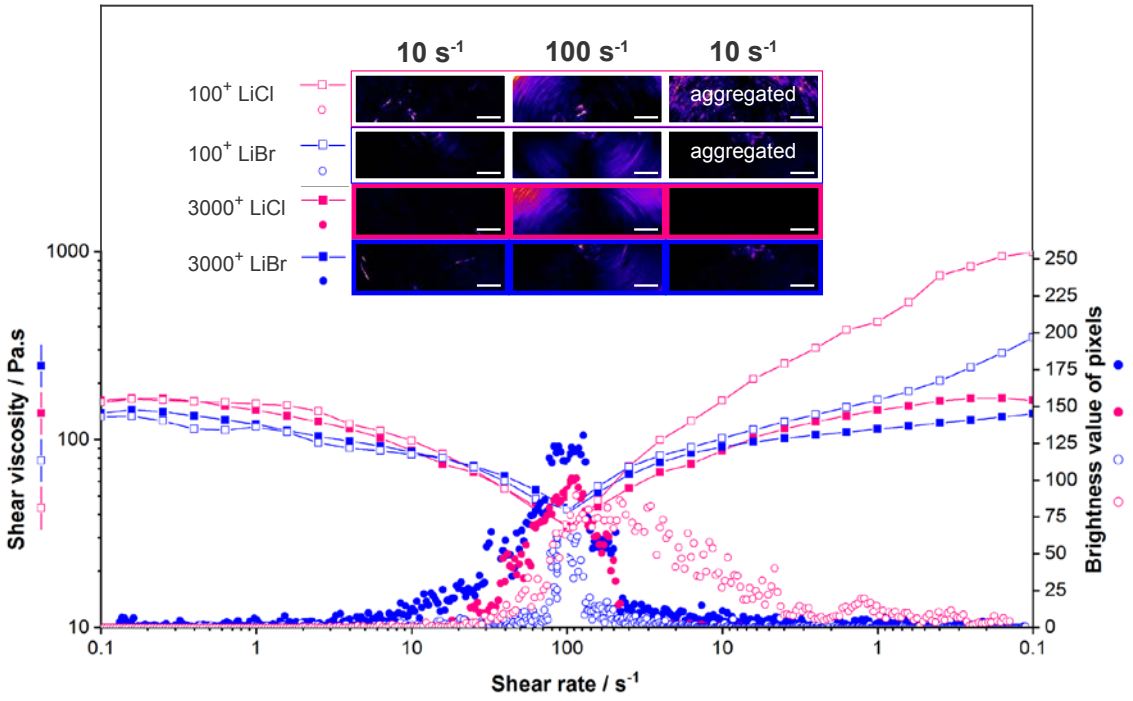

Figure 56: Shear viscosity and pixel brightness values for LiBr and LiCl.The results for 100 and 3000 positive charges per fibroin chain are plotted against a shear rate from 0.1s^{-1} to 100 s^{-1} and back to 0.1s^{-1}. The inset pictures show the micrographs at 10 s^{-1}, 100 s^{-1} and again 10s^{-1}. For better visualisation, each micrograph shows only half of the area of the 8 mm parallel plate. The scale bar is 1 mm and the flow direction is clockwise.

6.5 Conclusions

In this study I provide rheological evidence that metal ions can prepare silk proteins for either storage or spinning by altering their propensity to orient and aggregate under flow. I show that the addition of Ca^{2+} ions induces a stable, storage ready, feedstock by increasing viscosity, which we attribute to an increase in interchain interactions, presumably by salt bridge formation between charged side groups. In contrast, K^{+} ions prime silk for spinning by lowering feedstock viscosity and increasing protein sensitivity for molecular alignment and aggregation. However, there is a limit to suppression of salt bridge formation, by substituting K^{+} for Li^{+}, a common chaotrope for silk regeneration, I find that Li^{+} reduces molecular interactions to the extreme and ultimately prevents aggregation (see overview in Figure 57). Thus, from an evolutionary perspective the ability to control the bulk rheological properties of silk feedstocks through the simple addition of metal ions appears to be a very elegant and practical way to activate proteins for spinning. From an industrial perspective, not only does this work provide another process variable in bio-inspired silk production, but silk feedstocks themselves may provide insights into the design of biomaterials that are able to activate complex, hierarchical self-assembly processes on demand.

		100^{+} per fibroin chain		3000^{+} per fibroin chain	
Cation	Anion	Alignment	Aggregation	Alignment	Aggregation
K^{+}	Cl^{-}	✓	✓	✓✓✓	✓✓✓
Ca^{2+}	Cl^{-}	✓	✓	✗✗✗	✓
Li^{+}	Cl^{-}	✓✓✓	✓✓	✓✓✓	✗✗✗
Li^{+}	Br^{-}	✓✓	✓✓	✓✓	✗✗✗

Figure 57: Overview of how the combination of different cations and anions changes the sensitivity of the silk feedstock for alignment and aggregation

CHAPTER 7:

Summary and Future Outlook

The findings reported in this thesis provide the silk field with new insights into how silk proteins can assemble into strong fibres under benign conditions and therefore significantly further the current knowledge of silk spinning. The key findings of each chapter are listed in Table 7.

My initial results have shown that for silk spinning to be achievable it is not only about feedstock quality but also the correct processing. Native silk proteins, the current gold standard, for example, cannot be processed into strong and tough fibres under unnatural conditions such as precipitation in a coagulation bath.

In order to get a better understanding of the natural processing of silk, my thesis has investigated the influence of extensional flow on native silk proteins which to date has only been partially addressed despite being the main flow field occurring during fibre spinning. Although I show that silk is intrinsically suited for fibre spinning as the proteins strain harden when exposed to extensional fields, I also found that extensional flow alone is not responsible for creating the hierarchical structure in silk fibres. Structural features in silk fibres can only be created when the pH is dropped prior to extensional flow. The pH activation is required to induce protein gelation which conditions the silk feedstock to allow for work input via extensional flow. The properties of the fibres depend on the stretching speed as well as the degree of protein gelation (pH drop) whose combined influence can be described by the rate of work input. Therefore, my findings show that the complicated natural silk spinning process can be replicated by simply two mechanisms: pH activation and extensional flow.

Following, I have investigated the influence of metal ions have on the flow properties of the native silk feedstock. Firstly, I have shown that dilution and reconcentration of the native silk feedstock does not significantly alter its flow properties. Therefore, this method provides us with a means to successfully mix nanoparticles or metal ions with the high viscosity, shear sensitive silk proteins. By implementing this method and mixing silk with different

metal ions, I found that adding $CaCl_2$ to the silk proteins results in an increase in viscosity due to salt bridge formation which also prevents aggregation and alignment of the molecular chains. Therefore, $CaCl_2$ prepares the proteins for a storage state in which the proteins are less shear sensitive and do not aggregate. In contrast, adding KCl increases the sensitivity of silk for alignment and aggregation transforming the feedstock into a spinning state.

So, with this newly acquired knowledge about silk processing presented here does it mean that the problems surrounding artificial silk spinning are close to being solved? Well this would be a very strong claim and although I wish I could make it there are still obstacles that have to be overcome. Eventually, the knowledge presented here has to be transferred into processes that allow scaling up. A newly designed spinning rig has to implement a pH drop which is followed by extensional flow. Two possible approaches could be either by spinning the native silk feedstock into an acetic acid vapour atmosphere (a liquid solution would gel the proteins too quickly and prevent stretching) or adding chemicals to the feedstock that hydrolyse in water and release acidic compounds that gradually drop the pH. An example would be Glucono delta-lactone (GDL) which hydrolyses to gluconic acid.[316] The hydrolysis of such chemicals has to be perfectly timed so that the proteins can still be stretched out into fibres when leaving the nozzle.

Yet, the processing is not the only challenge. The quality of artificial silk proteins also has to be improved. Currently, it is very expensive to upscale reconstituted (redissolved silk in LiBr) and recombinant (produced by genetically modified organisms) silk feedstocks and they only have a low molecular weight that also lacks the pH responsiveness.[136, 143, 317] Therefore, such feedstocks cannot be processed the same way native silk proteins are in Nature. To address this problem, on the one hand, that means that better reconstitution processes have to be developed to reduce the degradation of redissolved silk proteins and preserve functional groups that allow a response to a drop in pH.[107-109, 114, 117] On the other

hand, longer proteins with functional groups have to be designed using recombinant methods.[75, 143] Both approaches are very challenging, and I suppose will need more research efforts to show success along these lines.

However, an alternative way could be the design new silk-inspired biopolymers that are water soluble and can be processed similar to native silk. Such biopolymers offer the advantage that they could be assembled into fibres using the same low energy-processing method as silk. Concerted efforts are currently focusing on addressing this challenge in an EU-funded research project called Flow-Induced Phase Transitions (FLIPT). A team of European researchers led by Dr. Chris Holland are investigating how materials such as cellulose or synthetic polymers can be modified so that they can be processed in a similar way to silk. In conclusion, although there are still challenges that have to be overcome to translate the learnings from spiders and silkworms into industrial processes, this thesis has helped to further our understanding how artificial silk proteins or newly designed biomaterials have to be designed to be processable with a low-energy impact route similar to silk.

Table 8: A summary of the key findings of each chapter of this thesis.

Chapter	Key findings
3	• Silk proteins cannot be pushed through a capillary with a similar geometry to the silkworm duct • Flow alone does not result in silk fibre formation • In order to align silk proteins via extensional flow, a very high pressure is required • Unnatural processing of natural silk proteins results in very weak and brittle fibres
4	• The surface tension of native silk proteins was determined • A conventional tensile tester can be used to characterise the extensional flow properties of silk • Silk proteins show strain hardening under extensional flow • Strain hardening behaviour of silk is independent of extension rate and silk's viscosity • Fibre formation under extensional flow is only possible at low extension rates due to dehydration
5	• Protein acidification prior to extensional flow is required for fibre formation • Protein acidification alone cannot induce structural changes in silk proteins • The structure of silk fibres and their mechanical properties depend on the amount of protein acidification prior to extensional stretching and the spinning speed • Rate of work input can describe the combined influence of protein acidification and spinning speed • Mechanical and structural properties depend on rate of work input during fibre formation • Fibres were spun from native silk proteins *ex vivo*
6	• Silk protein dilution and reconcentration does not change the flow behaviour of silk proteins • *Bombyx mori* silk proteins taken from different cocoon stages show a distinct flow and aggregation behaviour • Ca^{2+} ions form salt bridges between silk molecules and thus increase the viscosity and prevent molecular alignment and aggregation • K^{+} ions reduce molecular interaction between silk chains and allow alignment and aggregation • Adding LiBr and LiCl to silk proteins induces molecular alignment but prevents aggregation

APPENDIX A:

Supplementary Information

A.1 Information on data reported in Table 2

In literature, fibre properties are reported in different units. For a better comparison, all values were converted to MPa/GPa for strength and stiffness, % for extensibility, MJ/m³ for toughness and μm for fibre diameter. Below detailed information about the unit conversion is provided.

Conversion of toughness values:

- kJ/kg in MJ/m³

The density of silk is assumed to be 1.35 g/cm³ (1350 kg/m³)

Example:

50 kJ/kg · 1350 kg/m³ = 67.5 MJ/m³

Conversion of fineness values in diameter (μm):

- dtex in μm

A circular cross-sectional area and a density of 1.35 g/cm³ of the fibres are assumed for this calculation.[318-319]

The fineness of a fibre in dtex can be converted into a fibre diameter in μm with the following equation (A1):[318]

$$d = 1000 \cdot \sqrt{\frac{f \cdot 4}{\pi \cdot \rho_{silk} \cdot 10^4}} \qquad \text{(A1)}$$

where,

d - fibre diameter in μm.

f - fibre fineness in dtex.

ρ_{silk} - density of the silk fibre in g/cm³.

- den in μm

The fibre fineness in denier can be converted to dtex by multiplying the denier value by 10/9.

Example:

2 den · 10/9 = 2.22 dtex

For the conversion to diameter in μm the dtex value can be used with equation (1).

Conversion of stress and stiffness values:

- cN/dtex in MPa

The value in cN/dtex is first multiplied by the reported fibre fineness in dtex and divided by 100 to get N. The fineness is then converted into a diameter in mm. By dividing the value in N by the cross-sectional area of the fibre in mm^2, the stress value is converted to N/mm^2, which is equivalent to MPa.

- gf/d (also termed as gf/den, g/d or gpd) in MPa

The value in gf/d is multiplied by the reported fibre fineness in denier, and then converted from gf to N. The fineness in denier is then converted into a diameter in mm. By dividing the value in N by the cross-sectional area of the fibre in mm^2, the stress value is converted to N/mm^2, which is equivalent to MPa.

Missing values:

In some publications only some or none of the properties are directly reported. Where possible these values where extracted from stress-strain graphs or images.

Values from stress-strain graphs were extracted using the software PlotDigitizer. Diameter values from SEM images were measured using ImageJ[320].

All data that was either converted or extracted from a graph or image is clearly marked by a superscript.

A.2 Extensional flow videos

Video 1:

Video 2:

A.3 References

1. Koeppel, A.; Holland, C., Progress and Trends in Artificial Silk Spinning: A Systematic Review. *ACS Biomaterials Science & Engineering* **2017,** *3* (3), 226-237.
2. Vollrath, F.; Porter, D., Silks as ancient models for modern polymers. *Polymer* **2009,** *50* (24), 5623-5632.
3. Sutherland, T. D.; Young, J. H.; Weisman, S.; Hayashi, C. Y.; Merritt, D. J., Insect silk: One name, many materials. In *Annual Review of Entomology*, **2010,** *55*, 171-188.
4. Shultz, J. W., The origin of the spinning apparatus in spiders. *Biological Reviews* **1987,** *62* (2), 89-113.
5. Vollrath, F.; Knight, D. P., Liquid crystalline spinning of spider silk. *Nature* **2001,** *410* (6828), 541-548.
6. Vepari, C.; Kaplan, D. L., Silk as a biomaterial. *Progress in Polymer Science* **2007,** *32* (8-9), 991-1007.
7. Vollrath, F.; Porter, D.; Dicko, C., The structure of silk. In *Handbook of Textile Fibre Structure*, Woodhead Publishing: **2009**; Vol. 2, pp 146-198.
8. Babu, K. M., *Silk: processing, properties and applications*. Elsevier: **2013**.
9. FAOSTAT - Food and Agriculture Organization of the United Nations Statistics Division. http://faostat3.fao.org/download/Q/QP/E (accessed October 2016).
10. Holland, C.; Numata, K.; Rnjak-Kovacina, J.; Seib, F. P., The Biomedical Use of Silk: Past, Present, Future. *Advanced Healthcare Materials* **2019,** *8* (1), 1800465.
11. Asakura, T.; Kaplan, D., Silk production and processing. *Encyclopedia of agricultural science* **1994,** *4*, 1-11.
12. Heslot, H., Artificial fibrous proteins: a review. *Biochimie* **1998,** *80* (1), 19-31.
13. Keten, S.; Xu, Z.; Ihle, B.; Buehler, M. J., Nanoconfinement controls stiffness, strength and mechanical toughness of beta-sheet crystals in silk. *Nat Mater* **2010,** *9* (4), 359-367.
14. Holland, C.; Vollrath, F.; Ryan, A. J.; Mykhaylyk, O. O., Silk and synthetic polymers: Reconciling 100 degrees of separation. *Advanced Materials* **2012,** *24* (1), 105-109.
15. Mortimer, B.; Guan, J.; Holland, C.; Porter, D.; Vollrath, F., Linking naturally and unnaturally spun silks through the forced reeling of Bombyx mori. *Acta Biomaterialia* **2015,** *11*, 247-255.
16. Vollrath, F.; Madsen, B.; Shao, Z., The effect of spinning conditions on the mechanics of a spider's dragline silk. *Proceedings of the Royal Society B: Biological Sciences* **2001,** *268* (1483), 2339-2346.
17. Gosline, J. M.; Guerette, P. A.; Ortlepp, C. S.; Savage, K. N., The mechanical design of spider silks: From fibroin sequence to mechanical function. *Journal of Experimental Biology* **1999,** *202* (23), 3295-3303.
18. Bunsell, A. R., *Handbook of tensile properties of textile and technical fibres*. Elsevier: **2009**.
19. Vollrath, F.; Porter, D.; Holland, C., There are many more lessons still to be learned from spider silks. *Soft Matter* **2011,** *7* (20), 9595-9600.
20. Fu, C.; Shao, Z.; Fritz, V., Animal silks: Their structures, properties and artificial production. *Chemical Communications* **2009,** (43), 6515-6529.
21. Agnarsson, I.; Kuntner, M.; Blackledge, T. A., Bioprospecting Finds the Toughest Biological Material: Extraordinary Silk from a Giant Riverine Orb Spider. *Plos One* **2010,** *5* (9), e11234.
22. Zhao, H.-P.; Feng, X.-Q.; Shi, H.-J., Variability in mechanical properties of Bombyx mori silk. *Materials Science and Engineering: C* **2007,** *27* (4), 675-683.
23. Chen, F.; Porter, D.; Vollrath, F., Silk cocoon (Bombyx mori): Multi-layer structure and mechanical properties. *Acta Biomaterialia* **2012,** *8* (7), 2620-2627.
24. Hakimi, O.; Knight, D. P.; Knight, M. M.; Grahn, M. F.; Vadgama, P., Ultrastructure of insect and spider cocoon silks. *Biomacromolecules* **2006,** *7* (10), 2901-2908.
25. Poza, P.; Pérez-Rigueiro, J.; Elices, M.; Llorca, J., Fractographic analysis of silkworm and spider silk. *Engineering Fracture Mechanics* **2002,** *69* (9), 1035-1048.
26. Inoue, S.; Tanaka, K.; Arisaka, F.; Kimura, S.; Ohtomo, K.; Mizuno, S., Silk fibroin of Bombyx mori is secreted, assembling a high molecular mass elementary unit consisting of H-chain, L-chain, and P25, with a 6:6:1 molar ratio. *Journal of Biological Chemistry* **2000,** *275* (51), 40517-40528.
27. Shimura, K.; Kikuchi, A.; Ohtomo, K.; Katagata, Y.; Hyodo, A., Studies on silk fibroin of Bombyx mori. I. Fractionation of fibroin prepared from the posterior silk gland. *Journal of Biochemistry* **1976,** *80* (4), 693-702.
28. Tanaka, K.; Kajiyama, N.; Ishikura, K.; Waga, S.; Kikuchi, A.; Ohtomo, K.; Takagi, T.; Mizuno, S., Determination of the site of disulfide linkage between heavy and light chains of silk fibroin produced by Bombyx mori. *Biochimica et Biophysica Acta (BBA)-Protein Structure and Molecular Enzymology* **1999,** *1432* (1), 92-103.
29. Zhou, C. Z.; Confalonieri, F.; Jacquet, M.; Perasso, R.; Li, Z. G.; Janin, J., Silk fibroin: structural implications of a remarkable amino acid sequence. *Proteins: Structure, Function, and Bioinformatics* **2001,** *44* (2), 119-122.
30. Tanaka, K.; Inoue, S.; Mizuno, S., Hydrophobic interaction of P25, containing Asn-linked oligosaccharide chains, with the H-L complex of silk fibroin produced by Bombyx mori. *Insect Biochemistry and Molecular Biology* **1999,** *29* (3), 269-276.
31. Koh, L.-D.; Cheng, Y.; Teng, C.-P.; Khin, Y.-W.; Loh, X.-J.; Tee, S.-Y.; Low, M.; Ye, E.; Yu, H.-D.; Zhang, Y.-W.; Han, M.-Y., Structures, mechanical properties and applications of silk fibroin materials. *Progress in Polymer Science* **2015,** *46*, 86-110.
32. Asakura, T.; Okushita, K.; Williamson, M. P., Analysis of the Structure of Bombyx mori Silk Fibroin by NMR. *Macromolecules* **2015,** *48* (8), 2345-2357.

33. Mortimer, B.; Holland, C.; Vollrath, F., Forced reeling of bombyx mori silk: Separating behavior and processing conditions. *Biomacromolecules* **2013,** *14* (10), 3653-3659.
34. Shao, Z.; Vollrath, F., Materials: Surprising strength of silkworm silk. *Nature* **2002,** *418* (6899), 741-741.
35. Cunniff, P. M.; Fossey, S. A.; Auerbach, M. A.; Song, J. W.; Kaplan, D. L.; Adams, W. W.; Eby, R. K.; Mahoney, D.; Vezie, D. L., Mechanical and thermal properties of dragline silk from the spider Nephila clavipes. *Polymers for Advanced Technologies* **1994,** *5* (8), 401-410.
36. Jackson, C.; O'Brien, J. P., Molecular weight distribution of Nephila clavipes dragline silk. *Macromolecules* **1995,** *28* (17), 5975-5977.
37. Madsen, B.; Shao, Z. Z.; Vollrath, F., Variability in the mechanical properties of spider silks on three levels: Interspecific, intraspecific and intraindividual. *International Journal of Biological Macromolecules* **1999,** *24* (2-3), 301-306.
38. Vollrath, F.; Knight, D. P., Structure and function of the silk production pathway in the spider Nephila edulis. *International Journal of Biological Macromolecules* **1999,** *24* (2-3), 243-249.
39. Vollrath, F.; Holtet, T.; Thogersen, H. C.; Frische, S., Structural Organization of Spider Silk. *Proceedings of the Royal Society of London B: Biological Sciences* **1996,** *263* (1367), 147-151.
40. Kaplan, D.; Adams, W. W.; Farmer, B.; Viney, C., *Silk polymers: materials science and biotechnology*. ACS Publications: **1994**.
41. Scheibel, T., Spider silks: recombinant synthesis, assembly, spinning, and engineering of synthetic proteins. *Microbial cell factories* **2004,** *3*, 14.
42. Andersson, M.; Johansson, J.; Rising, A., Silk Spinning in Silkworms and Spiders. *International Journal of Molecular Sciences* **2016,** *17* (8).
43. Magoshi, J.; Magoshi, Y.; Nakamura, S. In *Mechanism of fiber formation of silkworm*, ACS symposium series (USA), **1994**.
44. Percot, A.; Colomban, P.; Paris, C.; Dinh, H. M.; Wojcieszak, M.; Mauchamp, B., Water dependent structural changes of silk from Bombyx mori gland to fibre as evidenced by Raman and IR spectroscopies. *Vibrational Spectroscopy* **2014,** *73*, 79-89.
45. Ochi, A.; Hossain, K. S.; Magoshi, J.; Nemoto, N., Rheology and dynamic light scattering of silk fibroin solution extracted from the middle division of Bombyx mori silkworm. *Biomacromolecules* **2002,** *3* (6), 1187-1196.
46. Domigan, L. J.; Andersson, M.; Alberti, K. A.; Chesler, M.; Xu, Q.; Johansson, J.; Rising, A.; Kaplan, D. L., Carbonic anhydrase generates a pH gradient in Bombyx mori silk glands. *Insect Biochemistry and Molecular Biology* **2015,** *65*, 100-106.
47. Asakura, T.; Umemura, K.; Nakazawa, Y.; Hirose, H.; Higham, J.; Knight, D., Some observations on the structure and function of the spinning apparatus in the silkworm Bombyx mori. *Biomacromolecules* **2007,** *8* (1), 175-181.
48. Foo, C. W. P.; Bini, E.; Hensman, J.; Knight, D. P.; Lewis, R. V.; Kaplan, D. L., Role of pH and charge on silk protein assembly in insects and spiders. *Appl. Phys. A* **2006,** *82* (2), 223-233.
49. Zhou, L.; Chen, X.; Shao, Z.; Huang, Y.; Knight, D. P., Effect of metallic ions on silk formation in the mulberry silkworm, Bombyx mori. *Journal of Physical Chemistry B* **2005,** *109* (35), 16937-16945.
50. Zhou, L.; Chen, X.; Shao, Z.; Zhou, P.; Knight, D. P.; Vollrath, F., Copper in the silk formation process of Bombyx mori silkworm. *FEBS Letters* **2003,** *554* (3), 337-341.
51. Laity, P. R.; Baldwin, E.; Holland, C., Changes in Silk Feedstock Rheology during Cocoon Construction: The Role of Calcium and Potassium Ions. *Macromolecular Bioscience* **2018,** 1800188.
52. Willcox, P. J.; Gido, S. P.; Muller, W.; Kaplan, D. L., Evidence of a cholesteric liquid crystalline phase in natural silk spinning processes. *Macromolecules* **1996,** *29* (15), 5106-5110.
53. Terry, A. E.; Knight, D. P.; Porter, D.; Vollrath, F., pH induced changes in the rheology of silk fibroin solution from the middle division of Bombyx mori silkworm. *Biomacromolecules* **2004,** *5* (3), 768-772.
54. Zong, X. H.; Zhou, P.; Shao, Z. Z.; Chen, S. M.; Chen, X.; Hu, B. W.; Deng, F.; Yao, W. H., Effect of pH and copper(II) on the conformation transitions of silk fibroin based on EPR, NMR, and Raman spectroscopy. *Biochemistry* **2004,** *43* (38), 11932-11941.
55. Dicko, C.; Kenney, J. M.; Knight, D.; Vollrath, F., Transition to a β-sheet-rich structure in spidroin in vitro: The effects of pH and cations. *Biochemistry* **2004,** *43* (44), 14080-14087.
56. Sparkes, J.; Holland, C., Analysis of the pressure requirements for silk spinning reveals a pultrusion dominated process. *Nat Commun* **2017,** *8* (1), 594.
57. Vollrath, F.; Knight, D. P.; Hu, X. W., Silk production in a spider involves acid bath treatment. *Proceedings of the Royal Society B: Biological Sciences* **1998,** *265* (1398), 817-820.
58. Viney, C., Natural silks: archetypal supramolecular assembly of polymer fibres. *Supramolecular Science* **1997,** *4* (1), 75-81.
59. Knight, D. P.; Knight, M. M.; Vollrath, F., Beta transition and stress-induced phase separation in the spinning of spider dragline silk. *International Journal of Biological Macromolecules* **2000,** *27* (3), 205-210.
60. Altman, G. H.; Diaz, F.; Jakuba, C.; Calabro, T.; Horan, R. L.; Chen, J.; Lu, H.; Richmond, J.; Kaplan, D. L., Silk-based biomaterials. *Biomaterials* **2003,** *24* (3), 401-416.
61. Mandal, B. B.; Kundu, S. C., Biospinning by silkworms: Silk fiber matrices for tissue engineering applications. *Acta Biomaterialia* **2010,** *6* (2), 360-371.

62. Radtke, C., Natural Occurring Silks and Their Analogues as Materials for Nerve Conduits. *International Journal of Molecular Sciences* **2016,** *17* (10), 1754.
63. Shah, D. U.; Porter, D.; Vollrath, F., Can silk become an effective reinforcing fibre? A property comparison with flax and glass reinforced composites. *Composites Science and Technology* **2014,** *101*, 173-183.
64. Laity, P. R.; Gilks, S. E.; Holland, C., Rheological behaviour of native silk feedstocks. *Polymer* **2015,** *67*, 28-39.
65. Laity, P. R.; Holland, C., Native Silk Feedstock as a Model Biopolymer: A Rheological Perspective. *Biomacromolecules* **2016,** *17* (8), 2662-2671.
66. Holland, C.; Terry, A. E.; Porter, D.; Vollrath, F., Natural and unnatural silks. *Polymer* **2007,** *48* (12), 3388-3392.
67. Xia, X.-X.; Qian, Z.-G.; Ki, C. S.; Park, Y. H.; Kaplan, D. L.; Lee, S. Y., Native-sized recombinant spider silk protein produced in metabolically engineered Escherichia coli results in a strong fiber. *P Natl Acad Sci USA* **2010,** *107*, 14059-63.
68. Fahnestock, S.; Bedzyk, L., Production of synthetic spider dragline silk protein in Pichia pastoris. *Applied microbiology and biotechnology* **1997,** *47* (1), 33-39.
69. Huemmerich, D.; Scheibel, T.; Vollrath, F.; Cohen, S.; Gat, U.; Ittah, S., Novel Assembly Properties of Recombinant Spider Dragline Silk Proteins. *Current Biology* **2004,** *14* (22), 2070-2074.
70. Lazaris, A.; Arcidiacono, S.; Huang, Y.; Zhou, J.-F.; Duguay, F.; Chretien, N.; Welsh, E. A.; Soares, J. W.; Karatzas, C. N., Spider Silk Fibers Spun from Soluble Recombinant Silk Produced in Mammalian Cells. *Science* **2002,** *295*, 472-476.
71. Scheller, J.; Gührs, K.-H.; Grosse, F.; Conrad, U., Production of spider silk proteins in tobacco and potato. *Nature biotechnology* **2001,** *19* (6), 573-577.
72. Albertson, A. E.; Teulé, F.; Weber, W.; Yarger, J. L.; Lewis, R. V., Effects of different post-spin stretching conditions on the mechanical properties of synthetic spider silk fibers. *J Mech Behav Biomed* **2014,** *29*, 225-234.
73. Copeland, C. G.; Bell, B. E.; Christensen, C. D.; Lewis, R. V., Development of a Process for the Spinning of Synthetic Spider Silk. *ACS Biomaterials Science & Engineering* **2015,** *1*, 577-584.
74. Jones, J. A.; Harris, T. I.; Tucker, C. L.; Berg, K. R.; Christy, S. Y.; Day, B. A.; Gaztambide, D. A.; Needham, N. J. C.; Ruben, A. L.; Oliveira, P. F.; Decker, R. E.; Lewis, R. V., More than just fibers: an aqueous method for the production of innovative recombinant spider silk protein materials. *Biomacromolecules* **2015,** *16*, 1418-25.
75. Bowen, C. H.; Dai, B.; Sargent, C. J.; Bai, W.; Ladiwala, P.; Feng, H.; Huang, W.; Kaplan, D. L.; Galazka, J. M.; Zhang, F., Recombinant Spidroins Fully Replicate Primary Mechanical Properties of Natural Spider Silk. *Biomacromolecules* **2018**.
76. Seidel, A.; Liivak, O.; Calve, S.; Adaska, J.; Ji, G.; Yang, Z.; Grubb, D.; Zax, D. B.; Jelinski, L. W., Regenerated Spider Silk : Processing , Properties , and Structure. **2000**, 775-780.
77. Seidel, A.; Liivak, O.; Jelinski, L. W., Artificial spinning of spider silk. *Macromolecules* **1998,** *31* (19), 6733-6736.
78. Cho, H. J.; Ki, C. S.; Oh, H.; Lee, K. H.; Um, I. C., Molecular weight distribution and solution properties of silk fibroins with different dissolution conditions. *International Journal of Biological Macromolecules* **2012,** *51*, 336-341.
79. Zhao, H.-P.; Feng, X.-Q.; Yu, S.-W.; Cui, W.-Z.; Zou, F.-Z., Mechanical properties of silkworm cocoons. *Polymer* **2005,** *46* (21), 9192-9201.
80. Rockwood, D. N.; Preda, R. C.; Yücel, T.; Wang, X.; Lovett, M. L.; Kaplan, D. L., Materials fabrication from Bombyx mori silk fibroin. *Nat Protoc* **2011,** *6* (10), 1612-1631.
81. Wang, Y. J.; Zhag, Y. Q. In *Three-layered sericins around the silk fibroin fiber from Bombyx mori cocoon and their amino acid composition*, Advanced Materials Research, Trans Tech Publ: **2011**; pp 158-163.
82. Ishizaka, H.; Watanabe, Y.; Ishida, K.; Fukumoto, O., Regenerated silk prepared from ortho phosphoric acid solution of fibroin. *Journal of Sericultural Science of Japan* **1989,** *58* (2), 87-95.
83. Yao, J. M.; Masuda, H.; Zhao, C. H.; Asakura, T., Artificial spinning and characterization of silk fiber from Bombyx mori silk fibroin in hexafluoroacetone hydrate. *Macromolecules* **2002,** *35* (1), 6-9.
84. Lee, K. H.; Baek, D. H.; Ki, C. S.; Park, Y. H., Preparation and characterization of wet spun silk fibroin/poly(vinyl alcohol) blend filaments. *Int J Biol Macromol* **2007,** *41* (2), 168-72.
85. Sashina, E. S.; Bochek, A. M.; Novoselov, N. P.; Kirichenko, D. A., Structure and solubility of natural silk fibroin. *Russian Journal of Applied Chemistry* **2006,** *79* (6), 869-876.
86. Phillips, D. M.; Drummy, L. F.; Conrady, D. G.; Fox, D. M.; Naik, R. R.; Stone, M. O.; Trulove, P. C.; De Long, H. C.; Mantz, R. A., Dissolution and regeneration of Bombyx mori silk fibroin using ionic liquids. *Journal of the American Chemical Society* **2004,** *126* (44), 14350-14351.
87. Yamada, H.; Nakao, H.; Takasu, Y.; Tsubouchi, K., Preparation of undegraded native molecular fibroin solution from silkworm cocoons. *Materials Science and Engineering C: Biomimetic and Supramolecular Systems* **2000,** *14* (1), 41-46.
88. Wang, H.-Y.; Zhang, Y.-Q., Effect of regeneration of liquid silk fibroin on its structure and characterization. *Soft Matter* **2013,** *9* (1), 138-145.
89. Perea, G. B.; Solanas, C.; Marí-Buyé, N.; Madurga, R.; Agulló-Rueda, F.; Muinelo, A.; Riekel, C.; Burghammer, M.; Jorge, I.; Vázquez, J.; Plaza, G. R.; Torres, A. L.; del Pozo, F.; Guinea, G. V.; Elices, M.; Cenis, J. L.; Pérez-Rigueiro, J., The apparent variability of silkworm (Bombyx mori) silk and its relationship with degumming. *European Polymer Journal* **2016,** *78*, 129-140.

90. Ko, J. S.; Yoon, K.; Ki, C. S.; Kim, H. J.; Bae do, G.; Lee, K. H.; Park, Y. H.; Um, I. C., Effect of degumming condition on the solution properties and electrospinnablity of regenerated silk solution. *Int J Biol Macromol* **2013,** *55*, 161-8.
91. Rnjak-Kovacina, J.; Wray, L. S.; Burke, K. A.; Torregrosa, T.; Golinski, J. M.; Huang, W.; Kaplan, D. L., Lyophilized Silk Sponges: A Versatile Biomaterial Platform for Soft Tissue Engineering. *ACS Biomaterials Science & Engineering* **2015,** *1* (4), 260-270.
92. Boulet-Audet, M.; Holland, C.; Gheysens, T.; Vollrath, F., Dry-spun silk produces native-like fibroin solutions. *Biomacromolecules* **2016**.
93. Wang, Q.; Chen, Q.; Yang, Y.; Shao, Z., Effect of various dissolution systems on the molecular weight of regenerated silk fibroin. *Biomacromolecules* **2013,** *14* (1), 285-289.
94. Wei, W.; Zhang, Y.; Shao, H.; Hu, X., Posttreatment of the dry-spun fibers obtained from regenerated silk fibroin aqueous solution in ethanol aqueous solution. *Journal of Materials Research* **2011,** *26* (09), 1100-1106.
95. Wei, W.; Zhang, Y. P.; Zhao, Y. M.; Luo, J.; Shao, H. L.; Hu, X. C., Bio-inspired capillary dry spinning of regenerated silk fibroin aqueous solution. *Mat Sci Eng C-Mater* **2011,** *31* (7), 1602-1608.
96. Sun, M.; Zhang, Y.; Zhao, Y.; Shao, H.; Hu, X., The structure–property relationships of artificial silk fabricated by dry-spinning process. *Journal of Materials Chemistry* **2012,** *22* (35), 18372.
97. Jin, Y.; Zhang, Y.; Hang, Y.; Shao, H.; Hu, X., A simple process for dry spinning of regenerated silk fibroin aqueous solution. *Journal of Materials Research* **2013,** *28* (20), 2897-2902.
98. Jin, Y.; Hang, Y. C.; Zhang, Y. P.; Shao, H. L.; Hu, X. C., Role of Ca^{2+} on structures and properties of regenerated silk fibroin aqueous solutions and fibres. *Mater. Res. Innov.* **2014,** *18*, 113-116.
99. Luo, J.; Zhang, L.; Peng, Q.; Sun, M.; Zhang, Y.; Shao, H.; Hu, X., Tough silk fibers prepared in air using a biomimetic microfluidic chip. *Int J Biol Macromol* **2014,** *66*, 319-24.
100. Yue, X.; Zhang, F.; Wu, H.; Ming, J.; Fan, Z.; Zuo, B., A novel route to prepare dry-spun silk fibers from CaCl2–formic acid solution. *Mater Lett* **2014,** *128*, 175-178.
101. Zhu, J. X.; Zhang, Y. P.; Shao, H. L.; Hu, X. C., Effects of Environment Parameters on Sol-Gel Transition and Dry-spinnability of Regenerated Silk Fibroin Aqueous Solution. *Fibers and Polymers* **2014,** *15* (3), 540-546.
102. Peng, Q.; Shao, H.; Hu, X.; Zhang, Y., Role of humidity on the structures and properties of regenerated silk fibers. *Progress in Natural Science: Materials International* **2015,** *25* (5), 430-436.
103. Yazawa, S., Spinning of concentrated aqueous silk fibroin solution. *Journal of Chemical Society of Japan* **1960,** *63*, 1428-1430.
104. Matsumoto, K.; Uejima, H.; Iwasaki, T.; Sano, Y.; Sumino, H., Studies on regenerated protein fibers. III. Production of regenerated silk fibroin fiber by the self-dialyzing wet spinning method. *Journal of Applied Polymer Science* **1996,** *60* (4), 503-511.
105. Liivak, O.; Blye, A.; Shah, N.; Jelinski, L. W., A microfabricated wet-spinning apparatus to spin fibers of silk proteins. Structure-property correlations. *Macromolecules* **1998,** *31* (9), 2947-2951.
106. Trabbic, K. A.; Yager, P., Comparative structural characterization of naturally- and synthetically-spun fibers of Bombyx mori fibroin. *Macromolecules* **1998,** *31* (2), 462-471.
107. Zhao, C.; Yao, J.; Masuda, H.; Kishore, R.; Asakura, T., Structural characterization and artificial fiber formation of Bombyx mori silk fibroin in hexafluoro-iso-propanol solvent system. *Biopolymers* **2003,** *69* (2), 253-9.
108. Um, I. C.; Ki, C. S.; Kweon, H.; Lee, K. G.; Ihm, D. W.; Park, Y. H., Wet spinning of silk polymer. II. Effect of drawing on the structural characteristics and properties of filament. *Int J Biol Macromol* **2004,** *34* (1-2), 107-19.
109. Um, I. C.; Kweon, H.; Lee, K. G.; Ihm, D. W.; Lee, J. H.; Park, Y. H., Wet spinning of silk polymer. I. Effect of coagulation conditions on the morphological feature of filament. *Int J Biol Macromol* **2004,** *34* (1-2), 89-105.
110. Ha, S. W.; Tonelli, A. E.; Hudson, S. M., Structural studies of Bombyx mori silk fibroin during regeneration from solutions and wet fiber spinning. *Biomacromolecules* **2005,** *6* (3), 1722-31.
111. Marsano, E.; Corsini, P.; Arosio, C.; Boschi, A.; Mormino, M.; Freddi, G., Wet spinning of Bombyx mori silk fibroin dissolved in N-methyl morpholine N-oxide and properties of regenerated fibres. *Int J Biol Macromol* **2005,** *37* (4), 179-88.
112. Phillips, D. M.; Drummy, L. F.; Naik, R. R.; De Long, H. C.; Fox, D. M.; Trulove, P. C.; Mantz, R. A., Regenerated silk fiber wet spinning from an ionic liquid solution. *Journal of Materials Chemistry* **2005,** *15* (39), 4206-4208.
113. Xie, F.; Zhang, H.; Shao, H.; Hu, X., Effect of shearing on formation of silk fibers from regenerated Bombyx mori silk fibroin aqueous solution. *Int J Biol Macromol* **2006,** *38* (3-5), 284-8.
114. Corsini, P.; Perez-Rigueiro, J.; Guinea, G. V.; Plaza, G. R.; Elices, M.; Marsano, E.; Carnasciali, M. M.; Freddi, G., Influence of the draw ratio on the tensile and fracture behavior of NMMO regenerated silk fibers. *Journal of Polymer Science Part B-Polymer Physics* **2007,** *45* (18), 2568-2579.
115. Ki, C. S.; Kim, J. W.; Oh, H. J.; Lee, K. H.; Park, Y. H., The effect of residual silk sericin on the structure and mechanical property of regenerated silk filament. *Int J Biol Macromol* **2007,** *41* (3), 346-53.
116. Ki, C. S.; Lee, K. H.; Baek, D. H.; Hattori, M.; Um, I. C.; Ihm, D. W.; Park, Y. H., Dissolution and wet spinning of silk fibroin using phosphoric acid/formic acid mixture solvent system. *Journal of Applied Polymer Science* **2007,** *105* (3), 1605-1610.
117. Zuo, B. Q.; Liu, L.; Wu, Z., Effect on properties of regenerated silk fibroin fiber coagulated with aqueous Methanol/Ethanol. *Journal of Applied Polymer Science* **2007,** *106* (1), 53-59.
118. Zhu, Z. H.; Ohgo, K.; Asakura, T., Preparation and characterization of regenerated Bombyx mori silk fibroin fiber with high strength. *Express Polymer Letters* **2008,** *2* (12), 885-889.

119. Plaza, G. R.; Corsini, P.; Marsano, E.; Perez-Rigueiro, J.; Biancotto, L.; Elices, M.; Riekel, C.; Agullo-Rueda, F.; Gallardo, E.; Calleja, J. M.; Guinea, G. V., Old Silks Endowed with New Properties. *Macromolecules* **2009,** *42* (22), 8977-8982.
120. Sohn, S.; Gido, S. P., Wet-spinning of osmotically stressed silk fibroin. *Biomacromolecules* **2009,** *10* (8), 2086-91.
121. Zhou, G.; Shao, Z.; Knight, D. P.; Yan, J.; Chen, X., Silk Fibers Extruded Artificially from Aqueous Solutions of Regenerated Bombyx mori Silk Fibroin are Tougher than their Natural Counterparts. *Advanced Materials* **2009,** *21* (3), 366-370.
122. Ko, J. S.; Lee, K. H.; Bae, D. G.; Um, I. C., Miscibility, Structural Characteristics, and Thermal Behavior of Wet Spun Regenerated Silk Fibroin/Nylon 6 Blend Filaments. *Fibers and Polymers* **2010,** *11* (1), 14-20.
123. Yan, J.; Zhou, G.; Knight, D. P.; Shao, Z.; Chen, X., Wet-spinning of regenerated silk fiber from aqueous silk fibroin solution: discussion of spinning parameters. *Biomacromolecules* **2010,** *11* (1), 1-5.
124. Zhu, Z.; Kikuchi, Y.; Kojima, K.; Tamura, T.; Kuwabara, N.; Nakamura, T.; Asakura, T., Mechanical properties of regenerated Bombyx mori silk fibers and recombinant silk fibers produced by transgenic silkworms. *Journal of biomaterials science. Polymer edition* **2010,** *21*, 395-411.
125. Cho, H. J.; Yoo, Y. J.; Kim, J. W.; Park, Y. H.; Bae, D. G.; Um, I. C., Effect of molecular weight and storage time on the wet- and electro-spinning of regenerated silk fibroin. *Polymer Degradation and Stability* **2012,** *97* (6), 1060-1066.
126. Ling, S.; Zhou, L.; Zhou, W.; Shao, Z.; Chen, X., Conformation transition kinetics and spinnability of regenerated silk fibroin with glycol, glycerol and polyethylene glycol. *Mater Lett* **2012,** *81*, 13-15.
127. Plaza, G. R.; Corsini, P.; Marsano, E.; Perez-Rigueiro, J.; Elices, M.; Riekel, C.; Vendrely, C.; Guinea, G. V., Correlation between processing conditions, microstructure and mechanical behavior in regenerated silkworm silk fibers. *Journal of Polymer Science Part B-Polymer Physics* **2012,** *50* (7), 455-465.
128. Chung, D. E.; Um, I. C., Effect of Molecular Weight and Concentration on Crystallinity and Post Drawing of Wet Spun Silk Fibroin Fiber. *Fibers and Polymers* **2014,** *15* (1), 153-160.
129. Kim, H. J.; Um, I. C., Effect of degumming ratio on wet spinning and post drawing performance of regenerated silk. *Int J Biol Macromol* **2014,** *67*, 387-93.
130. Zhou, H.; Shao, Z. Z.; Chen, X., Wet-spinning of regenerated silk fiber from aqueous silk fibroin solutions: Influence of calcium ion addition in spinning dope on the performance of regenerated silk fiber. *Chinese Journal of Polymer Science* **2014,** *32* (1), 29-34.
131. Zhang, F.; Lu, Q.; Yue, X.; Zuo, B.; Qin, M.; Li, F.; Kaplan, D. L.; Zhang, X., Regeneration of high-quality silk fibroin fiber by wet spinning from CaCl2-formic acid solvent. *Acta Biomater* **2015,** *12*, 139-45.
132. Chen, Z.; Zhang, H.; Lin, Z.; Lin, Y.; van Esch, J. H.; Liu, X. Y., Programing Performance of Silk Fibroin Materials by Controlled Nucleation. *Advanced Functional Materials* **2016**.
133. Fang, G.; Huang, Y.; Tang, Y.; Qi, Z.; Yao, J.; Shao, Z.; Chen, X., Insights into Silk Formation Process: Correlation of Mechanical Properties and Structural Evolution during Artificial Spinning of Silk Fibers. *ACS Biomaterials Science & Engineering* **2016**.
134. Teulé, F.; Furin, W. A.; Cooper, A. R.; Duncan, J. R.; Lewis, R. V., Modifications of spider silk sequences in an attempt to control the mechanical properties of the synthetic fibers. *Journal of Materials Science* **2007,** *42*, 8974-8985.
135. Brooks, A. E.; Stricker, S. M.; Joshi, S. B.; Kamerzell, T. J.; Middaugh, C. R.; Lewis, R. V., Properties of synthetic spider silk fibers based on Argiope aurantia MaSp2. *Biomacromolecules* **2008,** *9*, 1506-1510.
136. An, B.; Hinman, M. B.; Holland, G. P.; Yarger, J. L.; Lewis, R. V., Inducing beta-sheets formation in synthetic spider silk fibers by aqueous post-spin stretching. *Biomacromolecules* **2011,** *12*, 2375-2381.
137. Elices, M.; Guinea, G. V.; Plaza, G. R.; Karatzas, C.; Riekel, C.; Agulló-Rueda, F.; Daza, R.; Pérez-Rigueiro, J., Bioinspired Fibers Follow the Track of Natural Spider Silk. *Macromolecules* **2011,** *44*, 1166-1176.
138. An, B.; Jenkins, J. E.; Sampath, S.; Holland, G. P.; Hinman, M.; Yarger, J. L.; Lewis, R., Reproducing natural spider silks' copolymer behavior in synthetic silk mimics. *Biomacromolecules* **2012,** *13*, 3938-3948.
139. Gnesa, E.; Hsia, Y.; Yarger, J. L.; Weber, W.; Lin-Cereghino, J.; Lin-Cereghino, G.; Tang, S.; Agari, K.; Vierra, C., Conserved C-terminal domain of spider tubuliform spidroin 1 contributes to extensibility in synthetic fibers. *Biomacromolecules* **2012,** *13*, 304-12.
140. Teulé, F.; Addison, B.; Cooper, A. R.; Ayon, J.; Henning, R. W.; Benmore, C. J.; Holland, G. P.; Yarger, J. L.; Lewis, R. V., Combining flagelliform and dragline spider silk motifs to produce tunable synthetic biopolymer fibers. *Biopolymers* **2012,** *97*, 418-431.
141. Adrianos, S. L.; Teulé, F.; Hinman, M. B.; Jones, J. A.; Weber, W. S.; Yarger, J. L.; Lewis, R. V., Nephila clavipes Flagelliform silk-like GGX motifs contribute to extensibility and spacer motifs contribute to strength in synthetic spider silk fibers. *Biomacromolecules* **2013,** *14*, 1751-60.
142. Lin, Z.; Deng, Q.; Liu, X.-Y.; Yang, D., Engineered large spider eggcase silk protein for strong artificial fibers. *Advanced Materials* **2013,** *25*, 1216-20.
143. Heidebrecht, A.; Eisoldt, L.; Diehl, J.; Schmidt, A.; Geffers, M.; Lang, G.; Scheibel, T., Biomimetic Fibers Made of Recombinant Spidroins with the Same Toughness as Natural Spider Silk. *Advanced Materials* **2015,** *27*, 2189-2194.
144. Peng, Q.; Zhang, Y.; Lu, L.; Shao, H.; Qin, K.; Hu, X.; Xia, X., Recombinant spider silk from aqueous solutions via a bio-inspired microfluidic chip. *Scientific Reports* **2016,** *6*, 36473.

145. Andersson, M.; Jia, Q.; Abella, A.; Lee, X.-Y.; Landreh, M.; Purhonen, P.; Hebert, H.; Tenje, M.; Robinson, C. V.; Meng, Q.; Plaza, G. R.; Johansson, J.; Rising, A., Biomimetic spinning of artificial spider silk from a chimeric minispidroin. *Nat Chem Biol* **2017.**
146. Jin, H. J.; Fridrikh, S. V.; Rutledge, G. C.; Kaplan, D. L., Electrospinning Bombyx mori silk with poly(ethylene oxide). *Biomacromolecules* **2002,** *3* (6), 1233-9.
147. Kim, S. H.; Nam, Y. S.; Lee, T. S.; Park, W. H., Silk fibroin nanofiber. Electrospinning, properties, and structure. *Polymer Journal* **2003,** *35* (2), 185-190.
148. Ohgo, K.; Zhao, C. H.; Kobayashi, M.; Asakura, T., Preparation of non-woven nanofibers of Bombyx mori silk, Samia cynthia ricini silk and recombinant hybrid silk with electrospinning method. *Polymer* **2003,** *44* (3), 841-846.
149. Sukigara, S.; Gandhi, M.; Ayutsede, J.; Micklus, M.; Ko, F., Regeneration of Bombyx mori silk by electrospinning - part 1: processing parameters and geometric properties. *Polymer* **2003,** *44* (19), 5721-5727.
150. Zarkoob, S.; Eby, R. K.; Reneker, D. H.; Hudson, S. D.; Ertley, D.; Adams, W. W., Structure and morphology of electrospun silk nanofibers. *Polymer* **2004,** *45* (11), 3973-3977.
151. Chen, C.; Cao, C. B.; Ma, X. L.; Tang, Y.; Zhu, H. S., Preparation of non-woven mats from all-aqueous silk fibroin solution with electrospinning method. *Polymer* **2006,** *47* (18), 6322-6327.
152. Yoon, K.; Lee, H. N.; Ki, C. S.; Fang, D.; Hsiao, B. S.; Chu, B.; Um, I. C., Effects of degumming conditions on electro-spinning rate of regenerated silk. *Int J Biol Macromol* **2013,** *61*, 50-7.
153. Weisman, S.; Haritos, V. S.; Church, J. S.; Huson, M. G.; Mudie, S. T.; Rodgers, A. J. W.; Dumsday, G. J.; Sutherland, T. D., Honeybee silk: recombinant protein production, assembly and fiber spinning. *Biomaterials* **2010,** *31*, 2695-700.
154. Takajima, T., *Advanced fiber spinning technology*. Woodhead Publishing: **1994.**
155. Esselen, G. J. Production of silk fibers. US1934413 A, **1933.**
156. Mortimer, B.; Drodge, D. R.; Dragnevski, K. I.; Siviour, C. R.; Holland, C., In situ tensile tests of single silk fibres in an environmental scanning electron microscope (ESEM). *Journal of Materials Science* **2013,** *48* (14), 5055-5062.
157. Porter, D.; Guan, J.; Vollrath, F., Spider silk: super material or thin fibre? *Advanced Materials* **2013,** *25* (9), 1275-1279.
158. Hu, X.; Kaplan, D.; Cebe, P., Determining Beta-Sheet Crystallinity in Fibrous Proteins by Thermal Analysis and Infrared Spectroscopy. *Macromolecules* **2006,** *39* (18), 6161-6170.
159. Hu, X.; Shmelev, K.; Sun, L.; Gil, E.-S.; Park, S.-H.; Cebe, P.; Kaplan, D. L., Regulation of Silk Material Structure by Temperature-Controlled Water Vapor Annealing. *Biomacromolecules* **2011,** *12* (5), 1686-1696.
160. Guan, J.; Porter, D.; Vollrath, F., Thermally Induced Changes in Dynamic Mechanical Properties of Native Silks. *Biomacromolecules* **2013,** *14* (3), 930-937.
161. Koyanagi, R.; Zhu, Z.; Asakura, T., Regenerated Bombyx mori silk fiber with enhanced biodegradability. *Journal of Insect Biotechnology and Sericology* **2010,** *79* (1), 27-30.
162. Teulé, F.; Miao, Y.-G.; Sohn, B.-H.; Kim, Y.-S.; Hull, J. J.; Fraser, M. J.; Lewis, R. V.; Jarvis, D. L., Silkworms transformed with chimeric silkworm/spider silk genes spin composite silk fibers with improved mechanical properties. *Proceedings of the National Academy of Sciences* **2012,** *109* (3), 923-928.
163. Kinahan, M. E.; Filippidi, E.; Köster, S.; Hu, X.; Evans, H. M.; Pfohl, T.; Kaplan, D. L.; Wong, J., Tunable silk: using microfluidics to fabricate silk fibers with controllable properties. *Biomacromolecules* **2011,** *12*, 1504-11.
164. Martel, A.; Burghammer, M.; Davies, R.; DiCola, E.; Panine, P.; Salmon, J.-B.; Riekel, C., A microfluidic cell for studying the formation of regenerated silk by synchrotron radiation small- and wide-angle X-ray scattering. *Biomicrofluidics* **2008,** *2* (2), 024104.
165. Martel, A.; Burghammer, M.; Davies, R. J.; Di Cola, E.; Vendrely, C.; Riekel, C., Silk Fiber Assembly Studied by Synchrotron Radiation SAXS/WAXS and Raman Spectroscopy. *Journal of the American Chemical Society* **2008,** *130* (50), 17070-17074.
166. Rammensee, S.; Slotta, U.; Scheibel, T.; Bausch, A. R., Assembly mechanism of recombinant spider silk proteins. *P Natl Acad Sci USA* **2008,** *105*, 6590-5.
167. Rising, A.; Johansson, J., Toward spinning artificial spider silk. *Nature Chemical Biology* **2015,** *11* (5), 309-315.
168. Guan, J.; Porter, D.; Vollrath, F., Silks cope with stress by tuning their mechanical properties under load. *Polymer (United Kingdom)* **2012,** *53* (13), 2717-2726.
169. Yang, Y.; Kwak, H. W.; Lee, K. H., Effect of Residual lithium ions on the structure and cytotoxicity of silk fibroin film. *International Journal of Industrial Entomology* **2013,** *27* (2), 265-270.
170. Holland, C. Silk rheology. University of Oxford, **2008.**
171. Akai, H., The structure and ultrastructure of the silk gland. *Experientia* **1983,** *39* (5), 443-449.
172. Machida, J., On the Secretion of the Silk Substances of the Silkworm. *Proceedings of the Imperial Academy* **1926,** *2* (8), 421-422.
173. Joos P., Dynamic surface phenomena. VSP: **1999**.
174. Berry, J. D.; Neeson, M. J.; Dagastine, R. R.; Chan, D. Y. C.; Tabor, R. F., Measurement of surface and interfacial tension using pendant drop tensiometry. *Journal of Colloid and Interface Science* **2015**, 454, 226-237.
175. Andrade, J. D.; Ma, S. M.; King, R. N.; Gregonis, D. E., Contact angles at the solid—water interface. *Journal of Colloid and Interface Science* **1979,** *72* (3), 488-494.

176. Nakamura, T.; Hattori, M.; Kawasaki, H.; Miyamoto, K.; Tokita, M.; Komai, T., Surface tension of the polymer network of a gel. *Physical Review E* **1996,** *54* (2), 1663.
177. Stalder, A. F.; Melchior, T.; Müller, M.; Sage, D.; Blu, T.; Unser, M., Low-bond axisymmetric drop shape analysis for surface tension and contact angle measurements of sessile drops. *Colloids and Surfaces A: Physicochemical and Engineering Aspects* **2010,** *364* (1), 72-81.
178. Li, Z.; Giese, R. F.; van Oss, C. J.; Yvon, J.; Cases, J., The Surface Thermodynamic Properties of Talc Treated with Octadecylamine. *Journal of Colloid and Interface Science* **1993,** *156* (2), 279-284.
179. Osswald, T.; Rudolph, N., Rheometry. In *Polymer Rheology*, Carl Hanser Verlag GmbH & Co. KG: **2014**; pp 187-220.
180. McKinley, G. H.; Sridhar, T., Filament-stretching rheometry of complex fluids. *Annual Review of Fluid Mechanics* **2002,** *34* (1), 375-415.
181. Tropea, C.; Yarin, A. L., *Handbook of experimental fluid mechanics*. Springer Science & Business Media: **2007**; Vol. 1.
182. Münstedt, H., New Universal Extensional Rheometer for Polymer Melts. Measurements on a Polystyrene Sample. *Journal of Rheology* **1979,** *23* (4), 421-436.
183. Binding, D. M.; Jones, D. M.; Walters, K., The shear and extensional flow properties of M1. *Journal of Non-Newtonian Fluid Mechanics* **1990,** *35* (2), 121-135.
184. Schweizer, T.; Mikkelsen, K.; Cathey, C.; Fuller, G., Mechanical and optical responses of the M1 fluid subject to stagnation point flow. *Journal of Non-Newtonian Fluid Mechanics* **1990,** *35* (2), 277-286.
185. Laun, H. M.; Hingmann, R., Rheological characterization of the fluid M1 and of its components. *Journal of Non-Newtonian Fluid Mechanics* **1990,** *35* (2), 137-157.
186. James, D. F.; Chandler, G. M.; Armour, S. J., A converging channel rheometer for the measurement of extensional viscosity. *Journal of Non-Newtonian Fluid Mechanics* **1990,** *35* (2), 421-443.
187. Sridhar, T., An overview of the project M1. *Journal of Non-Newtonian Fluid Mechanics* **1990,** *35* (2), 85-92.
188. Anna, S. L.; McKinley, G. H.; Nguyen, D. A.; Sridhar, T.; Muller, S. J.; Huang, J.; James, D. F., An interlaboratory comparison of measurements from filament-stretching rheometers using common test fluids. *Journal of Rheology* **2001,** *45* (1), 83-114.
189. Matta, J.; Tytus, R., Liquid stretching using a falling cylinder. *Journal of Non-Newtonian Fluid Mechanics* **1990,** *35* (2), 215-229.
190. Sridhar, T.; Tirtaatmadja, V.; Nguyen, D. A.; Gupta, R. K., Measurement of extensional viscosity of polymer solutions. *Journal of Non-Newtonian Fluid Mechanics* **1991,** *40* (3), 271-280.
191. Tirtaatmadja, V.; Sridhar, T., A filament stretching device for measurement of extensional viscosity. *Journal of Rheology* **1993,** *37* (6), 1081-1102.
192. Bazilevsky, A. V.; Entov, V. M.; Rozhkov, A. N., Liquid Filament Microrheometer and Some of Its Applications. In *Third European Rheology Conference and Golden Jubilee Meeting of the British Society of Rheology*, Oliver, D. R., Ed. Springer Netherlands: Dordrecht, **1990**; pp 41-43.
193. Entov, V. M.; Hinch, E. J., Effect of a spectrum of relaxation times on the capillary thinning of a filament of elastic liquid. *Journal of Non-Newtonian Fluid Mechanics* **1997,** *72* (1), 31-53.
194. Spiegelberg, S. H.; Ables, D. C.; McKinley, G. H., The role of end-effects on measurements of extensional viscosity in filament stretching rheometers. *Journal of Non-Newtonian Fluid Mechanics* **1996,** *64* (2), 229-267.
195. Spiegelberg, S. H.; McKinley, G. H., Stress relaxation and elastic decohesion of viscoelastic polymer solutions in extensional flow. *Journal of Non-Newtonian Fluid Mechanics* **1996,** *67*, 49-76.
196. Gupta, R. K.; Nguyen, D. A.; Sridhar, T., Extensional viscosity of dilute polystyrene solutions: Effect of concentration and molecular weight. *Physics of Fluids* **2000,** *12* (6), 1296-1318.
197. McKinley, G. H.; Brauner, O.; Yao, M., Kinematics of filament stretching in dilute and concentrated polymer solutions. *Korea-Aust. Rheol. J* **2001,** *13* (1), 29-35.
198. Bhattacharjee, P. K.; Oberhauser, J. P.; McKinley, G. H.; Leal, L. G.; Sridhar, T., Extensional Rheometry of Entangled Solutions. *Macromolecules* **2002,** *35* (27), 10131-10148.
199. Rothstein, J. P.; McKinley, G. H., Inhomogeneous transient uniaxial extensional rheometry. *Journal of Rheology* **2002,** *46* (6), 1419-1443.
200. Rothstein, J. P.; McKinley, G. H., A comparison of the stress and birefringence growth of dilute, semi-dilute and concentrated polymer solutions in uniaxial extensional flows. *Journal of non-newtonian fluid mechanics* **2002,** *108* (1), 275-290.
201. Anna, S. L.; McKinley, G. H., Effect of a controlled pre-deformation history on extensional viscosity of dilute polymer solutions. *Rheologica acta* **2008,** *47* (8), 841-859.
202. Tuladhar, T. R.; Mackley, M. R., Filament stretching rheometry and break-up behaviour of low viscosity polymer solutions and inkjet fluids. *Journal of Non-Newtonian Fluid Mechanics* **2008,** *148* (1–3), 97-108.
203. Capillary thinning of polymeric filaments. *Journal of Rheology* **1999,** *43* (3), 609-625.
204. Arnolds, O.; Buggisch, H.; Sachsenheimer, D.; Willenbacher, N., Capillary breakup extensional rheometry (CaBER) on semi-dilute and concentrated polyethyleneoxide (PEO) solutions. *Rheologica Acta* **2010,** *49* (11), 1207-1217.
205. Rodd, L. E.; Scott, T. P.; Cooper-White, J. J.; McKinley, G. H., Capillary break-up rheometry of low-viscosity elastic fluids. **2004**.

206. Miller, E.; Clasen, C.; Rothstein, J. P., The effect of step-stretch parameters on capillary breakup extensional rheology (CaBER) measurements. *Rheologica Acta* **2009,** *48* (6), 625-639.
207. How dilute are dilute solutions in extensional flows? *Journal of Rheology* **2006,** *50* (6), 849-881.
208. Plog, J.; Kulicke, W.; Clasen, C., Influence of the molar mass distribution on the elongational behaviour of polymer solutions in capillary breakup. *Applied Rheology* **2005,** *15* (1), 28-37.
209. Dinic, J.; Zhang, Y.; Jimenez, L. N.; Sharma, V., Extensional Relaxation Times of Dilute, Aqueous Polymer Solutions. *ACS Macro Letters* **2015,** *4* (7), 804-808.
210. Bhardwaj, A.; Miller, E.; Rothstein, J. P., Filament stretching and capillary breakup extensional rheometry measurements of viscoelastic wormlike micelle solutions. *Journal of Rheology* **2007,** *51* (4), 693-719.
211. Chellamuthu, M.; Rothstein, J. P., Distinguishing between linear and branched wormlike micelle solutions using extensional rheology measurements. *Journal of Rheology* **2008,** *52* (3), 865-884.
212. Yesilata, B.; Clasen, C.; McKinley, G. H., Nonlinear shear and extensional flow dynamics of wormlike surfactant solutions. *Journal of Non-Newtonian Fluid Mechanics* **2006,** *133* (2), 73-90.
213. Haward, S. J.; Sharma, V.; Butts, C. P.; McKinley, G. H.; Rahatekar, S. S., Shear and Extensional Rheology of Cellulose/Ionic Liquid Solutions. *Biomacromolecules* **2012,** *13* (5), 1688-1699.
214. Sharma, V.; Haward, S. J.; Serdy, J.; Keshavarz, B.; Soderlund, A.; Threlfall-Holmes, P.; McKinley, G. H., The rheology of aqueous solutions of ethyl hydroxy-ethyl cellulose (EHEC) and its hydrophobically modified analogue (hmEHEC): extensional flow response in capillary break-up, jetting (ROJER) and in a cross-slot extensional rheometer. *Soft Matter* **2015,** *11* (16), 3251-3270.
215. Morozova, S.; Schmidt, P. W.; Metaxas, A.; Bates, F. S.; Lodge, T. P.; Dutcher, C. S., Extensional Flow Behavior of Methylcellulose Solutions Containing Fibrils. *ACS Macro Letters* **2018,** *7* (3), 347-352.
216. McKinley, G. H.; Tripathi, A., How to extract the Newtonian viscosity from capillary breakup measurements in a filament rheometer. *Journal of Rheology* **2000,** *44* (3), 653-670.
217. Bach, A.; Rasmussen, H. K.; Hassager, O., Extensional viscosity for polymer melts measured in the filament stretching rheometer. *Journal of Rheology* **2003,** *47* (2), 429-441.
218. Kolte, M. I.; Rasmussen, H. K.; Hassager, O., Transient filament stretching rheometer. *Rheologica Acta* **1997,** *36* (3), 285-302.
219. Szabo, P., Transient filament stretching rheometer. *Rheologica Acta* **1997,** *36* (3), 277-284.
220. Barth, A., Infrared spectroscopy of proteins. *Biochimica et Biophysica Acta (BBA) - Bioenergetics* **2007,** *1767* (9), 1073-1101.
221. Boulet-Audet, M. Why and how is silk spun? Integrating rheology with advanced spectroscopic techniques. University of Oxford, **2013.**
222. Larkin, P., Chapter 3 - Instrumentation and Sampling Methods. In *Infrared and Raman Spectroscopy*, Ed. Elsevier: Oxford, **2011**; pp 27-54.
223. Boulet-Audet, M.; Vollrath, F.; Holland, C., Identification and classification of silks using infrared spectroscopy. *The Journal of Experimental Biology* **2015,** *218* (19), 3138-3149.
224. Taddei, P.; Monti, P., Vibrational infrared conformational studies of model peptides representing the semicrystalline domains of Bombyx mori silk fibroin. *Biopolymers* **2005,** *78* (5), 249-258.
225. Petsko, G. A.; Ringe, D., Protein Structure and Function. *Blackwell Scientific Publications*: Oxford, **2004**; Vol. 7, p 1365.
226. Goormaghtigh, E.; Ruysschaert, J.-M.; Raussens, V., Evaluation of the Information Content in Infrared Spectra for Protein Secondary Structure Determination. *Biophysical Journal* **2006,** *90* (8), 2946-2957.
227. Colthup, N. B.; Daly, L. H.; Wiberley, S. E., *Introduction to Infrared and Raman Spectroscopy (Third Edition)*. Academic Press: San Diego, **1990;** xi-xii.
228. Kwak, H. W.; Ju, J. E.; Shin, M.; Holland, C.; Lee, K. H., Sericin Promotes Fibroin Silk I Stabilization Across a Phase-Separation. *Biomacromolecules* **2017,** *18* (8), 2343-2349.
229. Madurga, R.; Gañán-Calvo, A. M.; Plaza, G. R.; Guinea, G. V.; Elices, M.; Pérez-Rigueiro, J., Production of High Performance Bioinspired Silk Fibers by Straining Flow Spinning. *Biomacromolecules* **2017**.
230. Paul, G.; Sophia, L.; Paul, W., Characterization of Historic Silk by Polarized Attenuated Total Reflectance Fourier Transform Infrared Spectroscopy for Informed Conservation. *Appl Spectrosc* **2005,** *59* (10), 1242-1247.
231. Boulet-Audet, M.; Lefèvre, T.; Buffeteau, T.; Pézolet, M., Attenuated Total Reflection Infrared Spectroscopy: An Efficient Technique to Quantitatively Determine the Orientation and Conformation of Proteins in Single Silk Fibers. *Appl Spectrosc* **2008,** *62* (9), 956-962.
232. Murphy, D. B.; Spring, K. R.; Fellers, T. J.; Davidson, M. W. Principles of Birefringence. https://www.microscopyu.com/techniques/polarized-light/principles-of-birefringence (accessed 17/02/2020).
233. Anton Paar GmbH, The principles of dynamic light scattering. https://wiki.anton-paar.com/en/the-principles-of-dynamic-light-scattering (accessed 05/08/2019).
234. Anton Paar GmbH, The principles of dynamic light scattering. https://wiki.anton-paar.com/en/the-principles-of-dynamic-light-scattering (accessed 31/08/2019).
235. Pecora, R., Dynamic Light Scattering Measurement of Nanometer Particles in Liquids. *Journal of Nanoparticle Research* **2000,** *2* (2), 123-131.
236. Malvern Instruments -Technical Note. *Dynamic Light Scattering: An Introduction in 30 Minutes*; **2017**.
237. Davies, G. Natural and bioinspired silk spinning. University of Oxford, **2013.**

238. Koeppel, A.; Laity, P. R.; Holland, C., Extensional flow behaviour and spinnability of native silk. *Soft Matter* **2018,** *14* (43), 8838-8845.
239. Porter, D.; Vollrath, F., Silk as a biomimetic ideal for structural polymers. *Advanced Materials* **2009,** *21* (4), 487-492.
240. Lefèvre, T.; Boudreault, S.; Cloutier, C.; Pézolet, M., Conformational and orientational transformation of silk proteins in the major ampullate gland of Nephila clavipes spiders. *Biomacromolecules* **2008,** *9* (9), 2399-2407.
241. Dicko, C.; Vollrath, F.; Kenney, J. M., Spider silk protein refolding is controlled by changing pH. *Biomacromolecules* **2004,** *5* (3), 704-710.
242. He, Y.-X.; Zhang, N.-N.; Li, W.-F.; Jia, N.; Chen, B.-Y.; Zhou, K.; Zhang, J.; Chen, Y.; Zhou, C.-Z., N-Terminal Domain of Bombyx mori Fibroin Mediates the Assembly of Silk in Response to pH Decrease. *Journal of Molecular Biology* **2012,** *418* (3–4), 197-207.
243. Knight, D. P.; Vollrath, F., Changes in element composition along the spinning duct in a Nephila spider. *Naturwissenschaften* **2001,** *88* (4), 179-182.
244. Rogalski, J. J.; Bastiaansen, C. W. M.; Peijs, T., Rotary jet spinning review – a potential high yield future for polymer nanofibers. *Nanocomposites* **2017,** *3* (4), 97-121.
245. Cheng, J.; Jun, Y.; Qin, J.; Lee, S.-H., Electrospinning versus microfluidic spinning of functional fibers for biomedical applications. *Biomaterials* **2017,** *114*, 121-143.
246. Lenk, R. S., *Polymer rheology*. Springer Science & Business Media: **2012.**
247. Chappel, F. P.; Culpin, M. F.; Gosden, R. G.; Tranter, T. G., Some crystallisation phenomena in rapidly quenched 6.6 nylon. *Journal of Applied Chemistry* **1964,** *14* (1), 12-19.
248. Paten, J. A.; Siadat, S. M.; Susilo, M. E.; Ismail, E. N.; Stoner, J. L.; Rothstein, J. P.; Ruberti, J. W., Flow-Induced Crystallization of Collagen: A Potentially Critical Mechanism in Early Tissue Formation. *ACS nano* **2016,** *10* (5), 5027-5040.
249. Samon, J. M.; Schultz, J. M.; Hsiao, B. S.; Seifert, S.; Stribeck, N.; Gurke, I.; Saw, C., Structure Development during the Melt Spinning of Polyethylene and Poly(vinylidene fluoride) Fibers by in Situ Synchrotron Small- and Wide-Angle X-ray Scattering Techniques. *Macromolecules* **1999,** *32* (24), 8121-8132.
250. Tian, N.; Zhou, W.; Cui, K.; Liu, Y.; Fang, Y.; Wang, X.; Liu, L.; Li, L., Extension Flow Induced Crystallization of Poly(ethylene oxide). *Macromolecules* **2011,** *44* (19), 7704-7712.
251. Bischoff White, E. E.; Henning Winter, H.; Rothstein, J. P., Extensional-flow-induced crystallization of isotactic polypropylene. *Rheologica Acta* **2012,** *51* (4), 303-314.
252. Samon, J. M.; Schultz, J. M.; Hsiao, B. S.; Wu, J.; Khot, S., Structure development during melt spinning and subsequent annealing of polybutene-1 fibers. *Journal of Polymer Science Part B: Polymer Physics* **2000,** *38* (14), 1872-1882.
253. White, J. L.; Cakmak, M., Orientation development and crystallization in melt spinning of fibers. *Advances in Polymer Technology* **1986,** *6* (3), 295-337.
254. Kojic, N.; Bico, J.; Clasen, C.; McKinley, G. H., Ex vivo rheology of spider silk. *Journal of Experimental Biology* **2006,** *209* (21), 4355-4362.
255. Renault, A.; Rioux-Dubé, J.-F. o.; Lefèvre, T.; Beaufils, S.; Vié, V. r.; Paquet-Mercier, F. o.; Pézolet, M., Structure and Mechanical Properties of Spider Silk Films at the Air–Water Interface. *Langmuir* **2013,** *29* (25), 7931-7938.
256. Singh, B.; Panda, N.; Pramanik, K., A novel electrospinning approach to fabricate high strength aqueous silk fibroin nanofibers. *International journal of biological macromolecules* **2016,** *87*, 201-207.
257. Rider, P. M.; Brook, I. M.; Smith, P. J.; Miller, C. A., Reactive Inkjet Printing of Regenerated Silk Fibroin Films for Use as Dental Barrier Membranes. *Micromachines* **2018,** *9* (2), 46.
258. Daerr, A. a. M., A, Pendent_Drop:An ImageJ Plugin to Measure the Surface Tension from an Image of a Pendent Drop. *Journal of Open Research Software* **2016,** *4* (1).
259. Berry, J. D.; Neeson, M. J.; Dagastine, R. R.; Chan, D. Y. C.; Tabor, R. F., Measurement of surface and interfacial tension using pendant drop tensiometry. *Journal of Colloid and Interface Science* **2015,** *454*, 226-237.
260. Pallas, N. R.; Harrison, Y., An automated drop shape apparatus and the surface tension of pure water. *Colloids and Surfaces* **1990,** *43* (2), 169-194.
261. Melo-Espinosa, E. A.; Sánchez-Borroto, Y.; Errasti, M.; Piloto-Rodríguez, R.; Sierens, R.; Roger-Riba, J.; Christopher-Hansen, A., Surface Tension Prediction of Vegetable Oils Using Artificial Neural Networks and Multiple Linear Regression. *Energy Procedia* **2014,** *57*, 886-895.
262. Fisher, L.; Mitchell, E.; Parker, N., Interfacial tensions of commercial vegetable oils with water. *Journal of Food Science* **1985,** *50* (4), 1201-1202.
263. Yang, Y.; Dicko, C.; Bain, C. D.; Gong, Z.; Jacobs, R. M. J.; Shao, Z.; Terry, A. E.; Vollrath, F., Behavior of silk protein at the air-water interface. *Soft Matter* **2012,** *8* (37), 9705-9712.
264. Ryan, A., *Polymer processing and structure development*. Springer Science & Business Media: **1998.**
265. Niesten, M.; Krijgsman, J.; Harkema, S.; Gaymans, R., Melt spinnable spandex fibers from segmented copolyetheresteraramids. *Journal of applied polymer science* **2001,** *82* (9), 2194-2203.
266. Laity, P.; Holland, C., The Rheology behind Stress-Induced Solidification in Native Silk Feedstocks. *International Journal of Molecular Sciences* **2016,** *17* (11), 1812.

267. Liu, G.; Sun, H.; Rangou, S.; Ntetsikas, K.; Avgeropoulos, A.; Wang, S.-Q., Studying the origin of "strain hardening": Basic difference between extension and shear. *Journal of Rheology* **2013,** *57* (1), 89-104.
268. Tripathi, A.; Whittingstall, P.; McKinley, G. H., Using filament stretching rheometry to predict strand formation and "processability" in adhesives and other non-Newtonian fluids. *Rheologica Acta* **2000,** *39* (4), 321-337.
269. Erni, P.; Varagnat, M.; Clasen, C.; Crest, J.; McKinley, G. H., Microrheometry of sub-nanolitre biopolymer samples: non-Newtonian flow phenomena of carnivorous plant mucilage. *Soft Matter* **2011,** *7* (22), 10889-10898.
270. Kojic, N.; Kojic, M.; Gudlavalleti, S.; McKinley, G., Solvent Removal during Synthetic and Nephila Fiber Spinning. *Biomacromolecules* **2004,** *5* (5), 1698-1707.
271. Trouton, F. T., On the Coefficient of Viscous Traction and Its Relation to that of Viscosity. *Proceedings of the Royal Society of London. Series A* **1906,** *77* (519), 426-440.
272. Petrie, C. J. S., Extensional viscosity: A critical discussion. *Journal of Non-Newtonian Fluid Mechanics* **2006,** *137* (1–3), 15-23.
273. Narayanan, S.; Gokuldas, M., Influence of organic solvents on the structural and thermal characteristics of silk protein from the web of Orthaga exvinacea Hampson (Lepidoptera: Pyralidae). *J Chem Biol* **2016,** *9* (4), 121-125.
274. Craig, C. L., Evolution of arthropod silks. In *Annual Review of Entomology*, **1997**; Vol. 42, pp 231-267.
275. Keten, S.; Xu, Z.; Ihle, B.; Buehler, M. J., Nanoconfinement controls stiffness, strength and mechanical toughness of B-sheet crystals in silk. *Nat Mater* **2010,** *9* (4), 359-367.
276. Yarger, J. L.; Cherry, B. R.; van der Vaart, A., Uncovering the structure–function relationship in spider silk. *Nature Reviews Materials* **2018,** *3*, 18008.
277. Holland, C.; Terry, A. E.; Porter, D.; Vollrath, F., Comparing the rheology of native spider and silkworm spinning dope. **2006,** *5*, 870.
278. Wang, X.; Li, Y.; Liu, Q.; Chen, Q.; Xia, Q.; Zhao, P., In vivo effects of metal ions on conformation and mechanical performance of silkworm silks. *Biochimica et Biophysica Acta.*
279. Askarieh, G.; Hedhammar, M.; Nordling, K.; Saenz, A.; Casals, C.; Rising, A.; Johansson, J.; Knight, S. D., Self-assembly of spider silk proteins is controlled by a pH-sensitive relay. *Nature* **2010,** *465*, 236-8.
280. Zhong, J.; Liu, Y.; Ren, J.; Tang, Y.; Qi, Z.; Zhou, X.; Chen, X.; Shao, Z.; Chen, M.; Kaplan, D. L.; Ling, S., Understanding Secondary Structures of Silk Materials via Micro- and Nano-Infrared Spectroscopies. *ACS Biomaterials Science & Engineering* **2019,** *5* (7), 3161-3183.
281. Saric, M.; Scheibel, T., Engineering of silk proteins for materials applications. *Current Opinion in Biotechnology* **2019,** *60*, 213-220.
282. Chen, P.; Kim, H. S.; Park, C. Y.; Kim, H. S.; Chin, I. J.; Jin, H. J., pH-triggered transition of silk fibroin from spherical micelles to nanofibrils in water. *Macromolecular Research* **2008,** *16* (6), 539-543.
283. Schwarze, S.; Zwettler, F. U.; Johnson, C. M.; Neuweiler, H., The N-terminal domains of spider silk proteins assemble ultrafast and protected from charge screening. *Nat Commun* **2013,** *4*, 2815.
284. Hagn, F.; Thamm, C.; Scheibel, T.; Kessler, H., pH-Dependent Dimerization and Salt-Dependent Stabilization of the N-terminal Domain of Spider Dragline Silk—Implications for Fiber Formation. *Angewandte Chemie International Edition* **2011,** *50* (1), 310-313.
285. Strickland, M.; Tudorica, V.; Řezáč, M.; Thomas, N. R.; Goodacre, S. L., Conservation of a pH-sensitive structure in the C-terminal region of spider silk extends across the entire silk gene family. *Heredity* **2018,** *120* (6), 574-580.
286. Sparkes, J.; Holland, C., The Energy Requirements for Flow-Induced Solidification of Silk. *Macromolecular Bioscience,* **2019,** 1800229.
287. Laity, P. R.; Holland, C., Thermo-rheological behaviour of native silk feedstocks. *European Polymer Journal* **2017,** *87*, 519-534.
288. Sentmanat, M.; Delgadillo-Velázquez, O.; Hatzikiriakos, S. G., Crystallization of an ethylene-based butene plastomer: the effect of uniaxial extension. *Rheologica Acta* **2010,** *49* (9), 931-939.
289. Trebbin, M.; Steinhauser, D.; Perlich, J.; Buffet, A.; Roth, S. V.; Zimmermann, W.; Thiele, J.; Förster, S., Anisotropic particles align perpendicular to the flow direction in narrow microchannels. *P Natl Acad Sci USA* **2013,** *110* (17), 6706-6711.
290. Khan Md, M. R.; Morikawa, H.; Gotoh, Y.; Miura, M.; Ming, Z.; Sato, Y.; Iwasa, M., Structural characteristics and properties of Bombyx mori silk fiber obtained by different artificial forcibly silking speeds. *International Journal of Biological Macromolecules* **2008,** *42* (3), 264-270.
291. Wan, Q.; Abrams, K. J.; Masters, R. C.; Talari, A. C. S.; Rehman, I. U.; Claeyssens, F.; Holland, C.; Rodenburg, C., Mapping Nanostructural Variations in Silk by Secondary Electron Hyperspectral Imaging. *Advanced Materials* **2017,** *29* (47), 1703510.
292. Ebrahimi, D.; Tokareva, O.; Rim, N. G.; Wong, J. Y.; Kaplan, D. L.; Buehler, M. J., Silk–Its Mysteries, How It Is Made, and How It Is Used. *ACS Biomaterials Science & Engineering* **2015,** *1* (10), 864-876.
293. Zhou, C.-Z.; Confalonieri, F.; Medina, N.; Zivanovic, Y.; Esnault, C.; Yang, T.; Jacquet, M.; Janin, J.; Duguet, M.; Perasso, R.; Li, Z.-G., Fine organization of Bombyx mori fibroin heavy chain gene. *Nucleic Acids Research* **2000,** *28* (12), 2413-2419.
294. Guan, J., Vollrath, F. & Porter, D, Silk "Quality" Revealed Using Dynamic Mechanical Thermal Analysis (DMTA). In *6th BACSA International Conference: Building value Chains in Sericulture*, Padua, Italy, **2013**.

295. Sparkes, J.; Holland, C., The Energy Requirements for Flow-Induced Solidification of Silk. *Macromolecular Bioscience* **2018**.
296. Holland, C.; Hawkins, N.; Frydrych, M.; Laity, P.; Porter, D.; Vollrath, F., Differential Scanning Calorimetry of Native Silk Feedstock. *Macromolecular Bioscience* **2019,** *19* (3), 1800228.
297. Nova, A.; Keten, S.; Pugno, N. M.; Redaelli, A.; Buehler, M. J., Molecular and nanostructural mechanisms of deformation, strength and toughness of spider silk fibrils. *Nano Letters* **2010,** *10* (7), 2626-2634.
298. Koeppel, A.; Holland, C., Spinning beta silks requires both pH activation and extensional stress. *submitted to Advanced Materials* **2019**.
299. Lee, S.-M.; Pippel, E.; Gösele, U.; Dresbach, C.; Qin, Y.; Chandran, C. V.; Bräuniger, T.; Hause, G.; Knez, M., Greatly Increased Toughness of Infiltrated Spider Silk. *Science* **2009,** *324* (5926), 488.
300. Liu, Q.; Wang, X.; Tan, X.; Xie, X.; Li, Y.; Zhao, P.; Xia, Q., A strategy for improving the mechanical properties of silk fiber by directly injection of ferric ions into silkworm. *Materials & Design* **2018,** *146*, 134-141.
301. Wang, X.; Zhao, P.; Li, Y.; Yi, Q.; Ma, S.; Xie, K.; Chen, H.; Xia, Q., Modifying the Mechanical Properties of Silk Fiber by Genetically Disrupting the Ionic Environment for Silk Formation. *Biomacromolecules* **2015,** *16* (10), 3119-3125.
302. Liu, Y.; Yu, T.; Yao, H.; Yang, F., PIXE Analysis of Silk. *Journal of Applied Polymer Science* **1997,** *66* (2), 405-408.
303. Xin Wang, P. Z., Yi Li, Qiying Yi, Sanyuan Ma, Kang Xie, Huifang Chen, Qingyou Xia, Modifying the Mechanical Properties of Silk Fiber by Genetically Disrupting the Ionic Environment for Silk Formation. *Biomacromolecules* **2015,** *16*, 3119-25.
304. Hofmeister, F., *Archiv f. experiment. Pathol. u. Pharmakol* **1888,** *24*
305. Bosshard, H. R.; Marti, D. N.; Jelesarov, I., Protein stabilization by salt bridges: concepts, experimental approaches and clarification of some misunderstandings. *Journal of Molecular Recognition* **2004,** *17* (1), 1-16.
306. Vrbka, L.; Vondrášek, J.; Jagoda-Cwiklik, B.; Vácha, R.; Jungwirth, P., Quantification and rationalization of the higher affinity of sodium over potassium to protein surfaces. *Proceedings of the National Academy of Sciences* **2006,** *103* (42), 15440.
307. Hess, B.; van der Vegt, N. F. A., Cation specific binding with protein surface charges. *Proceedings of the National Academy of Sciences* **2009,** *106* (32), 13296.
308. Rembert, K. B.; Paterová, J.; Heyda, J.; Hilty, C.; Jungwirth, P.; Cremer, P. S., Molecular Mechanisms of Ion-Specific Effects on Proteins. *Journal of the American Chemical Society* **2012,** *134* (24), 10039-10046.
309. Rotilio, G., Interaction of metal ions with proteins: an overview. *Inorganica Chimica Acta* **1980,** *40*, X49.
310. Ruan, Q.-X.; Zhou, P.; Hu, B.-W.; Ji, D., An investigation into the effect of potassium ions on the folding of silk fibroin studied by generalized two-dimensional NMR–NMR correlation and Raman spectroscopy. *The FEBS Journal* **2008,** *275* (2), 219-232.
311. Bush, A. I., The metallobiology of Alzheimer's disease. *Trends in Neurosciences* **2003,** *26* (4), 207-214.
312. Millhauser, G. L., Copper Binding in the Prion Protein. *Accounts of Chemical Research* **2004,** *37* (2), 79-85. DOI: 10.1021/ar0301678.
313. Schaeffer, C.; Laity, P.; Hollandd, C.; McLeish, T, manuscript in preparation.
314. Collins, K. D., Charge density-dependent strength of hydration and biological structure. *Biophysical Journal* **1997,** *72* (1), 65-76.
315. Bello, J.; Bello, H. R., Interaction of Model Peptides with Water and Lithium Bromide. *Nature* **1961,** *190* (4774), 440-441.
316. Pocker, Y.; Green, E., Hydrolysis of D-glucono-.delta.-lactone. I. General acid-base catalysis, solvent deuterium isotope effects, and transition state characterization. *Journal of the American Chemical Society* **1973,** *95* (1), 113-119.
317. Thamm, C.; Scheibel, T., Recombinant production, characterization and fiber spinning of an engineered short major ampullate spidroin (MaSp1s). *Biomacromolecules* **2017**. DOI: 10.1021/acs.biomac.7b00090.
318. Albrecht, W.; Fuchs, H.; Kittelmann, W., *Vliesstoffe: Rohstoffe, Herstellung, Anwendung, Eigenschaften, Prüfung*. John Wiley & Sons: **2012.**
319. Zemlin, J. *A study of the mechanical behavior of spider silks*; DTIC Document: 1968.
320. Schneider, C. A.; Rasband, W. S.; Eliceiri, K. W., NIH Image to ImageJ: 25 years of image analysis. *Nat Meth* **2012,** *9* (7), 671-675